Analyzing a curved suspension timber bridge
- Connections and durability based on the project “A Pilgrim’s walk”

Miriam Paola Emmi Kleinhenz

Avdelningen för Konstruktionsteknik
Lunds Tekniska Högskola
Lunds Universitet, 2012

Rapport TVBK - 5217

Avdelningen för Konstruktionsteknik
Lunds Tekniska Högskola
Box 118
221 00 LUND

Division of Structural Engineering
Faculty of Engineering, LTH
P.O. Box 118
S-221 00 LUND
Sweden

Analyzing a curved suspension timber bridge

- Connections and durability based on the project ”A Pilgrim’s Walk”

Miriam Paola Emmi Kleinhenz

2012

Rapport TVBK-5217
ISSN 0349-4969
ISRN: LUTVDG/TVBK-12/5217+148p

Examensarbete
Handledare: Roberto Crocetti
September 2012

PREFACE

The extraordinary opportunity of writing the diploma thesis in Sweden for half a year was given to me by Professor Hans-Joachim Blaß, head of the Institute of Timber Construction and Structural Engineering at the Karlsruhe Institute of Technology (KIT). I want to thank him for encouraging me to pursue my thesis abroad. My many thanks also go to Dietrich Töws, scientific assistant, for his very important help through the entire process of the thesis.

The idea for joining the bridge project "A Pilgrim's Walk" was presented to me by Roberto Crocetti, professor at the Department of Structural Engineering at Lunds Tekniska Högskola (LTH). Combining the diploma thesis in the field of structural timber bridge engineering with the timber bridge case of a real project enhanced enormously my work satisfaction. Special thanks go to him for being my supervisor in Lund, Sweden.

Special thanks go to Eva Frühwald Hansson, assistant professor, supplying me until the end of the thesis and to Hassan Mehri, PhD student, always helping me with the software SAP2000 v.14.

The thesis would never have been possible without my parents supporting and encouraging me from the start.

ABSTRACT

The curved suspension bridge is characterized by a light-weighted and remarkable structure. This bridge construction represents from the architect's as well as from the engineer's point of view a more unusual construction.

Understanding the statics in the right way opens up the possibility of using the interplay of forces and the different materials' advantages in an optimal way. Diverse options of suspending the bridge's deck change the behavior of the bridge.

This diploma thesis describes basically the statics of a curved and suspended structure. It takes consequences out of the conclusions for modeling the structure of the "A Pilgrim's Walk" bridge, a pedestrian bridge of a project taking place near Lomma in Southern Sweden.

During the modeling process, the software SAP2000 v.14 is used. It becomes clear that suspending the deck structure along the outer edge brings more benefits for the project's bridge. The final model is divided into two arches, the timber deck and the steel tension arch, which are connected to each other by timber frames. In order to have smaller section forces, the connection point between the two arches and the suspension should be in a position inside the deck structure.

Since the middle of the 20th century the attractiveness of timber is increasing again thanks to big developments in technology and timber products. Ever since, timber is the only perpetually renewable material and can be used without any harm for the environment. The aim of this thesis is to use the material timber as much as possible while designing the project's bridge.

Nevertheless, the durability of the timber constructions needs to be considered well to assure a long lifespan. The connections of the bridge are strongly connected to the important aspect of durability. Therefore, it will be concentrated, in particular, on the connection between deck structure and cable arrangement.

TABLE OF CONTENTS

1. Introduction

1.1 Background

The first bridges used by humans have probably been made out of wood. Since the middle of the 20th century the attractiveness of timber is increasing again thanks to big developments in technology and timber products. In the field of bridge constructions timber is not only useful because of its good weight-to-strength ratio but also attracts attention because of its aesthetic and haptic values.

In general, engineers started already centuries ago to include the idea of a cultural and aesthetically purpose instead of just having the functional purpose of the construction in mind. Bridges, especially footbridges, can be special objects. During the design process it should not just be focused on the application of codes' requirements. Footbridges can be more than simple crossing devices. They are elements of connection between areas and buildings. At the same time, they create new public areas for pedestrians, visitors and local residents. By designing no standard solution engineers are able to create statically more challenging and aesthetically more pleasing constructions.

Nowadays, a very important aspect is sustainability. Footbridges are tools of infrastructure that enable alternative mobility. Using the material timber in addition gives the unique opportunity of saving more CO_2 than has been produced during manufacturing. Timber structures give the opportunity of entering into a cycle of regeneration. In order to enter into this cycle efficiently, the timber structures have to be as highly durable as structures out of other materials. The assurance of well considered durability is needed. Therefore, concepts of structural timber preservation need to be worked out during the project's design process.

In the project "A Pilgrim's Walk" timber was chosen as main construction material. In this project a pedestrian bridge will be designed at Borgeby Castle near Lomma in Southern Sweden. Among other concepts, the striking and more unusual concept of a slender and two-curved timber bridge suspended from a cable structure aroused most interest. Joining this project means not to deal with a standard solution.

1.2 Objectives and limitations

By joining the project "A Pilgrim's Walk" the main topic of this thesis is to work with the structure of a curved timber bridge suspended along one edge. The aim is to analyze the statics of a curved structure and the influence of the suspension, in general. The decision has to be made along which side the suspension seems more advantageous.

Afterwards it will be concentrated on the most important connection point between cable structure and timber deck under the aspect of load carrying capacity as well as durability of the bridge.

Therefore, the load-bearing design according to the Eurocode standards is made for bridge elements directly linked to the connection point. In order to demonstrate the distribution of section forces in the system, the finite element program SAP2000 v.14 is used. The live load is distributed evenly over the whole timber deck. It is no aim of the thesis to study a series of influence lines.

The first examples as well as the final model are modelled as one-curved structure although the developed concept of the project is a two-curved structure. This decision is made for reasons of simplification.

Daniel Asp, a student at the Chalmers University of Technology, focuses on the dynamics of the bridge. That is the reason for leaving out dynamic analyses.

1.3 Outline of the thesis

In this thesis it is worked on the subject of a timber bridge. Chapter 2 gives a short introduction to the field of timber bridges by summarizing the most important improvements of timber engineering and outlining the future of timber bridge engineering.

Chapter 3 presents the project “A Pilgrim’s Walk” and summarizes the architectural work of the Chalmers’ student Daniel Asp. In this chapter the development of the concept of a curved suspension bridge is outlined.

In order to be able to model the bridge in the right way and to discuss the results of the section forces, it is important to start the analysis with basic examples. In chapter 4 the focus shifts to the statics of the complex curved structure. It is explained what kind of section forces can be observed and which effects are generated thanks to the curvature and the suspension.

The conclusions of chapter 4 are used to develop the final model, which is defined and assigned in chapter 5.

Chapter 6 deals with the load-bearing design of parts of the bridge. At the end of the thesis the connection point between timber deck and hangers is discussed.

Chapter 7 summarizes the conclusions of the thesis and offers an incentive for further research.

2. Aspects of timber bridges

2.1 Important means in the development of timber

Wood has always been at hand and was most likely one of the first materials which humans used to construct a bridge. Nowadays, wooden bridge constructions impress by the beauty of their light structure. After having almost entirely been replaced by steel and concrete during the 20th century, architects and engineers started again to appreciate this lightweight material which assures load-bearing capacity, serviceability and environmental friendliness, at the same time. To increase the suitability and competiveness of wood for modern bridge applications, improvements in modern timber engineering were needed.

During the early 20th century, a mistaken industrialization lead to a process of alienation from nature. Concrete, steel and synthetic materials replaced wood as major material even in cases in which the use of wood was more suitable. (*NATTERER, J. et al. 1991*)

While the technology of other bridge materials developed rapidly, progress in timber bridge development slowed. It was not until the mid 1940ies that innovative improvements in timber materials, connections and structures made it possible to counteract this process. (*RITTER, M.A. 1990*)

Extensive development work and research accomplished the transition from conventional wood construction to modern timber engineering. Standardizations completed empirical values with valid methods of calculation, static systems and exact numerical values for the physical and mechanical values of timber. This led to an assurance of the necessary requirements in notifications and standards. (*NATTERER, J. et al. 1991*)

The mainstay of timber engineering was made by the advent of glued-laminated timber, in short, glulam. Glulam consists of parallel laminations of solid timber which are bonded together under pressure. Compared to solid timber glulam has a homogenous structure which means that natural strength reducing features have a reduced effect. Other advantages are its increased resistance and rigidity as well as the larger size possibilities. (*SÉTRA 2006 (2007)*)

Other structural timber composites followed and increased the alternatives for designers. During the past four or five decades, new technologies in the field of connection design have been very important, as well. Using the material steel to connect timber elements has created effective joining techniques with high quality and refined solutions. Examples for innovative techniques are compact connections formed with multiple or slotted-in steel plates and dowel-type fasteners. (*METTEM, C.J. 2011*)

All in all, longer spans, larger cross-sections and new evolved bridge designs were possible thanks to the continuing development of technologies and with the help of high-quality workmanship. As a result, the interest in timber as a bridge material has increased until today and an increasing number of timber bridges have been constructed. Designers have re-learned to use and to include this natural material in their designing process. Especially in the northern latitudes hundreds of new bridges have been the result of initiatives like the Nordic Timber Bridge Program. This program started in 1994 with the aim to increase the competitiveness of timber bridges in order "(…) to construct more timber bridges at the sacrifice of steel and concrete bridges." (*KLEPPE, O. & AASHEIM, E. 1996*)

A misconception prevails that wooden materials are limited bridge materials in the field of constructing structures of appreciable size. Fact is that due to the important means in the development durable and economic timber bridge structures could and can be built for high loading and large spans. Based on the Nordic Timber Bridge Program, "(m)any of these bridges are pedestrian bridges, but the number of new bridges for heavy traffic is increasing rapidly." (*AASHEIM, E.1999*) Elsewhere in Europe, like in France or in German-speaking countries, timber engineering is also on the increase. (*METTEM, C.J. 2011*)

2.2 Benefits of timber constructions

Using timber in construction means to use a living building material. In order to use it appropriately, the engineer has to know and to accept its characteristics.

Its characteristics provide many advantages which have to be compared with the advantages of other construction materials in order to evaluate them against each other. The pros and cons help to find a final bridge design.

At first, it will be taken a look on the most obvious benefit of timber structures. Wooden surfaces please with their aesthetic attractiveness. They appear warm, natural and vivid. Since there exists a high variety of timber species, a wide range of different appearances is available. Timber members are structural and design elements, at the same time. This very pleasant effect is appreciated by designers and architects.

Physical properties of wood

Due to the physical characteristics of wood the impression of warmness is caused by its high thermal storage capacity. Its thermal conductivity is in comparison to materials like stone, steel or concrete very low. This fact prevents the risk of heat loss caused by thermal bridges. Closely linked is the physical ability of wood "to breathe": the admission and submission of

humidity. As a consequence, pedestrians have a feeling of warmness and pleasant atmosphere walking over a timber bridge, especially, if it is covered. (*NATTERER, J. et al. 1991*)

Owing to the classification of timber as combustible material a widespread antipathy to timber constructions is common. It should be mentioned here that the fire properties of wood are perhaps the most misunderstood physical characteristics. In fact, heavy timber members "(…) provide a fire resistance comparable to, or greater than, that of other construction materials." In the case of a fire, a char layer is formed at the surface of the timber member which retards the heat penetration (Fig. 2.1). The unburned internal cross-section remains at a relatively low temperature. The depth of the char layer depends on the wood specie and on fire exposure conditions. But it means that in the event of fire the behavior of timber is resulting in slower failure compared to the one of unprotected steel. Important is the capacity of the remaining cross-section. (*RITTER, M.A. 1990*)

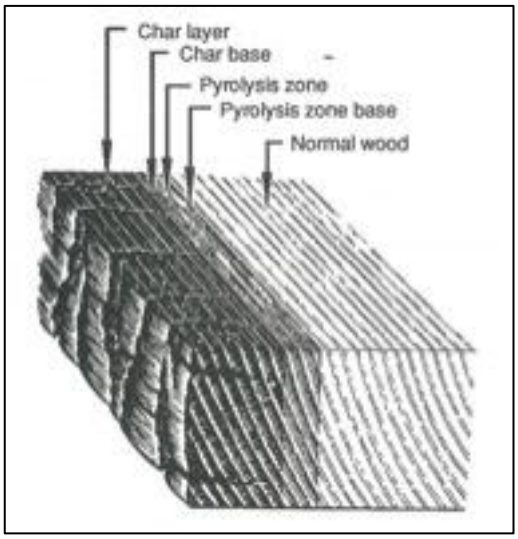

Figure 2.1 Degradation zones in a wood section exposed to fire (*RITTER, M.A. 1990*)

The most important physical property of wood is its very beneficial strength-to-weight ratio. In comparison to its density, wooden materials provide a very high strength. The following generated Table 2.1 demonstrates the density of reinforced concrete and steel in relation to the density of wood with a humidity of 20 percent. (*NATTERER, J. et al. 1991*)

Ratio	Material	Density
x 1	Timber	600 kg/m^3
x 4	reinforced concrete	2500 kg/m^3
x 10	Steel	7800 kg/m^3

Table 2.1 Densities of reinforced concrete and steel in relation to timber

Mechanical properties

Other materials may have in comparison higher strength values. The advantage of the beneficial strength-to-weight ratio of timber has to be evaluated in conjunction with the load-bearing capacities of timber. In fact, timber is not only the most light-weighted material compared to stone, reinforced concrete, cast iron or steel. It also bears considerable compressive and tensile stresses and, simultaneously, it is capable of transferring bending loads. Before the advent of steel no other construction material besides timber was so versatile. (*INFORMATIONSDIENST HOLZ 2000 (a)*)

Advantages during the manufacturing process

Another advantageous aspect is that wood is a closely available resource and that timber structures can easily be processed mechanically. Thanks to the simple workability and the light-weighted structure of timber, high levels of prefabrication, more simple constructions of foundation and relatively low transport and installation costs can be achieved. Consequently, the manufacturing proceeds under beneficial conditions for the environment. The process does consume no noteworthy amount of fossil energy. That is the reason why using timber includes "(…) very low embodied energy during manufacture" (*METTEM, C.J. 2011*).

Sustainability

Using timber structures has the unique feature to lock up substantial volumes of carbon. Timber can be classified as 'CO_2-positive' material. Of course, it is necessary to use 'CO_2-negative' materials in a certain amount. Such 'CO_2-negative' materials are steel or reinforced concrete and are used efficiently in the field of connection design or foundation construction. Constructing timber bridges does not mean neglecting the use of other materials in parts where they are much more suitable than timber. Because of this, the total result of a timber bridge project may not be totally 'carbon neutral', but "(…) it is likely to be significantly more benign than when structural timber is omitted" (*METTEM, C.J. 2011*).

However, timber structures give the opportunity of entering into a cycle of regeneration. Timber can be restructured and recycled easily. It is the only perpetually renewable material and can be used without any harm for the environment. Therefore, a sustainable management of forests and woodland is essential. (*METTEM, C.J. 2011*).

Summary

All mentioned benefits indicate that timber constructions are more related to nature and are more beneficial for the environment. They attract attention through their natural and aesthetically pleasing appearance, especially in natural surroundings. A very important aspect is the feature of sustainability.

In general, the sense of responsibility is growing and leads to an increasing awareness of the benefits of timber. As a reason, the aspect of building timber bridges is gaining more and more importance. (*INFORMATIONSDIENST HOLZ 2000 (a)*)

Matthias Gerold's book "Holzbruecken am Weg" is an impressing summary of the most interesting timber bridge constructions in Germany and Switzerland. The many examples are successfully in design and construction and make it clear that timber bridge constructions are not just caused by a short-dated trend. They demonstrate the gaining importance of timber bridge constructions, by now.

2.3 Classic types of timber bridges

Innovative materials and techniques extend the goal setting of bridges. Previously, climatic and topographic conditions influenced mostly the type of construction and raw materials were chosen depending on their domestic availability. Already centuries ago, architects and engineers started to include the idea of a cultural and aesthetically purpose instead of just having the functional purpose of the bridge project in mind. Bridges were not just crossing elements, any more. Expectations regarding the bridges' effect were set higher.

This is reflected in the development of different bridge types and configurations from early history through different historical periods till the present day. "Some of these bridges evolved from designs developed many years ago, while others have developed as a result of modern technological advances in timber design and fabrication." (*RITTER, M.A. 1990*)

The following rough summary of timber bridge types is not taking into account their exact chronological development. The aim of this subchapter is to classify through basic forms of structural arrangement. It should be mentioned that most of the timber bridges are hybrids of these highly simplified bridge types. The information has been taken out of the following references: *DTI & TRADA undated; METTEM, C.J. 2011*; *RITTER, M.A. 1990*; *SCHICKHOFER, G. 2000*; *SÉTRA 2006 (2007)*.

The visualizations of the basic forms have been used from reference *DTI & TRADA undated*.

Beams

Figure 2.2 Pedestrian and cyclist bridge over the Leinbach in Heilbronn, Germany (GEROLD, M. 2007)

Figure 2.3 Basic form: Beam

One of the first superstructures has been the beam (Fig. 2.2 and 2.3). It is the simplest and most common timber bridge type. A deck system is supported by several timber beams between two or more supports. The deck resists all applied loads.

Larger spans forced bridge builders to reach forward with the length. Multiple span and cantilever arrangements followed. In the absence of efficient joining systems, cantilevering is an instinctive method to shorten the span of the main structure.

The structure is restricted because of its limited spanning potential. Especially in the case of limited vertical clearance these bridge structures are useful and economical.

Arches

Figure 2.4 Pedestrian and cyclist bridge over the Wupper near Hueckeswagen, Germany (GEROLD, M. 2007)

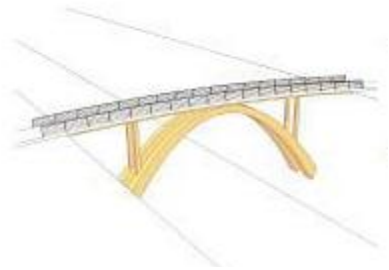

Figure 2.5 Basic form: Arch

A structure working mainly in axial compression is the arch. Especially with the development of glulam cross-sections, arched forms have been highly developed and became quite competitive.

Different variants are possible. A distinction is made between arches above the deck ("suspended deck", cf. Fig. 2.4) and arches below the deck ("standing deck", cf. Fig. 2.5).

Site and terrain or the wish of an architecturally commanding form can lead to an arched form. Larger spans than with beam structures are possible.

Trusses

Figure 2.6 Bridge over the Loisach near Garmisch-Partenkirchen, Germany (GEROLD, M. 2007)

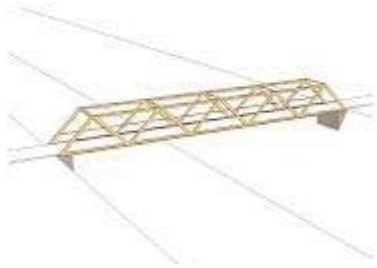

Figure 2.7 Basic form: Truss

The improvements in connection design led to effective node configurations which are also able to bear high tension. Trusses consist of straight members connected together in form of triangles (Fig. 2.6). The truss system minimizes the material consumption due to the fact that truss members are located where needed the most (Fig. 2.7).

Thanks to that, the truss bridge becomes a light-weighted and aesthetically attractive structure. With this modern structure greater load-carrying capacities and stiffness can be achieved than with simple beams. On the other hand, the large number of members and joints makes it more costly and more difficult to maintain. Still, the light-weighted and relatively small members bring advantages for transportation, prefabrication and erection.

Cable-stayed / Suspension bridges

Figure 2.8 Pedestrian and cyclist cable-stayed bridge over the Lahn near Limburg, Germany (GEROLD, M. 2007)

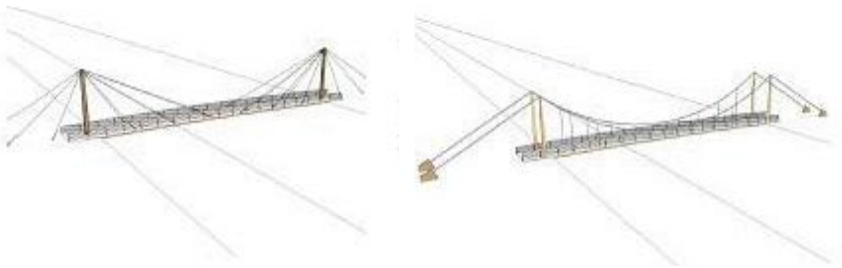

Figure 2.9 Basic forms: Cable-stayed and suspension bridge

Originally, a timber walkway has been supported by other natural materials to form a cable stayed bridge (Fig. 2.8 and 2.9 left). Nowadays, the support is ensured by abutments and flexible steel cables holding or suspending the timber deck structure (Fig. 2.9 right). These cables are connected to striking structures like pylons or towers. In that way, the timber deck can become slender and visually light.

With this efficient system long clear spans are possible. The whole cable arrangement needs a high vertical clearance. Therefore, these types are mostly used when other bridge types do not reach the required spans or the dramatically structure is in demand.

Note: The pedestrian bridge of the project “A Pilgrim’s Walk” has a span of approximately 80m.

2.4 General concepts of durability

During the last centuries, timber structures of all different bridge types demonstrated that they can last for many hundreds of years or only a few years. That experience makes it obvious that varying lifetimes depend on differences in design and details. No construction material lasts unendingly. It is important to have the knowledge about the right treatment. Also timber constructions are able to assure 100 years of lifespan if its characteristics are considered in the right way. (*INFORMATIONSDIENST HOLZ 2000 (c)*)

As already mentioned, it has always to be considered that using timber means to use a living building material. Wood is an organic material. Its natural decay is provoked by a long term moisture content of above 20%. Under the influence of permanent moisture wood grows sustainably, decays and retransforms into new nutrients in a closed circuit. In order to break this circuit, wood has to be dried and kept dry. Therefore, constructive solutions are needed to prevent damages by decay. By doing so, wooden constructions fulfill their function certainly and constantly during their lifetime. (*INFORMATIONSDIENST HOLZ 2000 (a)*)

Unfortunately, bridges are outdoor structures continuously subjected to the weather. The risk of humidity is particularly high. Wrong understanding and a lack of knowledge cause most likely damages in these structures. It is important to understand that under the influence of high moisture the loading resistance of timber decreases, while its deformations increase. The probability of an appearance of fungi or insects becomes more likely. As a consequence, uncontrollable shrinkage cracks, an increasing process of decay and a dramatic decrease of strength values can be observed.

The right treatment is able to prevent this process right from the start. In general, it must be ensured that the timber elements are manufactured and installed at appropriate initial moisture contents (exterior use: less than 20%). On this basis, improvements in the treatment of surfaces, the use of natural durable timber types and, especially, concepts of structural timber preservation assure the durability of timber structures.

The aim of structural timber preservation is to control the moisture penetration during the structure's lifetime by structural and constructive measures. The protective design seeks to avoid the concentration of moisture and organic matter as well as to assure a fast drainage and ventilation. That means as little water as possible should stay in the structure, the elements have to be able to drain off as fast as possible and air ventilation must be able to reach the structures' elements as much as possible. (*NATTERER, J. et al. 1996*)

Since the main principle of structural timber protection is to protect, above all, the key parts of the bridge construction from moisture, a structure of light-weighted elements can be used as protective layer of the main structure. This second structure does only serve to increase the lifespan of the load-bearing structure and can be replaced easily thanks to the easy workability of timber (cf. subchapter 2.2). "The concept is that the boarding will suffer deterioration first and can be replaced more easily than the principal structural members." (DTI & TRADA undated)

Examples of structural or constructive measures have been found in the following references: *INFORMATIONSDIENST HOLZ 2000 (c)*; *METTEM, C.J. 2011*; *NATTERER, J. et al. 1991*; *SÉTRA 2006 (2007)*. It will be focused on the most general methods.

- Precipitation has to be kept away from the key parts of the structure. Protruding edges of the roof help to keep the main elements dry under a rain falling and should have an angle of shelter of 30 degrees to the vertical (Fig. 2.10).

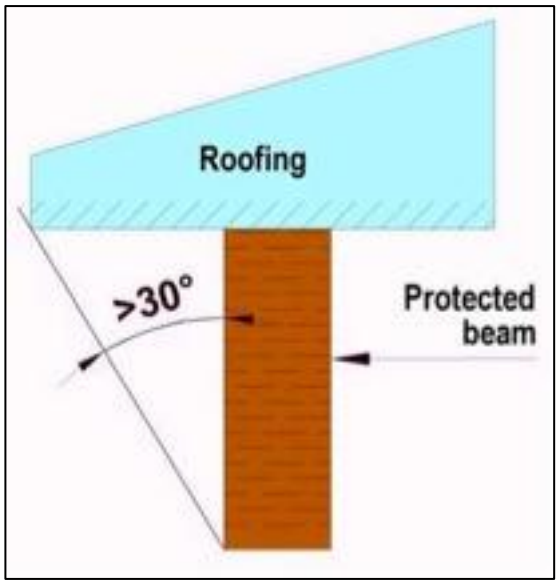

Figure 2.10 Angle to protect a beam of the main structure (SÉTRA 2006 (2007))

- Standing water on timber parts has to be limited. Through appropriate inclination horizontal surfaces can be avoided and an accumulation of water or humidity can be eliminated.
- Especially the main timber parts should remain unhidden in order to assure a better control during the maintenance.
- The second structure protects the main structure in the form of claddings. Protective layers can be wooden boarding for lateral faces as well as metal covers and concrete or masonry surfaces for horizontal surfaces (Fig. 2.11).

- A very important aspect of timber preservation is to protect the end grain of planks or beams in order to avoid water absorption in the fibers of the wood. This direct absorption can be inhibited by shielding with more resistant edge grain of other members, by efficient ventilation or also by cover plates (Fig. 2.12).

Figure 2.11 Beams protected under roadway (SÉTRA 2006 (2007))

Figure 2.12 Protected horizontal beam (INFORMATIONSDIENST HOLZ 2000 (c))

- The direct contact of timber with organic matter or dirt has to be prevented. Assuring a certain distance to the ground also protects from the penetration of spraying water. Ground clearances of at least 30cm are highly commended (Fig. 2.13).
- To avoid rising ground damp, concrete foundations are required (Fig. 2.13).

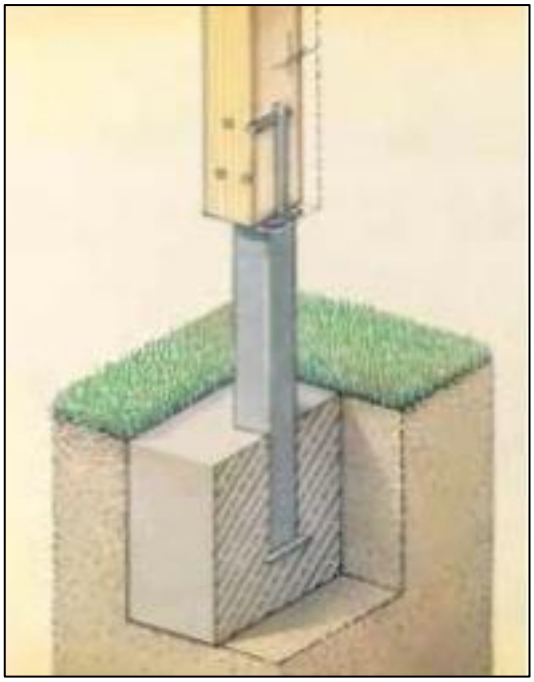

Figure 2.13 Design of column base with square tube: certain ground clearance and concrete foundation are shown (INFORMATIONSDIENST HOLZ 2000 (c))

- In the field of connection design minimized surface of contact, round and convex surfaces and the avoidance of continuous metal work are required to ensure a better drainage. Structural timber protection does not mean that the contact with water has to be avoided totally. The important aspect is giving the possibility of drying out again. For this reason, the key parts need to have a contact surface with other elements as minimized as possible (Fig. 2.14 and 2.15).

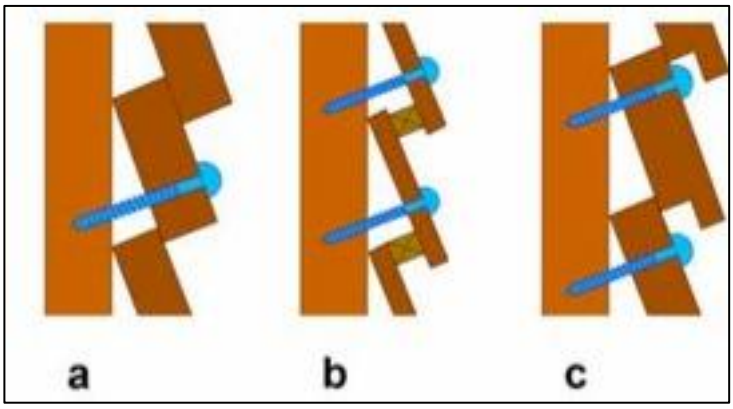

Figure 2.14 Boarding arrangements: a) badly ventilated, no drip groove; b) well ventilated, with drop groove; c) as b) with well protected fixings (SÉTRA 2006 (2007))

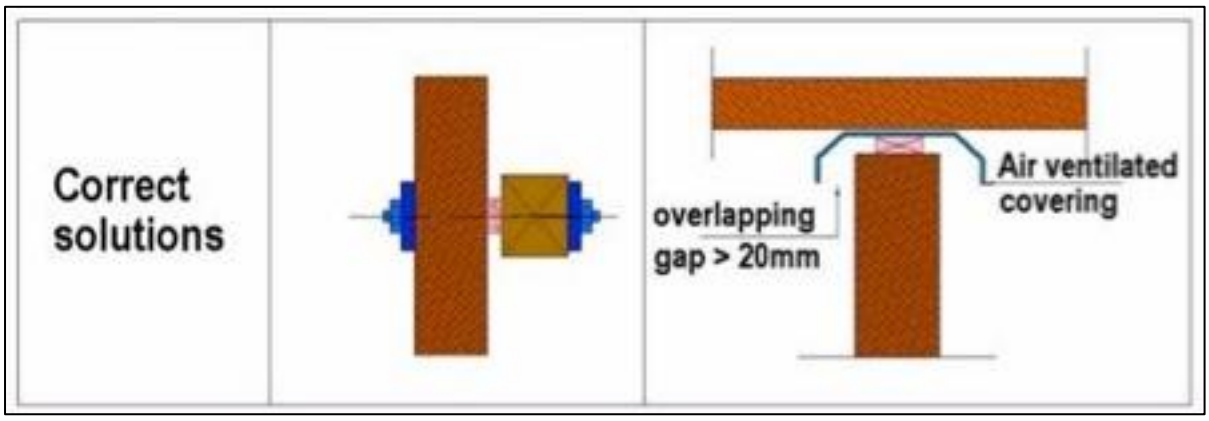

Figure 2.15 Ventilation in connections: minimized surface of contact, spacing the wood pieces sufficiently (SÉTRA 2006 (2007))

Thanks to the improvements in design and details, there is no longer any distinction needed between timber bridges "without protective roof" and "with protective roof". It seems more useful to differentiate between "unprotected" and "protected" timber bridges. That means, a bridge does not need to have a roof to be called "protected" but it has to be differentiated between a bridge with or without protective measures. (*GEROLD, M. 2006*)

In case of real moisture damage caused by fungi or insects, chemical or biological preventive measures can be considered. But in fact, chemical protection should be avoided as much as possible from the ecological point of view. Using only chemical protective measures is not

efficient enough to obtain a reasonable durability. In the long term, higher costs of maintenance and in the case of decay a complete rehabilitation have to be considered. Designing and detailing carefully as well as the choice of durable timbers for exposed applications reduce reliance upon chemical preservatives. The exchange of certain parts is often easier and in the long run more efficient. (*cf. INFORMATIONSDIENST HOLZ 2000 (b)*; *METTEM, C.J. 2011; NATTERER, J. et al. 1991*)

In summary, there are three strategies of efficiently protecting the wood from decay: either using very durable timber species or using treated timber with moderate covering or using less durable species in combination with thorough covering and cladding screening. Good ventilation and drainage is necessary in all cases. (*METTEM, C.J. 2011*) Using durable timber species is a very useful addition to the design. Chemical preventives contain toxic substances and should be avoided. The best way of assuring a long term protection is the strategy of using structural and constructive measures to protect the main structure. By doing so, well protected timber bridges evince low costs of maintenance like comparable constructions built out of other building materials. (*INFORMATIONSDIENST HOLZ 2000 (a)*)

The Eurocode 5 fixes the minimum lifespan of timber bridges at 100 years; 25 years for replaceable elements. Contrary to many prejudices, long life spans can be assured with the help of the right protection strategy. Evidences can be found especially in Alpine countries. An example is shown in Figure 2.16: the 1333 constructed Chapel Bridge in Luzern. The embedded wooden piles of this bridge remain undegenerated until today.

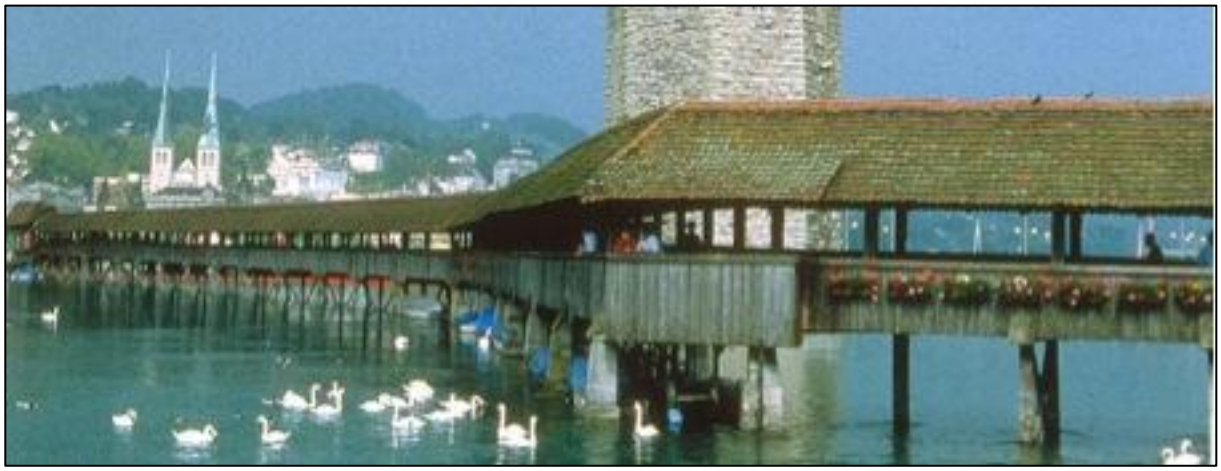

Figure 2.16 Chapel Bridge over the Reuss in Luzern, Switzerland (GEROLD, M. 2007)

2.5 Future of timber bridge constructions

It became obvious that timber is an interesting alternative for the construction of challenging bridge concepts. Besides its wide range of possibilities in design, it is an environmentally friendly material. Timber bridges demonstrate to have an efficient supporting structure (*SCHICKHOFER, G. 2000*) what makes the construction of timber structures more than just an aesthetic option. The right treatment in form of particular design and structural preservation assures the durability of this material.

A growing sense of responsibility and a high level of environmental awareness encourages using this unique growing material. Using timber in constructions helps attaining a neutral carbon balance. In future projects it should be achievable to compensate the "CO_2-negative" effect of materials like concrete by adding the "CO_2-positive" material timber (*METTEM, C.J. 2011*).

Solutions should include timber as an alternative and a complement to other building materials (*INFORMATIONSDIENST HOLZ 2000 (b)*). All materials have different properties and can help to improve the capacity of the structure. An association of timber with other materials in form of reasonable composites constructions has to be achieved. Therefore, each material has to be used in its preferred field. Concrete is an advantageous material when its high compressive strength is in demand and if it is needed to protect timber from penetration or organic matter. Steel has excellent tensile characteristics and makes it possible to increase enormously spans and width of timber deck structures. (*SÉTRA 2006 (2007)*)

All in all, timber has continued to be economically and structurally competitive with other bridge materials. Improvements in the field of connection design and the development of structural timber composites, in particular glulam, made timber constructions economically and statically efficient. Over the last decades, big improvements in the field of structural timber preservation added benefits regarding life-cycle costs. Thanks to right treatments regarding the design and the following maintenance, properly designed timber bridges have been built demonstrating a good performance and long service lives (*RITTER, M.A. 1990*).

3. Joining the project “A Pilgrim’s Walk”

3.1 Description of the pedestrian timber bridge project

During the year 2012, Daniel Asp a student at the Chalmers University of Technology is writing his master thesis in Gothenburg. His thesis includes both architecture and engineering and is going to last for a period of one year. The task of this double master thesis is to design a wooden pedestrian bridge at Borgeby Castle outside of Lomma in the south of Sweden. The town Lomma is located 10 km away from Lund, in the Swedish province Scania.

The bridge’s aim will be to connect two historical sites of this area, to make them part of the pilgrimage route of Scania and to add this new pilgrim walk to the European pilgrim network, including the Way of Saint James.

3.2 Historical background and location of the bridge

The Way of Saint James unites many old pilgrimage routes all over Europe to one important pilgrim stream (Fig. 3.1), which leads to the destination city Santiago de Compostela in the northwest of Spain (*CAMINO DE SANTIAGO 08/04/2012*).

Figure 3.1Pilgrim path network of Europe (CAMINOS DE EUROPA 08/04/2012)

In Northern Europe the connection point to Santiago de Compostela is located in the Norwegian city Trondheim. In Trondheim the Nidaros Cathedral is the center of the Scandinavian network of many remnant pilgrim ways of Denmark, Sweden and Norway (*TRONDHEIM 08/04/2012*).

The connection of these two important European locations could be expanded in the future by a developed route through Scania in Southern Sweden. Next to Lomma near the old city Lund lays the Castle Borgeby. The addition of footpaths in this area could give pilgrims the opportunity to pass by the castle on their journey. A new pilgrim route could be the result of this expansion.

Originally a pilgrim walk has been a spiritual action in the direction of a sacred place in order to gain divine help or to achieve absolution from sins. People all over Europe started their journey at their local church and hoped to find on their way forgiveness, answers or a sign of god. Nowadays, the real movement's pattern can be another kind. Enjoying nature, peace and historical leftovers can be the motivation for a pilgrim journey. Near Lomma around Borgeby a pilgrim experiences southern Swedish nature and history.

Since the history of Southern Sweden is influenced not only by Sweden but also by Denmark, it has many old reminders of this double influence.

Being burned in 1452 by the Swedes and in 1658 by the Danes, Borgeby Castle has been characterized by different time periods. Today the main parts are Börjes Tower standing alone after the demolition of the eastern wing in 1860, the main building built between 1650 and 1660 as well as the stables built of bricks in 1744 (*BORGEBY CASTLE 09/04/2012*).

Figure 3.2 Photos of stables (left) and Börjes Tower (right)

The castle lies about 100 meters aside the largest river in Scania, Kävlingeån. It is surrounded by a line of trees on the southern side of the river and by large fields on the northern side. Nearby the castle on each side of the river two churches are to be found, buildings of particular interest for pilgrims. Until now, the two churches and the castle are only connected

by street. Nevertheless, footpaths through the fields parallel to the street would end at the river. There is no possibility to cross the river.

Not only for visitors but also for local people it could be important to develop the infrastructure. With all the historic background a lot of activities like medieval markets and tourney games, cultural festivals or workshops are taken place in the area. Today the castle is under a preservation order and one of the stables became a museum for the paintings of the artist Ernst Nordlind (*BORGEBY CASTLE 09/04/2012*). All these cultural activities do not cooperate with each other since there is no connection between the two sides of the river.

The following figure is a photomontage made by Daniel Asp to show this splitting of locations and events. The white lines are the streets combining the castle (middle square) with Lomma in the north.

Figure 3.3 Photomontage showing the split locations and events (by Daniel Asp)

The development of the area around Borgeby Castle could be enriching for Scania's cultural offer and worthwhile for Scania's connecting to the Way of Saint James. The castle itself is well connected to the infrastructure of South Sweden including the airports of Copenhagen and Malmö and offers a beautiful stay with restaurant, café and accommodation.

The creation of a new footpath as alternative to the streets through fields and nature and over a bridge to the historic monuments located near Lomma is the aim of the project "A Pilgrim's Walk".

3.3 Architectural work of the Chalmers' student Daniel Asp

3.3.1 Aims and objectives

The essential part of this "Pilgrim's Walk" represents a bridge which is able to link the two sides of the river stronger together and is able to make the area available for pilgrims, inhabitants, visitors, in short for pedestrians.

In the following map (Fig. 3.4) Daniel Asp has outlined the bridge's function in the "Pilgrim's Walk" (blue path) and between the two churches (black crosses).

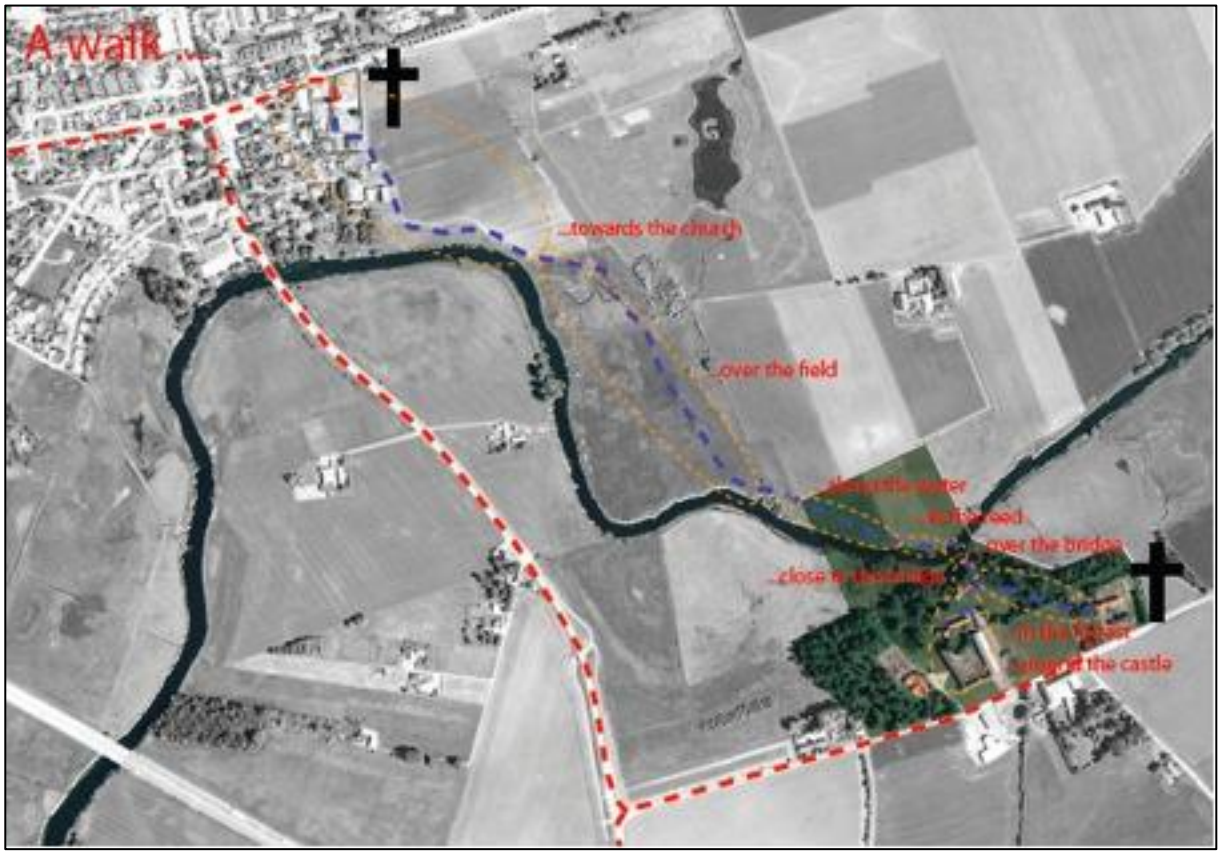

Figure 3.4 Functional allocation of the footpath "A Pilgrim's Walk" (by Daniel Asp)

Until the beginning of May he developed in the architectural part of his master thesis the impact on the site and, as a result, a concept for the project. As he explained in one meeting, the bridge should be able to stand out and, at the same time, not overpower its context. The new bridge should revalue this pilgrim walk but not upstage the historical background.

In order to develop a good concept it is important to understand the surrounding of the site. Flat landscape, small forests, rough big fields and sunny summers characterize the Southern Swedish countryside. In this project one aim is to save the relation to the surrounding nature. Consequently, an aesthetically pleasant pedestrian bridge made out of the natural material wood would fit well in the context.

Not only the landscape but also the historical background needs to be considered. Next to the bridge the church and the castle are located, both buildings with strong and historic character. The wooden bridge's design needs to be adapted to these striking buildings of the site.

However, the bridge is expected to keep its own identity. That means it invites to explore the two sides of the river as well as it serves as an attention-getter. In my eyes, that is a nice purpose for this pedestrian bridge.

In the end, one more objective has been added. Another task for the bridge is to give the possibility of experiencing the landscape in a new way. Pedestrians should feel the connection to the nature while walking over the bridge. In the same way, they should be intrigued to interrupt their crossing and to look consciously at the surroundings.

In summary, Daniel Asp wants the bridge to be an element of completion as well as of independence. It should match with the strong materiality of the nature and the historic monuments as well as it should attract attention. In this context and the fact that it will serve as a pedestrian bridge, I think a timber bridge seems a good choice. Furthermore, a final task of the bridge will be not only to make it possible to cross the river but also to be enriching for experiencing the region.

3.3.2 Design process

After having analyzed the historical background, the site and the objectives of the bridge, the design will be presented as an iterative process from different possibilities and ideas to the most promising option. It is important to examine the object from different points of view in order to reach the best final design. Following the aims of the project the discussion topics are view, accessibility, movement, impact on the site and perception of the bridge.

These topics help most of all to discuss an important aspect: the position of the bridge.

A high value was attached to the saving of the panoramic view. Visitors should not just cross the bridge and forget about their surroundings. To experience the area in the best way, we decided that Daniel Asp's idea of a change of direction on the way over the bridge should be kept. That means, if you are walking for example in direction of the fields, you will experience a little turn halfway. In this way, the pedestrians pay first particular attention to the upcoming objects, in this example the fields, and afterwards to the passed objects, in this example the castle and the little forest on the southern riverside. We both agreed that this turn would enhance the crossing's attractiveness enormously.

The connection to the water is a natural aspect if it comes to bridges. In some way, it is not always considered, with the result that people crossing the bridge do not feel connected to the element they are passing, the water. In order to prevent this, Daniel Asp wanted to make the north end of the bridge parallel to the riverbank and keep a height clearance that is high enough to walk under the construction. This should give people the possibility to be lingering, fishing and boating around and below the bridge.

The aspects of the view and the connection to the water make it obvious that visitors are expected to memorize what they see and to remember what they experience on their visit of the region.

Besides these more static topics, the movement between the different objects of the site is another interesting topic. The paths through the fields do not exist, yet, so that they can be adapted to the vision of a walk parallel to the riverbank. Between the castle and the church on the south side some paths already exist. This connection should not be disturbed by an element in the middle, the bridge.

Figure 3.5 Panorama photo of the site looking in direction of the northern riverside (by Daniel Asp); the approximate location of the bridge is outlined by the red circle

Three alternatives regarding the location of the bridge are presented. In these three alternatives the southern bridge end between castle and church and the bridge position's impact on the site has to be discussed. In doing so, it should be taken into account that no object of the site is neglected during the consideration.

In the following Figures 3.6, 3.7 and 3.8, the three alternatives are presented by showing the location of each alternative in sectional view and top view. The buildings sketched in various perspectives demonstrate the Börjes Tower, the main building and the stables of Borgeby Castle. The dashed lines depict the footpaths on the south riverside. The two connection points of each alternative stretch a different length over the river; from 70m for Alternative AA to 45m for Alternative CC. The two connection points have in no alternative a height difference higher than 5m. The drawings shall visualize only roughly the different

possibilities of the bridge's localization at a scale of about 1:2000. The information and the drawings of the sectional views were provided by Daniel Asp.

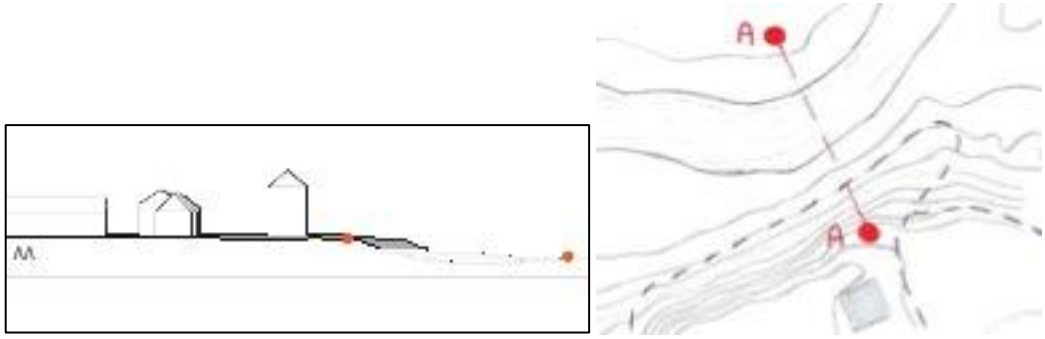

Figure 3.6 Sectional view and top view of Alternative A

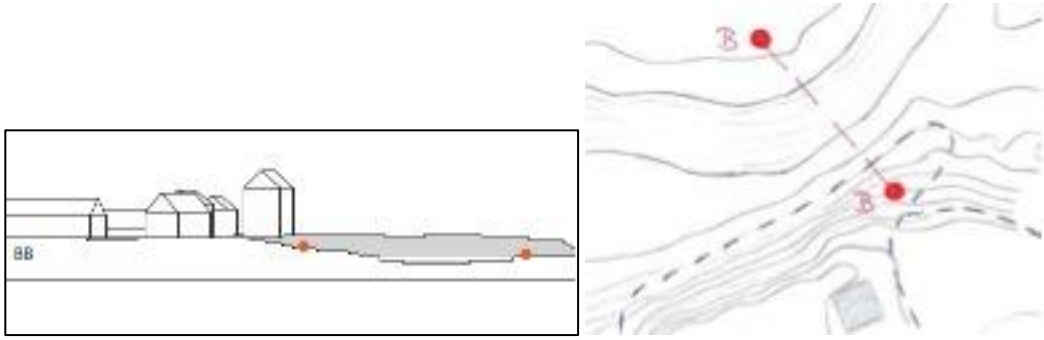

Figure 3.7 Sectional view and top view of Alternative B

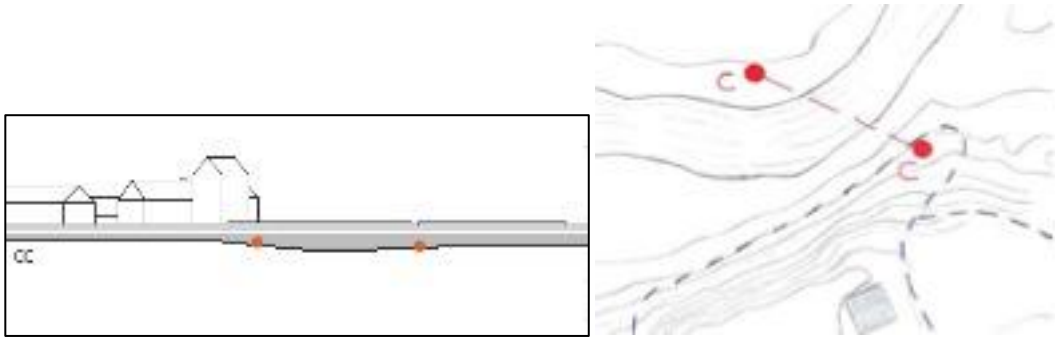

Figure 3.8 Sectional view and top view of Alternative C

All three alternatives have their advantages: Version A gives the major height clearance, Version B lies at the connection point of the paths between castle and church and Version C has the best connection to the water. However, lying so near to the castle Version A could overpower the site and lying at the end of the slope Version C could lose the connection to its surrounding buildings.

These were the aspects Daniel Asp outlined in a meeting with his supervisors Karl-Gunnar Olsson, Professor at Chalmers University of Technology, and Professor Roberto Crocetti in early March. I was able to participate in this meeting and to visit, at the same time, the site.

All of us have been in agreement that with these aspects in mind Version B seems like the best compromise among the alternatives.

Furthermore, Version B accomplishes the topic of the perception of the bridge in the best way. Being not too far away from the castle the bridge can be seen from the viewpoint at the top of the slope and arouses, in this way, anticipation about crossing the bridge to the other riverside. Simultaneously, having a certain distance to the buildings the bridge tries not to overpower the site. This leads again to the central object illustrated in the last chapter: the right balance between completion and independence.

All in all, the most important decisions to define the bridge's system lines have been described in this chapter. In summary, the bridge has a change of direction, starts halfway of the slope at the connection point of the buildings laying on the south riverside and ends in direction of the fields.

3.3.3 Final project proposals

At the meeting in early March the professors helped Daniel Asp to choose three final project proposals. He had tried out a lot of different concepts, always having in mind the objects and the chosen main material of this pedestrian bridge. On the day of the meeting three final proposals have been picked out of all his suggestions.

Concept 1: Cable supported single-span girder with a suspended deck

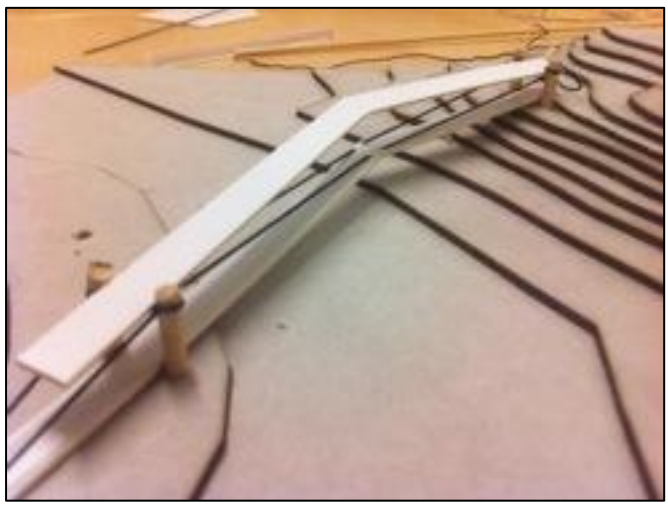

Figure 3.9 Model of Concept 1 modeled by Daniel Asp (view towards south riverside/castle)

Concept 1 (Fig. 3.9) is the simplest of all concepts. The structural system of this roofed bridge concept is in fact a single-span girder supported by cables. The deck works as a plate and is suspended by a tension cable system. These cables are connected to the main restraints, the

four pylons, at the ends of the bridge. The roof rests mainly on these pylons, which lead the vertical and horizontal loads from the roof down to the abutment. The roof should also be supported along the length by several columns, which prevent the roof from buckling and connect the roof with the bridge deck. The roof protects the deck and acts as stiffening system.

The simple design, construction and erection make this variant economically attractive.

Concept 2: One-curved suspension bridge

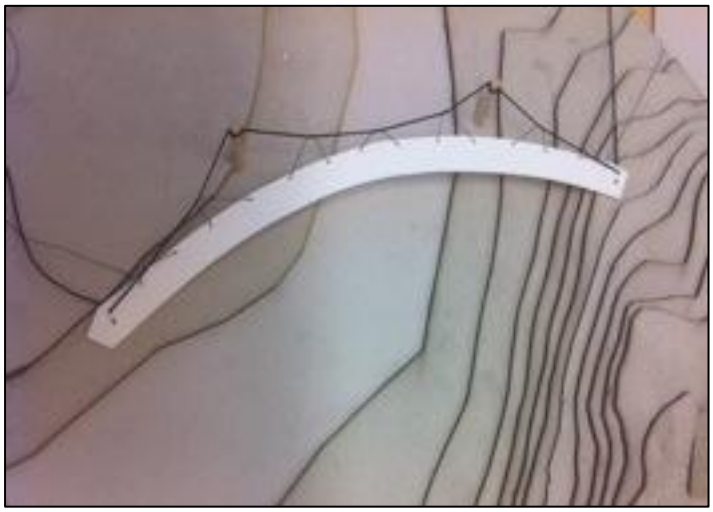

Figure 3.10 Model of Concept 2 modeled by Daniel Asp (castle located on the right side of the picture)

In the second concept tension cables suspend the deck of the bridge (Fig. 3.10). Thanks to the curvature of the deck the suspension is needed only along one side of the bridge. The same concept with a straight deck would be instable and tip sideways. The static structure of this curved deck will be explained more in detail in chapter 4. In chapter 4 the advantage of locating the suspension cables on the outer edge of the deck, in other words, on the edge with the bigger curvature will be outlined from the static point of view.

On the whole, the curved shape has not only the benefit of being aesthetically of interest but also of giving a more unobstructed view. This creates a feeling of openness encouraging pedestrians to look around perhaps more observantly. As already described in chapter 3.3.2, the attention should turn from the upcoming to the passed objects which is another reason for locating the suspension cables on the outer edge of the deck. In this way, the view goes unobstructed in direction of the castle and the path through the fields.

The unusual design and the obvious turn of direction make this variant aesthetically attractive.

Concept 3: Two-curved suspension bridge

Figure 3.11 Model of Concept 3 modeled by Daniel Asp (view towards south riverside/castle)

The only difference to Concept 2 is the more obvious change of direction thanks to the more rough shape. Actually this rough shape should be outlined by a two-curved deck. In Figure 3.11 the concept of a two-curved suspension bridge is still not pointed out well. Daniel Asp developed this aspect further in his final design process. At the end of this development he outlined the break on the bridge with a change of curvature at the middle of the deck. In the following rendering (Fig. 3.12) the final design for his presentation of the architectural thesis part is shown.

The specific turn of direction makes this concept aesthetically attractive. The double curvature makes it interesting for the static point of view. That is the reason why both of us decided to work with Concept 3, the two-curved suspension bridge.

Figure 3.12 Rendering of the two-curved suspension concept made by Daniel Asp (view towards south riverside)

4. Understanding the statics of a curved suspension bridge

4.1 Summary of the approach

A good way to understand the statics of a more complex structure is to start with a simpler example. By starting from basic examples this chapter ought to help to understand the statics of a curved suspension bridge. The sketches are made by hand and serve to roughly emphasize the most important details.

In the first step, the analysis' beginning is made by the example of the simple bending beam. The suspension is disregarded. Just the curved deck is of interest. As a result, a curved beam will be compared with its straight equivalent. Which effects does the curvature generate? What kind of section forces can be observed?

In the second step, different simple models are presented to show how the visualization of the section forces of a curved beam suspended along one edge can be developed. In order to model, some software was needed. Therefore, the finite element program SAP was used to demonstrate the distribution of forces in the system.

Since the curved bridge is not just restrained at its ends like a simply supported beam on two supports but is suspended along one edge by several cables, the influence of this suspension has to be considered. To simplify the demonstration of this influence the suspension is simulated at first by fixed restraints along the edge. It would be closer to reality to replace them by springs. However, to analyze the general behavior of the deck this simplification seems sufficient. Afterwards a look is taken at the impact of the angled suspension cables. During the last steps, it is becoming increasingly evident that the decision about an inner or an outer edge suspension has an important role to play.

At the end of the chapter, a bridge that is located in the "Deutsches Museum" in Munich since May 7 1998 is taken as a real example in the field of curved suspension bridges. This bridge demonstrates the concept of the inner edge suspension and was designed by Schlaich, Bergermann and Partners, Stuttgart, Germany (*DEUTSCHES MUSEUM et al. 1999*).

Finally, it is explained why the concept of the outer edge suspension is used in the case of the "A Pilgrim's Walk" Bridge. In this way, the project's advantage of positioning the suspension cables on the outer edge of the deck is outlined from the static point of view after it has been outlined from the architectural point of view in subchapter 3.3.3.

4.2 Derivation of the section forces of a curved beam

At first, a look is taken on a straight single-span beam loaded with a distributed load in gravity direction and supported with simple restraints at its ends (Fig. 4.1). This system gives the typical section force results of a bending beam. The moment has a maximum value in the middle of the span where at the same time the shear force is zero. The load distribution occurs just two-dimensional.

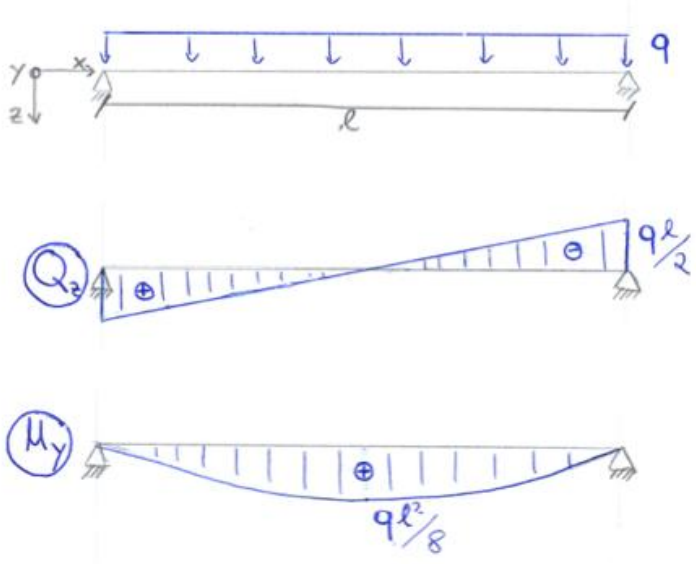

Figure 4.1 Section forces of the bending beam

Giving the beam a certain curvature determined by the angle α and the radius R the load distribution has to be analyzed now from the three-dimensional point of view (Fig. 4.2 and 4.3).

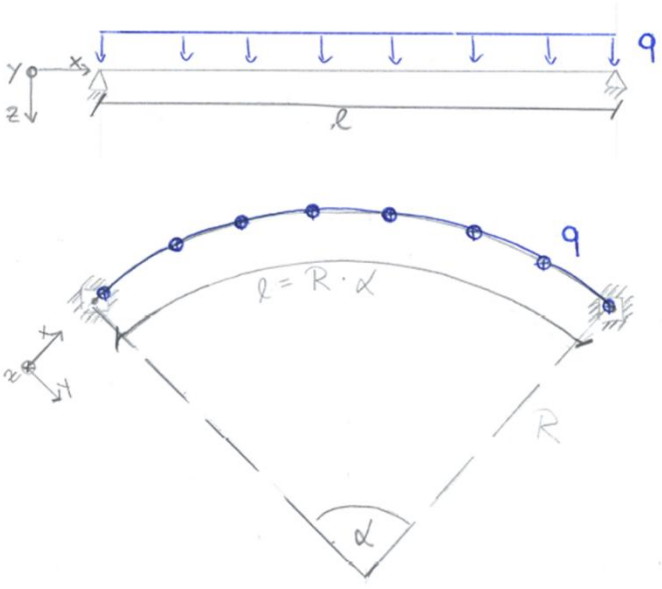

Figure 4.2 System of the curved beam (top view)

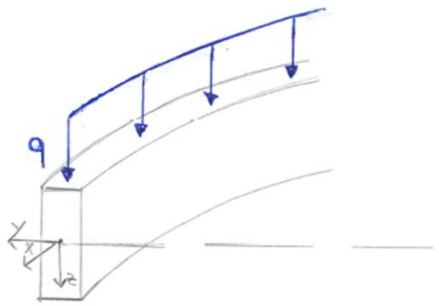

Figure 4.3 Three dimensional sketch of the cross-section

The line load q is distributed over the length l, which is the radian measure of the angle α and the radius R.

$$l = R \cdot \alpha \tag{4.2.1}$$

In direction parallel to the beam the bending moment M_y creates a deflection of the structure and can be divided into a compression force C and a tension force T (Fig. 4.4). The magnitude of this bending moment depends on the vertical line load q, which itself depends on the beam's load method and the beam's width b.

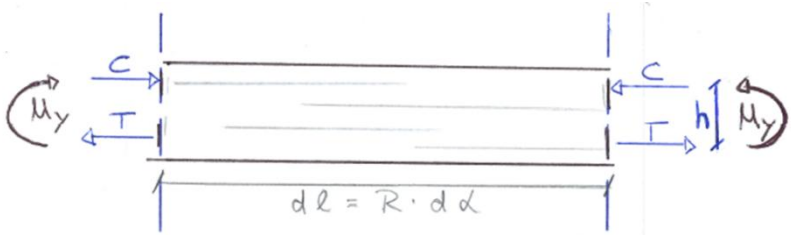

Figure 4.4 Division of bending moment M_y in compression C and tension T

$$C = T = \frac{M_y}{\square} \tag{4.2.2}$$

$$M_y = f(q) \tag{4.2.3}$$

A new feature is that the distributed line load has an influence on the vertical and the radial force progression. Thanks to the curvature the compression component C and the tension component T of the bending moment M_y can be split into axial and radial force components. The former are in charge of the beam's deflection, further on. The latter cause radial resulting forces H_R. These radial resultant forces, in turn, distribute a uniformly line load q_R over the length l (Fig. 4.5).

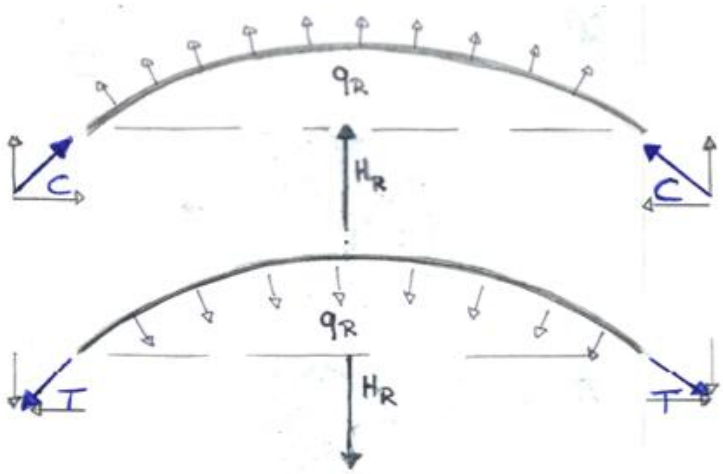

Figure 4.5 Distribution of a uniformly line load q_R

The caused radial forces of the curved beam can be illustrated more in detail using a beam element with the length dl (Fig. 4.6).

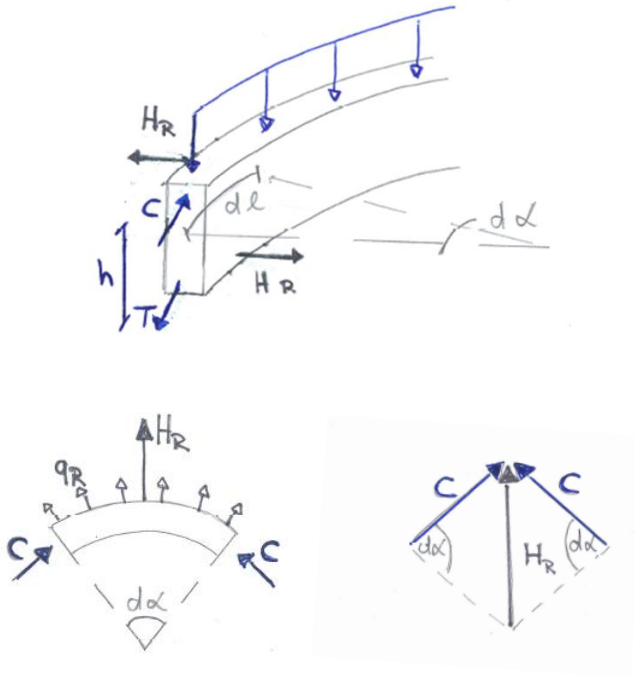

Figure 4.6 Sketches about the curved beam element with the length dl

It is obvious, that the radial resultant forces H_R depend totally on the curvature's angle α. Is the angle α=0°, then we have again the case of the straight beam and compression C and tension T have no radial force components, respectively, no radial forces are caused.

In the case of α≠0° the following equations are valid.

According to equation (4.1.1):

$$dl = R \cdot d\alpha \tag{4.2.4}$$

Considering Figure 4.6:

$$H_R = q_R \cdot dl \tag{4.2.5}$$

$$H_R = 2 \cdot C \cdot sin\frac{d\alpha}{2} \tag{4.2.6}$$

In the case of $\alpha << 1$ is $\sin\alpha \approx \alpha$. As a consequence and with use of equation (4.2.4):

$$H_R \approx 2 \cdot C \cdot \frac{d\alpha}{2} = C \cdot d\alpha = C \cdot \frac{dl}{R} \tag{4.2.7}$$

(4.1.5) equated with (4.1.7):

$$q_R \cdot dl = C \cdot \frac{dl}{R} \tag{4.2.8}$$

Solving the equation for the radial force q_R:

$$\boxed{q_R = \frac{C}{R}} \tag{4.2.9}$$

Taking again a look on Figure 4.6, it is evident that these radial loads q_R generate along the beam an uniformly distributed torsion moment with the lever arm h.

$$m_t = q_R \cdot \square = \frac{C}{R} \cdot \square = \frac{C \cdot \square}{R} = \frac{M_y}{R} \tag{4.2.10}$$

Finally, the effects of the curvature are derived. Compared to the former example of the straight beam, a torsion moment is caused along the whole length of the curved beam. Reflecting, this torsion could be the reason for the feeling of insecurity when one looks at the curved structure that is supported only by simple restraints at its ends.

In sum, the following additional section forces can be observed in comparison with the classical straight bending beam.

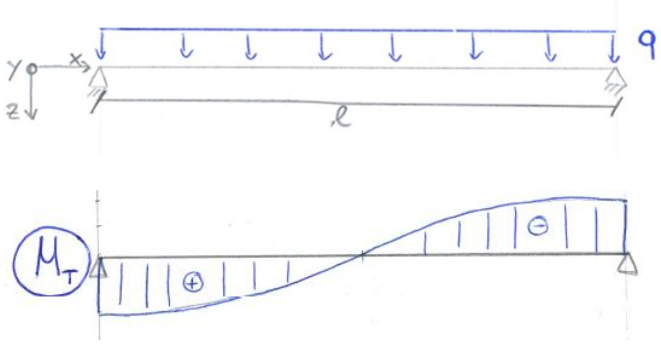

Figure 4.7 Additional section forces of a curved beam (frontal view) in addition to Figure's 4.1 section forces

4.3 Distribution of the system forces: Using the Software SAP

In order to visualize the section forces some software was needed. Therefore, the finite element program SAP was used to demonstrate the distribution of forces in the system.

4.3.1 General Information about SAP2000 v.14

Since the structure of the curved deck stands for a more complex system, the use of a finite element program seems to be very useful to analyze the complex structure of a curved suspension bridge.

SAP 2000 is a common structural FE-program. It is able to analyze most structural cases from a simple 2D bending beam case to a more complex 3D nonlinear case. The use of SAP 2000 meant getting to know a new, more international program and practicing to model with its help from beginner examples to the final structure of the thesis' bridge. In this thesis SAP 2000 version 14 has been used.

4.3.2 Limitations of the program

Although the program is relatively easy to use, at the same time, it has a couple of disadvantages.

SAP 2000 already has some predefined materials like steel and concrete and is able to change easily the material settings for these materials. However, it does not have any predefined settings for timber materials. To define a new material like timber it is only possible to define the modulus of elasticity and its density but not its strength capacities. Due to the fact that for this thesis the program is only needed to provide the section forces of the system and not to design the structure, this limitation is no significant problem.

To take into account that the suspension cables cannot take any compressive forces it is necessary to use a static nonlinear model. This can be considered easily when defining the load cases for the calculation.

4.4 Analyzing the effects of the suspension

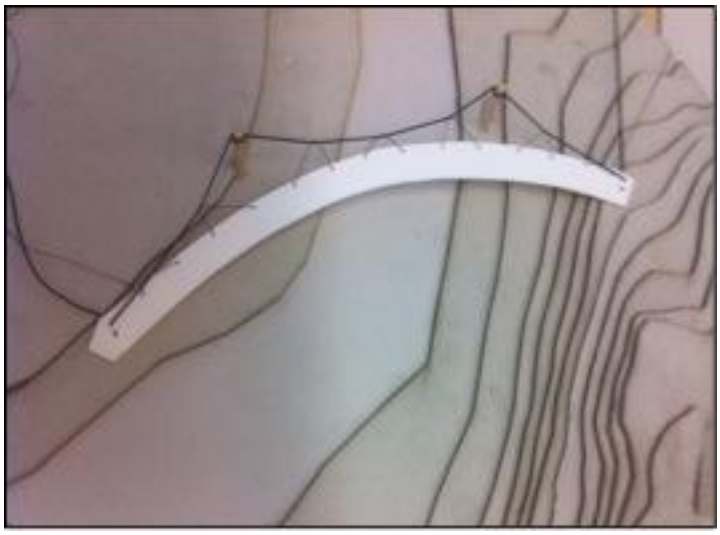

Figure 4.8 Model of the one-curved suspension bridge (by Daniel Asp)

In the next step the influence of the suspension will be analyzed. Figure 4.8 shows one of the former models Daniel Asp has worked out in his architectural thesis, outlined in chapter 3. Since the curved bridge is not just restrained at its ends like a simply supported beam but is suspended along one edge by several cables, fixed restraints along one edge will demonstrate the influence of this suspension. It would be closer to reality to replace them by springs. However, to analyze the general behavior of the deck this simplification seems sufficient.

Supporting a straight deck only along one edge, it would turn to the side. A support along both edges or a rigid clamping along one edge would be needed to stabilize the system. Compared to its straight equivalent the restraints of a curved deck do not lie all on one line. Thanks to its curvature it is sufficiently supported along one edge; the inner or the outer edge.

That means always one edge of the deck will be supported linearly. This linear support prevents the former deflection of the deck explained in subchapter 4.2.

The section force analysis of this suspended deck is of interest. In the following examples a system of beam elements will be compared to a system of shell elements. Further on, both systems will be compared to each other as well as the location of the linear support will be analyzed.

4.4.1 Basics of the models

In the following examples the same basic geometry has been used. This geometry has been settled, with reference to the Schlaich Bridge of the "Deutsches Museum" mentioned in subchapter 4.1. A circular segment simulates the structure of the curved deck. At the beginning, a circular segment has been defined and chosen to be the inner edge of the deck. The outer edge is determined by the deck's width. On half way lies the structure's system line characterized by a certain length. Therefore, the following system parameters have been chosen (Fig. 4.9).

- The chord of the circular segment: s = 30m → The radius: R = 25m
- The height of the circular segment: h = 5m → The angle α = 73,74°
- The width of the deck: b = 3m → The length of the deck: l = 34,11m
- The thickness of the deck: d = 0,20m

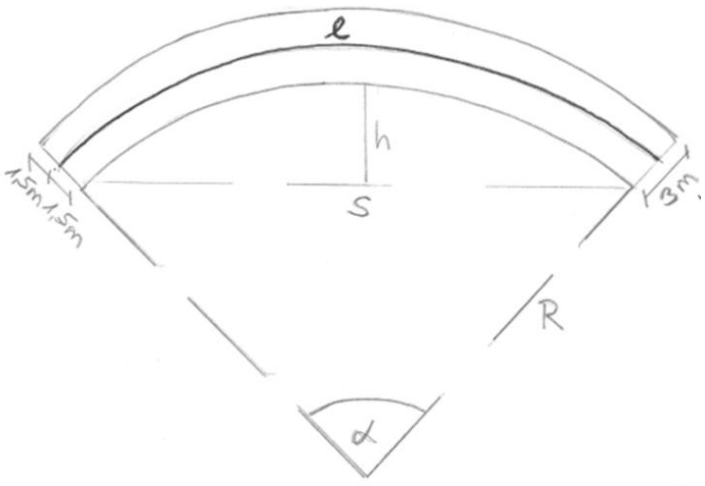

Figure 4.9 Draft of the basic circular segment

Always one edge of the deck will be supported linearly. Therefore, the whole circular segment has been divided into ten equal parts to draw the deck step by step along the curvature. Because of these ten circular parts, 10 fixed restraints will be situated uniformly along the inner or the outer edge as a replacement for the suspension cables.

For these general analyses steel will be defined for the whole structure.

To simulate the self-weight of the deck a distributed dead load q will be assigned along the system line. Hence, defining the load patterns the self-weight multiplier will be set to zero.

$$q = \gamma \cdot b \cdot d = 76{,}97\,\frac{kN}{m^3} \cdot 3m \cdot 0{,}20m = 46{,}18\,\frac{kN}{m} \approx 45\,\frac{kN}{m} \qquad (4.4.1)$$

Where: $\gamma = 76{,}97\,\frac{kN}{m^3}$ density of steel

4.4.2 Modeling the deck with beam elements

In the first example the deck is modeled with beam elements. The beams are located along the system line. Their width and height are chosen according to the assumptions in subchapter 4.4.1. Since a connection was needed between the beam elements and the supports, rigid elements, which have a higher modulus of elasticity than steel and a density set to zero, are used as connectors.

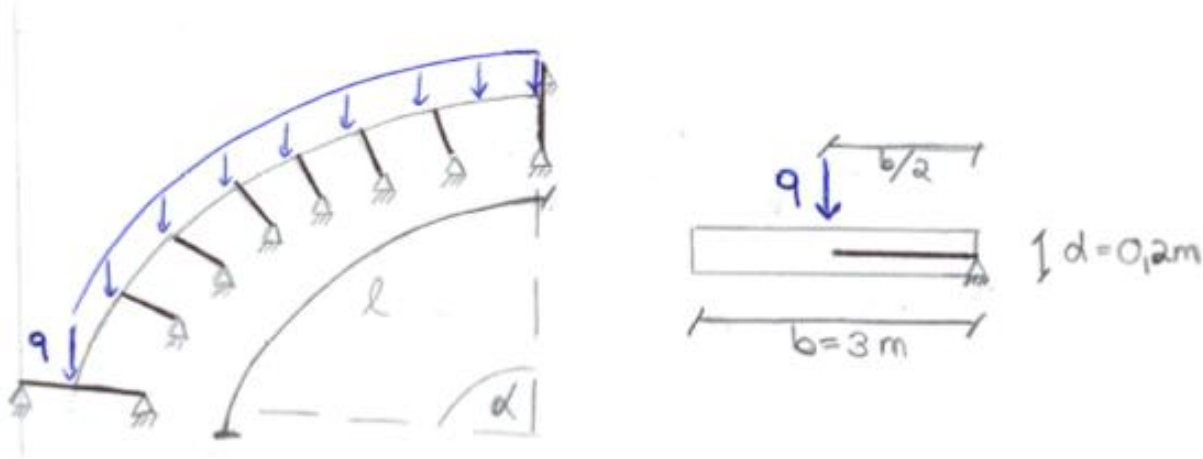

Figure 4.10 Beam element system with inside suspension

Figure 4.10 makes clear what happens due to the linear support. Although the former deflection of the deck is prevented, the distributed load q is still able to rotate around the supported side. This creates a local bending moment in the cross-section and, respectively, a global twisting moment along the total length.

$$m_t = q \cdot \frac{b}{2} \tag{4.4.2}$$

In the following part, the beam deck will be restrained along the inner edge first and then the outer edge. The results are taken from SAP 2000. The system has been drawn regarding to the former explained geometrical system and is loaded in gravity direction with the distributed line load $q = 45 \frac{kN}{m}$ (eq. 4.4.1).

Supports along the inner edge:

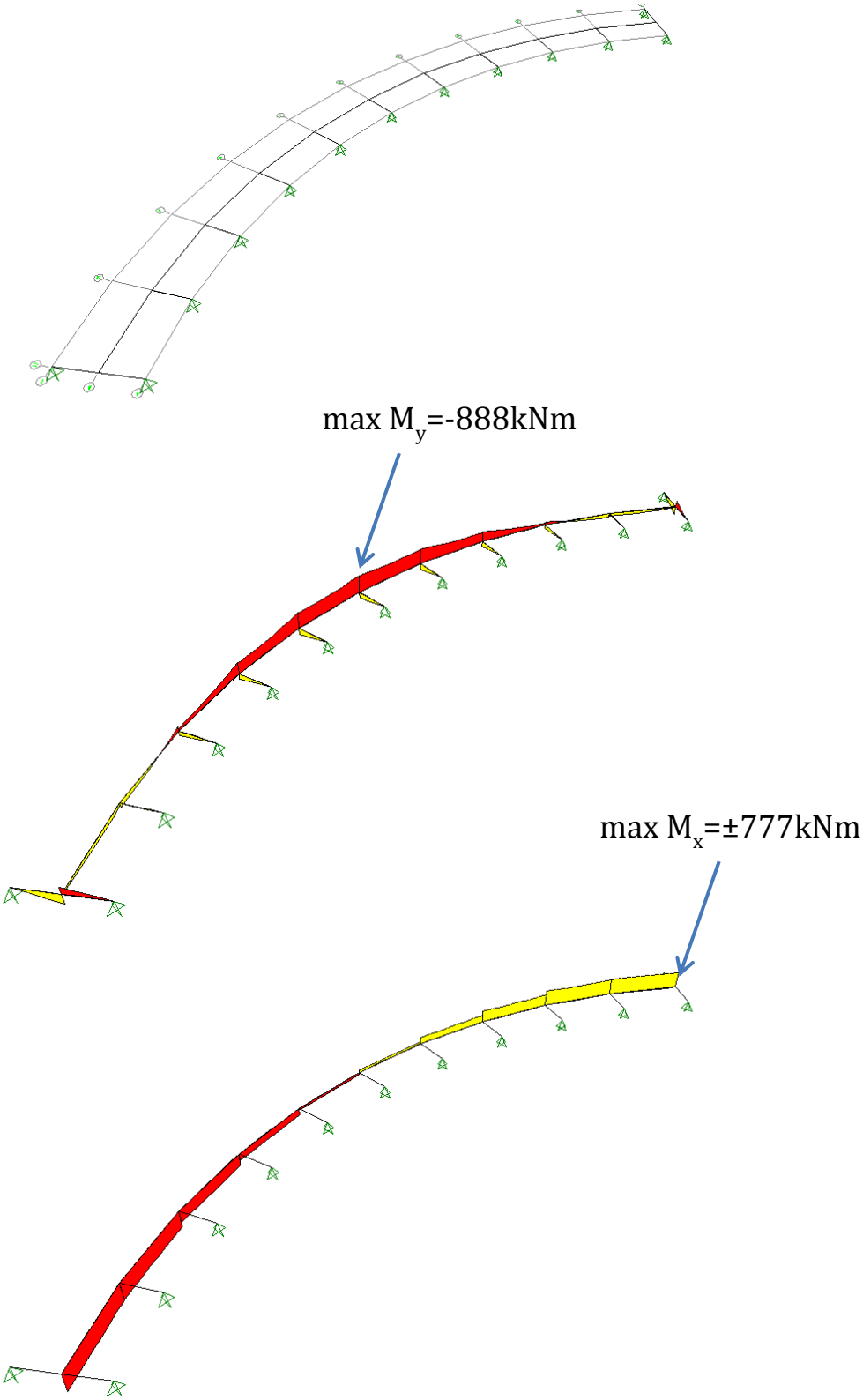

Figure 4.11 System, bending moment M_y (maxM_y=888kNm) and torsion moment M_x (maxM_x=777kNm) of beam element system with suspension on the inner side

Supports along the outer edge:

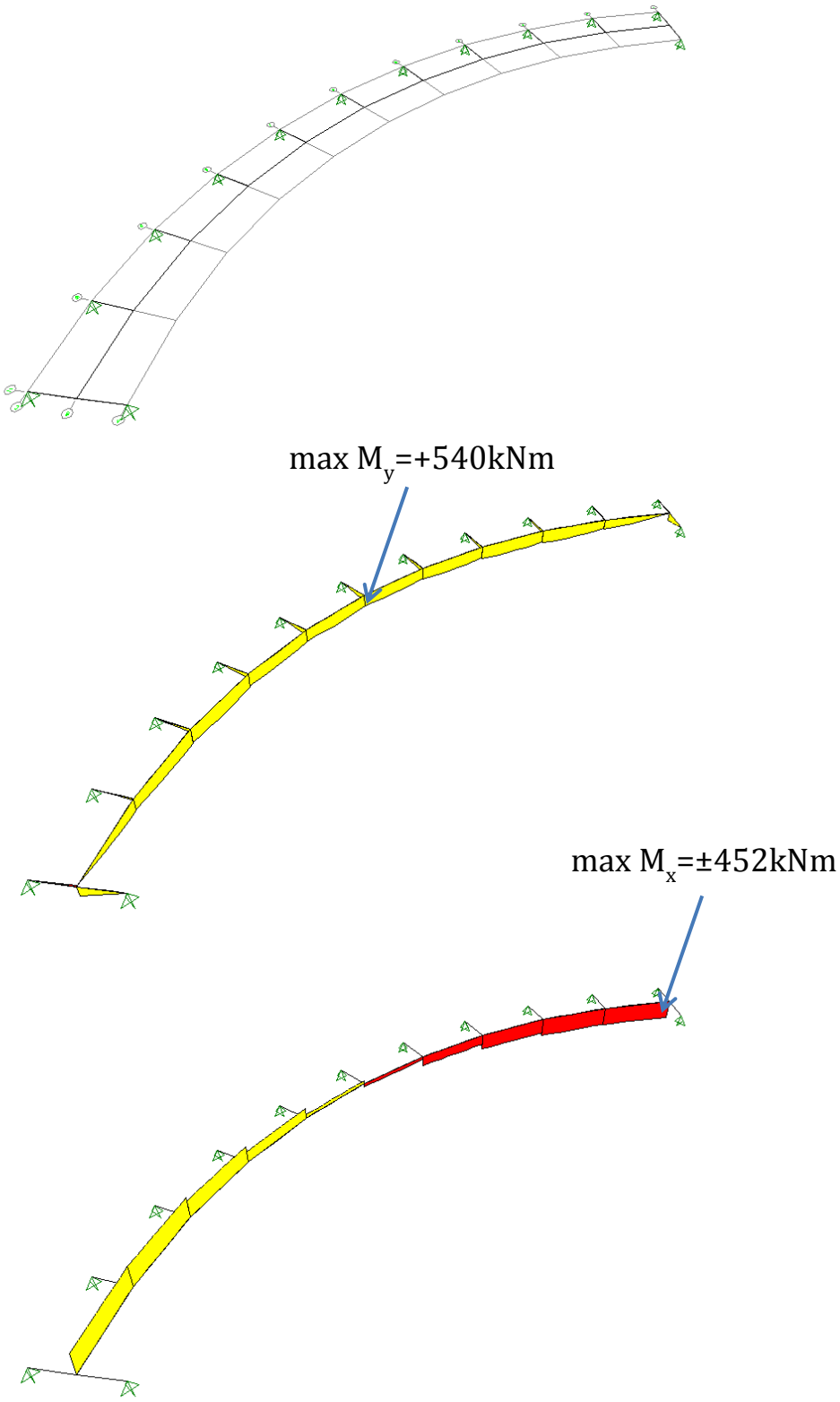

Figure 4.12 System, bending moment M_y (maxM_y=540kNm) and torsion moment M_x (maxM_x=452kNm) of beam elements system with suspension on the outer side

Both systems are only loaded in vertical direction. The only section forces that can be observed besides the shear force V_z are a bending moment M_y and a torsion moment $M_t=M_x$.

The bending moment is caused by the distributed vertical load. The graphs show a different progression of the bending moment. Supported along the inner edge the main part of the beam suffers a negative moment M_y^-. The beam bends upwards. Supported along the outer edge the beam suffers over its whole length a positive moment M_y^+. The beam bends downwards.

The twisting of the beam is caused by the linear support along one edge and the resulting global torsion moment. As it can be seen in the graphs, the twisting occurs in different directions depending on the side of support. The beam twists in direction of the free edge.

All in all, it is apparent that the curved deck will twist and bend due to the suspension and that the type of behavior depends on the side of the suspension.

4.4.3 Modeling the deck with shell elements

In the second example, the same system is modeled with shell elements. The width of the shells is set by the system's geometry and corresponds just like the thickness of the shells with the assumptions of subchapter 4.4.1.

The former distributed line load q $[\frac{kN}{m}]$ is assigned on the shell elements as uniformly distributed area load q $[\frac{kN}{m^2}]$ (eq. 4.4.2).

$$q = \frac{45\frac{kN}{m}}{b} = \frac{45\frac{kN}{m}}{3m} = 15\,\frac{kN}{m^2} \tag{4.4.3}$$

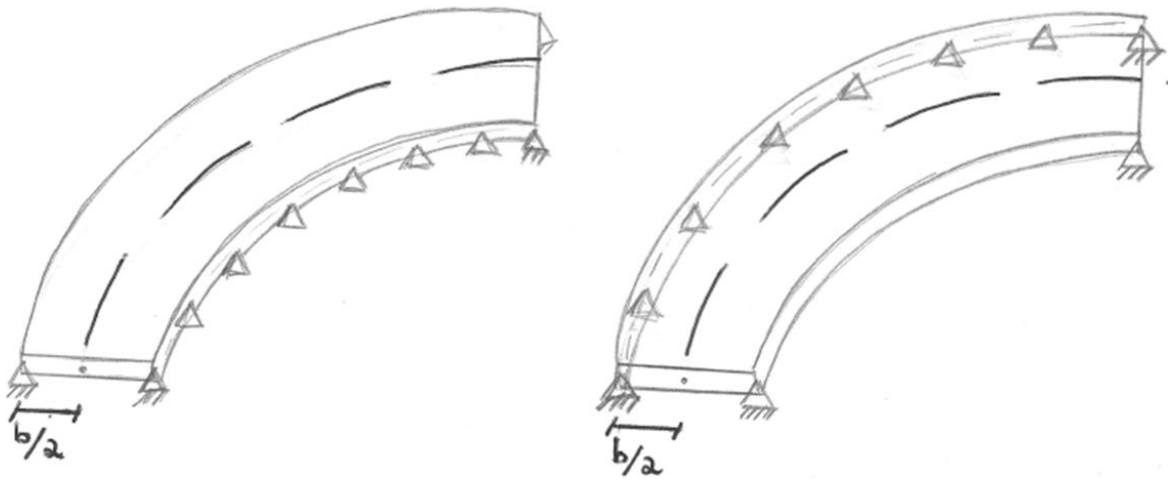

Figure 4.13 Shell element system with inside suspension (left) and outside suspension (right)

Supports along the inner edge:

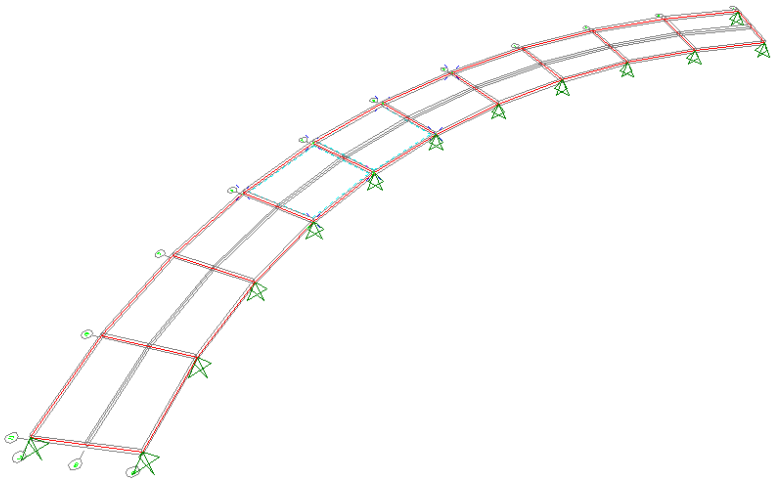

Figure 4.14 Shell element system with inside suspension

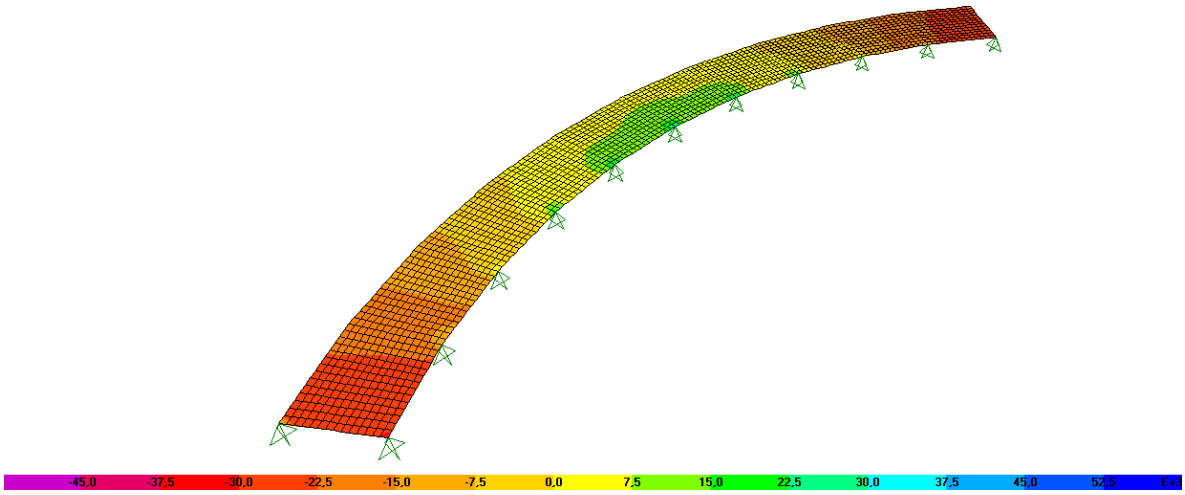

Figure 4.15 Longitudinal stresses S11, top face

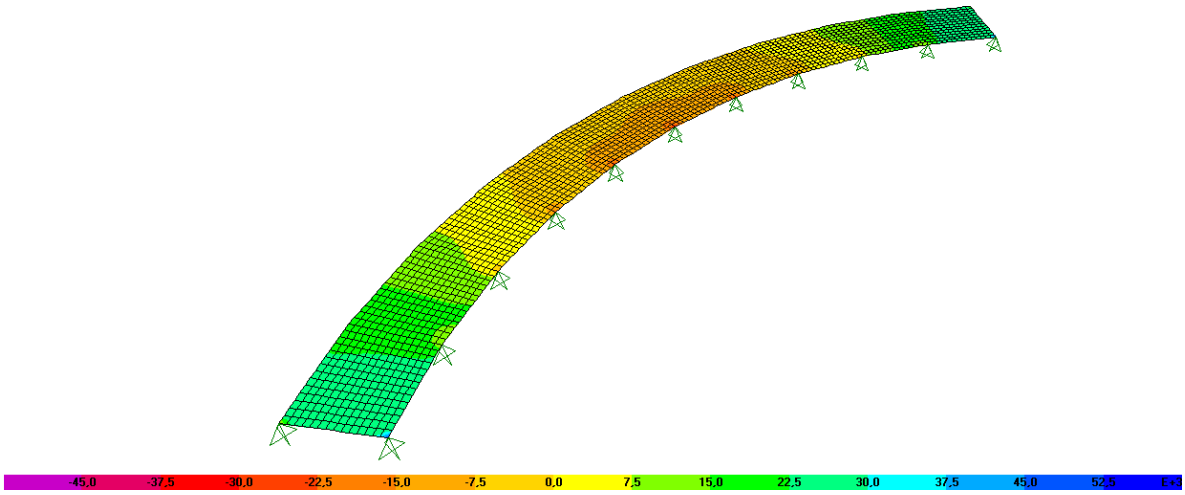

Figure 4.16 Longitudinal stresses S11, bottom face

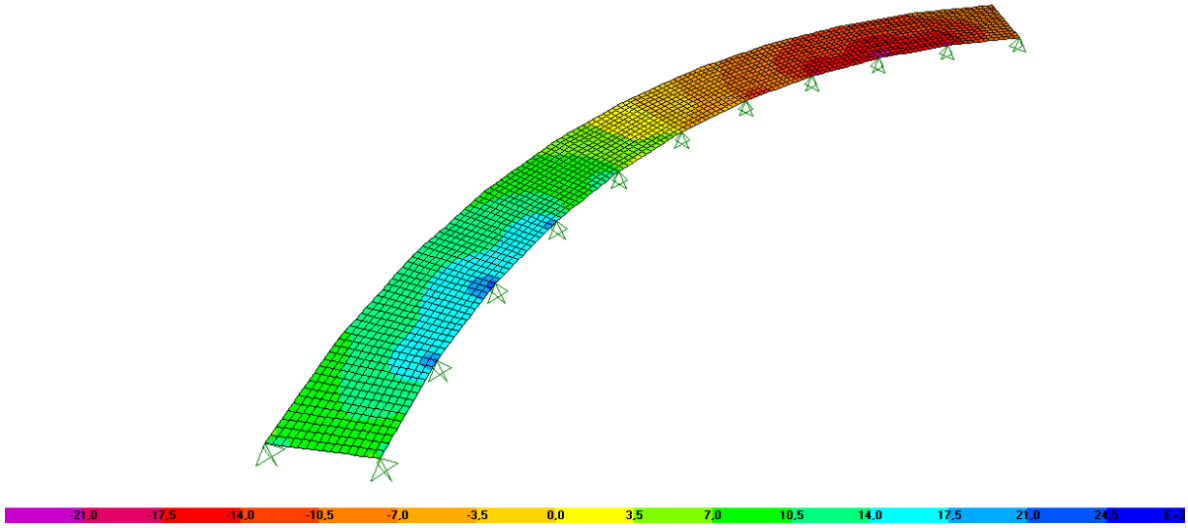

Figure 4.17 Torsion stresses S12

Supports along the outer edge:

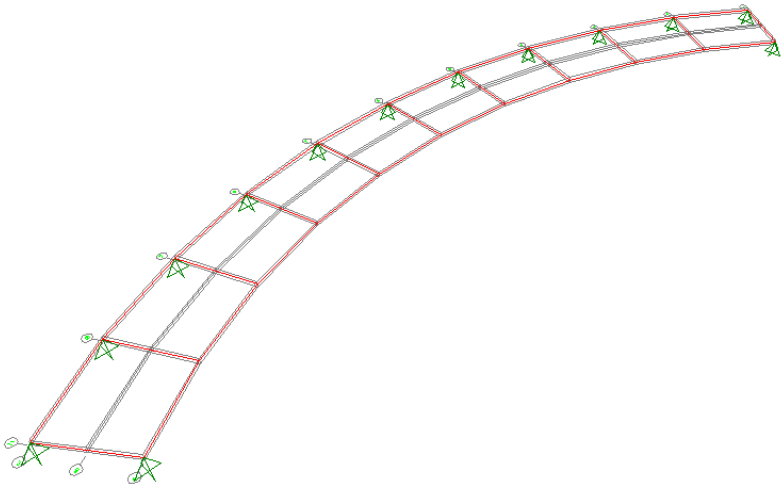

Figure 4.18 Shell element system with outside suspension

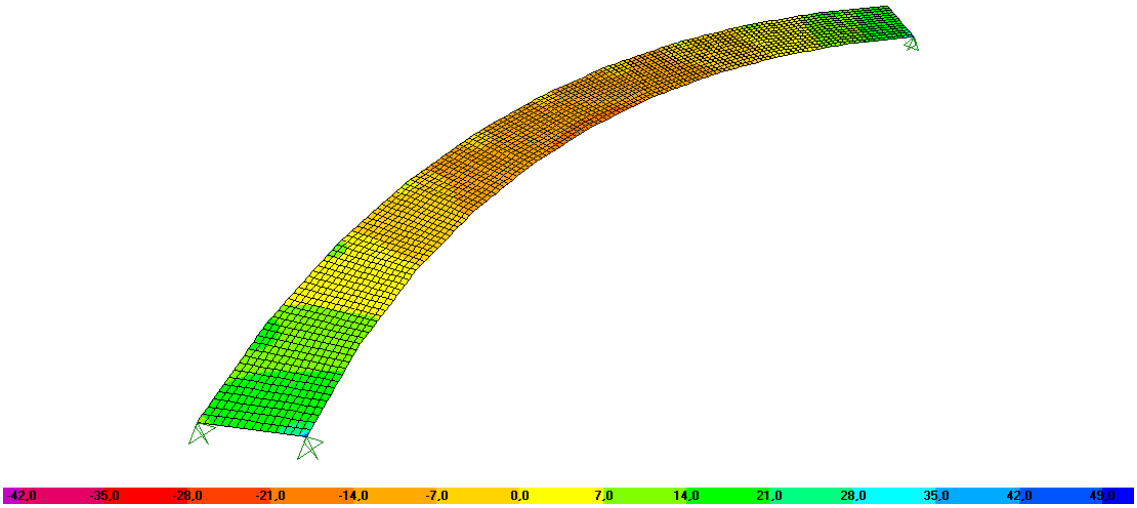

Figure 4.19 Longitudinal stresses S11, top face

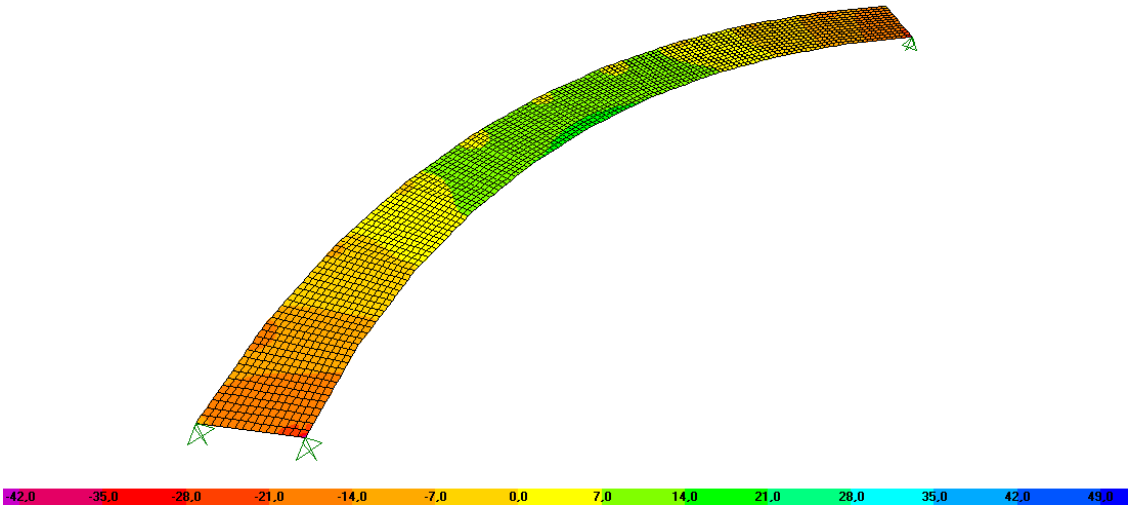

Figure 4.20 Longitudinal stresses S11, bottom face

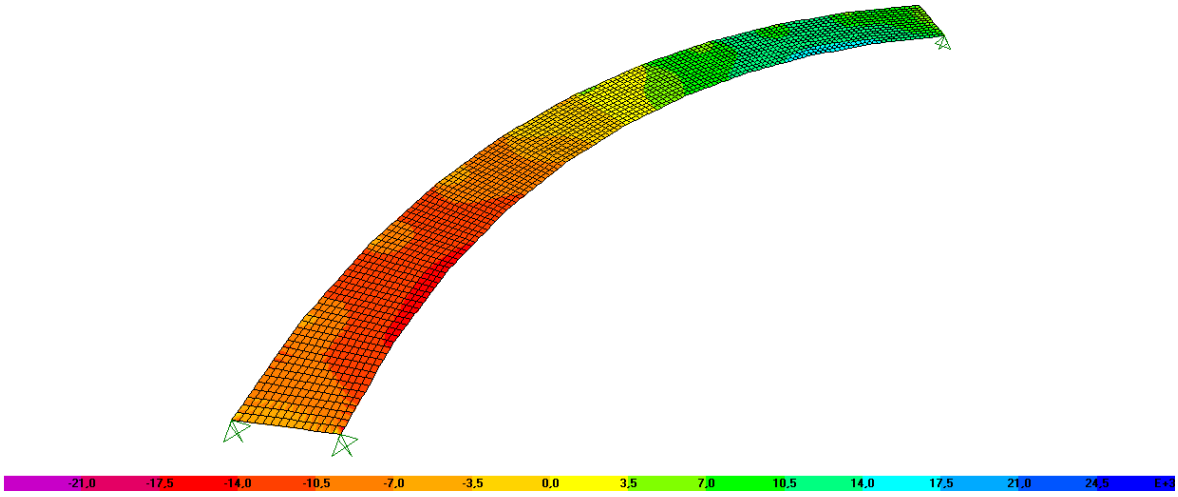

Figure 4.21 Torsion stresses S12

The results in Figures 4.15/4.16 and 4.19/4.20 show the stresses S11 of the shell elements in longitudinal direction. A distinction is made between stresses on the top face and stresses on the bottom face of the elements. Furthermore, the results show the absolute maximum of the stresses S12, which are interpreted as the stresses caused by torsion (Fig. 4.17/4.21).

For the shells a mesh area design of 14x14 objects per shell has been chosen. This generates objects of about 10x12cm size.

Like already demonstrated in subchapter 4.4.2 the behavior of the deck is changing totally when modifying the location of the point supports. Focusing on the middle part of the deck it can be summarized as follows: Supported along the inner edge the deck suffers tension on the top face and compression on the bottom face. The deck curves upwards. Supported along the

outer edge the deck suffers compression on the top face and tension on the bottom face. The deck curves downwards.

As in the system modeled with beams, a twisting of the deck around the longitudinal axis is induced by a global torsion moment. This moment twists the deck in direction of the unsupported edge.

This means that the behavior is just the other way around focusing on the location of the linear support and that the results of this shell element system match exactly with the ones of the beam element system of subchapter 4.4.2.

4.4.4 Comparison of the different systems

All in all, the deck system has been modeled with shell elements in order to analyze its differences to the system modeled with beam elements. As the former system is much more complicated in analyzing its results, it would be very helpful if the use of the beam element system had most of the advantages. This would simplify the analyses of following models.

Stresses in the deck:

In the system modeled with beam elements: The values of the bending moments have to be converted in order to be able to compare them with longitudinal stress values. Figures 4.11 and 4.12 show the progress of the bending moment with their extrema of $M_y^- = 888kNm$ and $M_y^+ = 540kNm$.

$$\sigma = \frac{M_y}{W_y} \tag{4.4.4}$$

Where: the moment of resistance $W = \frac{b \times \square^2}{6} = \frac{3m \times (0{,}2m)^2}{6} = 0{,}02m^3$

the bending moment $M_y = -888kNm \; / + 540kNm$

For inner edge suspension: $\sigma = \frac{0{,}888MNm}{0{,}02m^2} = 44{,}4\frac{MN}{m^2} = \pm 44{,}4\frac{N}{mm^2}$

For outer edge suspension: $\sigma = \frac{0{,}540MNm}{0{,}02m^2} = 27{,}0\frac{MN}{m^2} = \mp 27{,}0\frac{N}{mm^2}$

In the system modeled with shell elements: Figures 4.15, 4.16, 4.19, 4.20 show the stresses per area element of the deck. In the SAP file detailed information and diagram can be given just by right clicking on any element. Taking a look on the middle of the deck where the beam elements had their maximal bending moment the stresses can be read out.

In Table 4.1 the stresses are summarized.

Joint reaction forces:

This thesis will focus mainly on the connections of the cables with the deck. Therefore, it is necessary to take a closer look at the reaction forces of the restraints. Until now these restraints are replacements for the further suspension cables.

In Table 4.1 the maximum reaction forces are summarized. These are the tension forces of the most loaded joint located in the middle of the system.

	Inner edge suspension			Outer edge suspension		
	Beam elements	Shell elements	Δ [%]	Beam elements	Shell elements	Δ [%]
Bending moment [kNm]	-888	-	-	+540	-	-
Corresponding bending stress [N/mm^2]	±44,4	±9,2	80%	∓27,0	∓11,6	57%
Support reaction [kN]	215	167	22%	160	142	11%

Table 4.1 Summary of section forces and stresses

Summary:

Both systems illustrate the same behavior of the deck. First of all, the deck suffers a bending moment over its whole length. Secondly, it twists in direction of the free edge.

The stress results of the deck and the results of the joint reaction forces are not totally in the same range of magnitude. However, it seems sufficient enough to model the deck with beam elements since this system gives results on the safe side. Additionally, systems modeled with beam elements are in general more reliable (*Crocetti 2012*).

When it comes to the stress results, they demonstrate clearly the big influence of the location of the linear support. Supported along the inner edge the deck suffers positive stresses on the top face and negative stresses on the bottom face. Supported along the outer edge the deck suffers negative stresses on the top face and positive stresses on the bottom face.

As a consequence, the choice of suspending the bridge along one side has a bigger influence on the further proceeding than it seemed to have at the beginning. The design process depends very much on the decision of the suspended bridge edge.

Before, in chapter 3, it has been already mentioned that the concept of a curved bridge suspended along the outer edge will be progressed. That is why it should be pointed out here

that the concept of the outer edge suspension provides in general lower results than the one of the inner edge suspension. Figures 4.19 and 4.20 demonstrate that the stresses are distributed wider over the whole deck area compared to the stresses of Figures 4.15 and 4.16. Especially, the joint reaction forces are in the case of the shell element system 15% and in the case of the beam element system even 25% smaller. Since the outer edge is the border of the deck with the bigger curvature, in other words, the border with the longer length, it seems logical that the forces do not accumulate as much as along the shorter edge.

4.5 Consequences for designing a curved suspension bridge

The conclusion of this chapter about the statics of a curved suspension bridge is the need of stabilization in order to prevent the bridge deck from twisting. The global torsion moment has to be taken by an adequate preload system. The description of the radial uniform forces caused by the curvature and described in subchapter 4.2 has given the background which is needed to understand the explanations of the following part.

Especially the summary of subchapter 4.4 has emphasized that the behavior of the deck varies. When selecting the concept of the inner edge suspension the upper part of the deck has to take tension while the lower part has to take compression. When selecting the concept of the outer edge suspension the forces are just the other way around (Fig. 4.22).

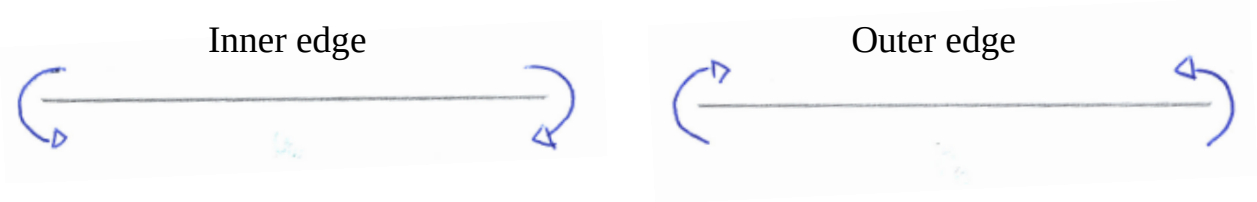

Figure 4.22 Simple demonstration of the deck's bending moment depending on inside (left) or outside (right) suspension

In subchapter 4.2 it has been developed how the tension force T and the compression force C create uniformly radial forces thanks to the curvature of the structure. In a preload system inward looking deviation forces u can be caused by a tension arch and outward looking deviation forces u can be caused by a compression arch (Fig. 4.23).

According to equation (4.1.9):

$$u = \frac{C}{R} = \frac{T}{R} \tag{4.5.1}$$

Where: u deviation force

C / T axial forces

R radius of the circular segment

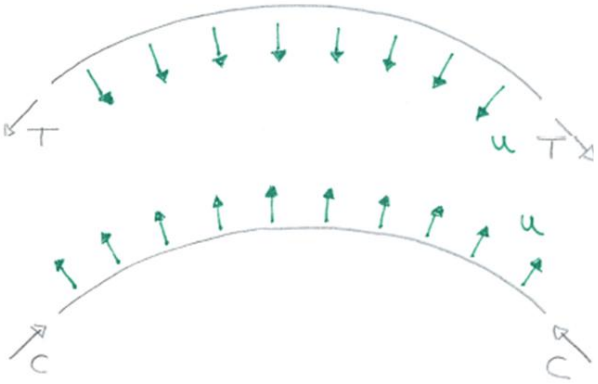

Figure 4.23 Inward (above) and outward (below) looking radial deviation forces u

In a global view it is evident that these radial forces u generate over the length dl a uniformly distributed torsional moment with the lever arm e (Fig. 4.24).

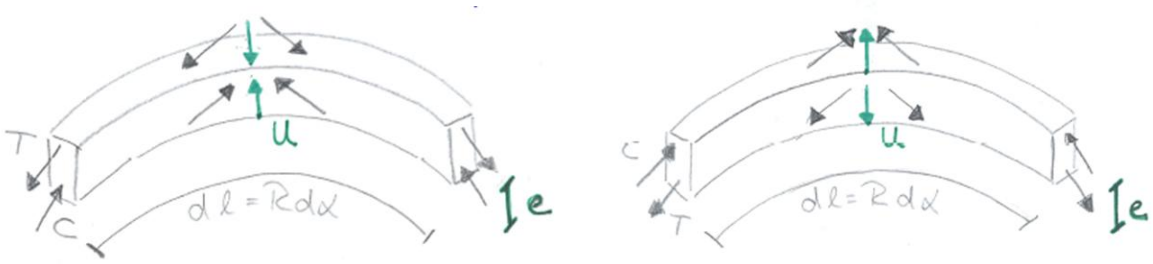

Figure 4.24 Global view of the radial deviation forces u along an element with the length dl

Globally this deviation forces are able to inhibit the twisting of the deck. The equilibrium of the forces is ensured (Fig.4.25).

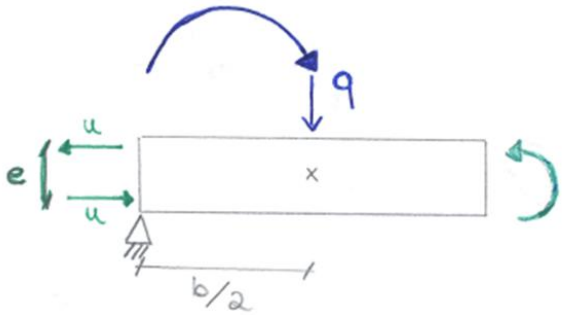

Figure 4.25 Equilibrium of the cross-section

In summary, it can be said that the deviation forces keep the balance against the local bending moment of the cross-section.

$$u \cdot e = q \cdot \frac{b}{2} \tag{4.5.2}$$

4.6 Case example: the Bridge in the "Deutsches Museum" in Munich, Germany

Figure 4.26 Picture of the museum's exhibition bridge (DEUTSCHES MUSEUM 16/06/2012)

In this real case, as shown in Figures 4.26 to 4.31, a steel bridge is curved in its horizontal and vertical direction.

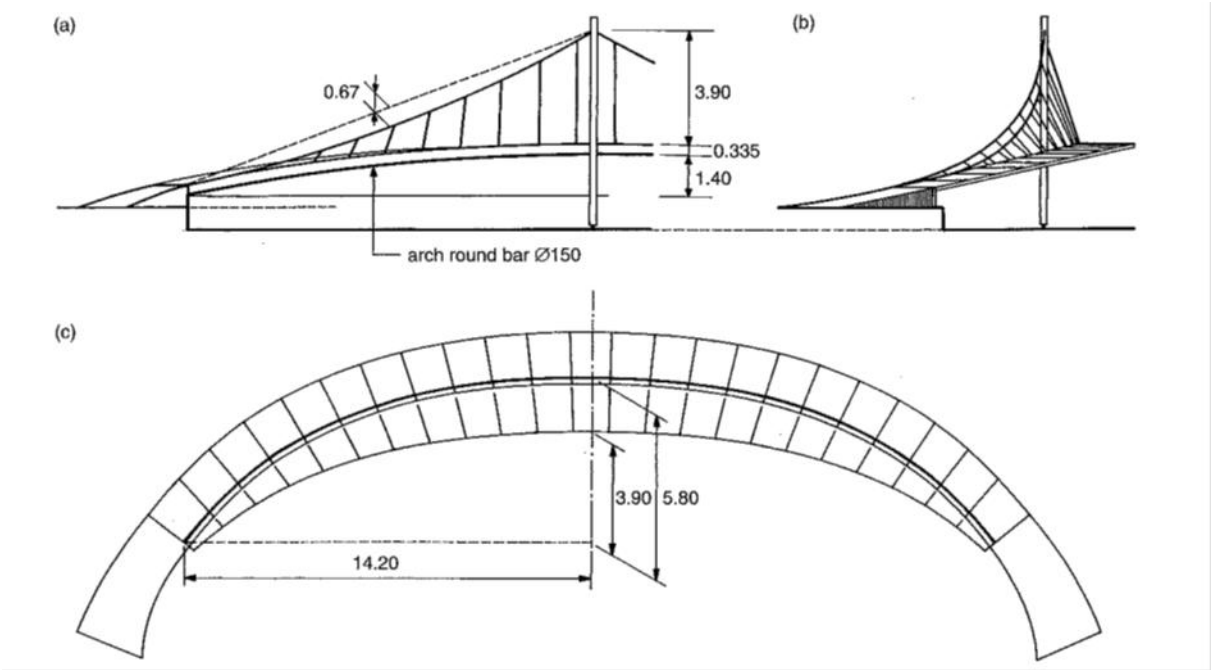

Figure 4.27 a) elevation b) cross-section c) plan (STRASKY, J. 2005)

Hangers on the inside of the curve suspend the bridge. The hangers are connected to main cables, which span from the bridge end abutment to the pin-ended pylon in the middle of the

structure. The ends of the bridge are fixed to the abutments. At a certain distance a horizontal arch supports radial diaphragms. They serve as connections for the anchored hangers and the horizontal cables and ensure a bending stiffness that is needed as a result of the circular ring effect. These diaphragms are asymmetric to reduce as much as possible the twisting moment.

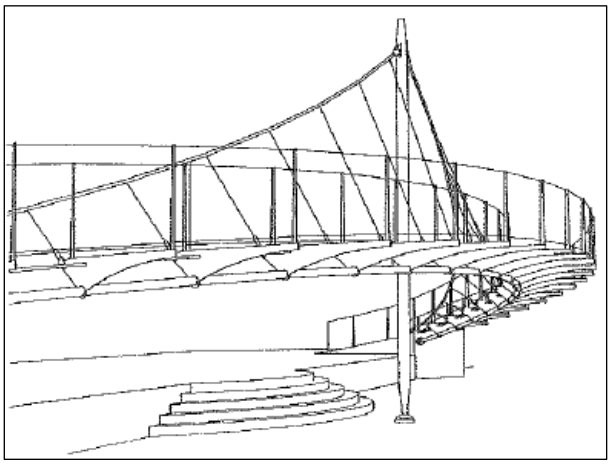

Figure 4.28 Structural arrangement, (STRASKY, J. 2005)

Figure 4.29Detailed view of a diaphragm, (DEUTSCHES MUSEUM et al. 1999)

The deck is able to counteract the torsion of the glass deck by an inner pair of forces. In the case of this exhibition bridge "(…) these forces are visible in the form of circular cables above a circular arch beneath a glass deck." (*STRASKY, J. 2005*) The circular cables, which are in tension, and the circular arch, which is in compression, are responsible for a torsional moment that balances the moment created by the glass deck.

Figure 4.30 Balancing of moments in the cross-section (DEUTSCHES MUSEUM 16/06/2012)

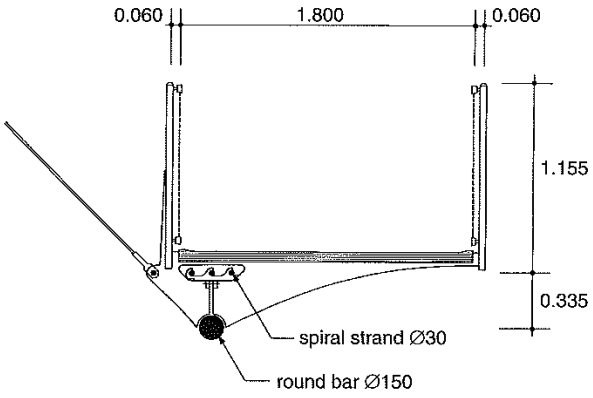

Figure 4.31 Cross-section of the bridge deck (STRASKY, J. 2005)

This prime example of a cable-supported pedestrian bridge demonstrates how a curved bridge can be suspended only on one side of the deck. At the same time, it indicates the need of compression and tension components in the deck in order to inhibit the twisting of the deck.

The angled suspension hangers are not comparable any more with the fixed restraints of the former models. They induce horizontal force components in addition to the former vertical joint reaction forces. These adding components cause additional stresses and moments.

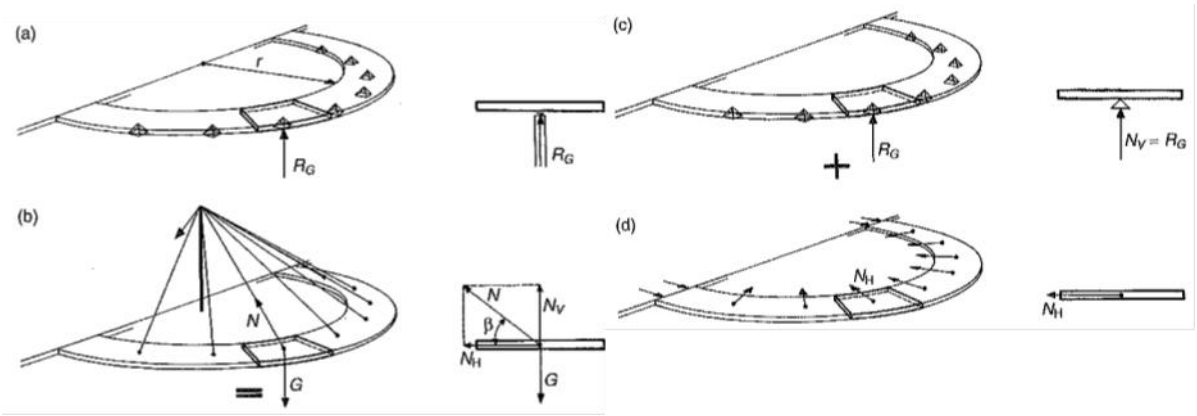

Figure 4.32 a) continuous beam b) cable-stayed structure; effects of the c) vertical and d) horizontal components (STRASKY, J. 2005)

Figure 4.32 a) shows the up to now structure, the continuous curved beam supported by single supports, where the joint reactions forces correspond to the vertical load G.

Figure 4.32 b) in contrast makes it evident that in the cable-stayed structure "(…) the vertical component of the cable force substitutes single supports and the horizontal component creates radial forces that stress the deck in horizontal direction." (*STRASKY, J. 2005*)

In the case of the Museum's Bridge the compression steel arch stiffens the system against these horizontal forces.

In fact, the hangers are anchored at the inner edge and not in the bridge axis. This evokes new lever arms for both components of the cable forces. How the horizontal components "(…) create significant transverse moments in the deck" (*STRASKY, J. 2005*), will be explained further in the next chapter about the design of the thesis' bridge "A Pilgrim's Walk".

4.7 Project concept: “A Pilgrim’s Walk” Bridge

In the previous chapters, it has only been mentioned which are the benefits of the outer edge suspended concept from the architectural and the static point of view: nice advantages for experiencing the surrounding (subchapter 3.3.3) and the advantageous distribution of loads in deck and cables (subchapter 4.4.4). Now it is important to screen the issue from the point of view of the load-bearing design.

The characteristic tensile strength of structural timber is in general less than its characteristic compressive strength. The reason for this is the timber’s sensitivity towards the effects of knots, spiral grain, compression wood and other anomalies. These are normal features of the living material wood. The anomalies have a stronger impact on tension failure, which proceeds in a more brittle than ductile way, than on compression failure. Compression and especially tension perpendicular to the fiber direction should be avoided totally.

That is why it is desirable to use the material timber mostly for taking axial compressive forces, preferably in full section. The material steel, on the other hand, would be perfect to take the tensile forces of the system.

In this timber bridge the visual or main part of the deck is ought to be made out of timber. Having the explanation of subchapter 4.5 in mind and taking especially a look back on Figure 4.22, it is evident that the upper part of the structure, in this case the deck, can only be stressed in compression by suspending the bridge on the outside of the deck. In fact, this is the most important reason for having chosen the outer edge concept even before having done the analyses of the concepts.

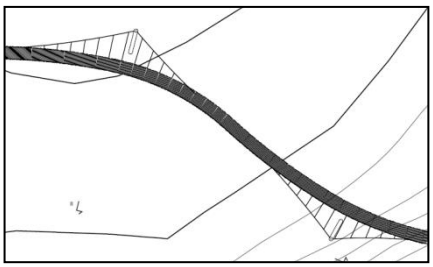

Figure 4.33 Top view of the two-curved suspension bridge (by Daniel Asp)

Following the design of the Museum’s Bridge a prestressing two-layer system will be responsible for a torsional moment that balances the moment created by the twisting structure. An inner pair of forces just has to be caused the other way around than in the case of the inner edge suspension.

In the case of the outer edge suspension the upper part of the deck, the timber arch deck, will be in compression, while an additional circular member will take care of the tension. This tension arch has to be situated below the timber deck with a sufficient distance (Fig. 4.34).

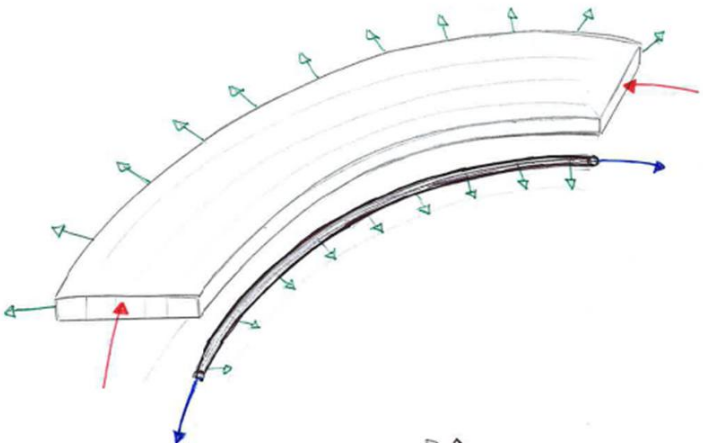

Figure 4.34 Two-layer system with its radial deviation forces: compression timber deck and tension steel arch

Basically, the structural behavior of this cable-supported and curved bridge is characterized by bending moments M_y around the horizontal axis and by torsion moments M_t around the bridge axis (see subchapter 4.4). Also in the project of "A Pilgrim's Walk" Bridge a space arrangement of cables minimize the bending and the shear stresses of the system while the prestressing arches are able to counteract the torsion by an inner radial pair of forces. The vertical force-components of the cables balance the vertical weight.

Meanwhile, the horizontal force-components of the cables burden additionally the structure with radial shear forces V_y (blue arrow) as well as with torsion moments M_t (blue moment) and globally with significant bending moments around the vertical axis M_z (Fig. 4.35).

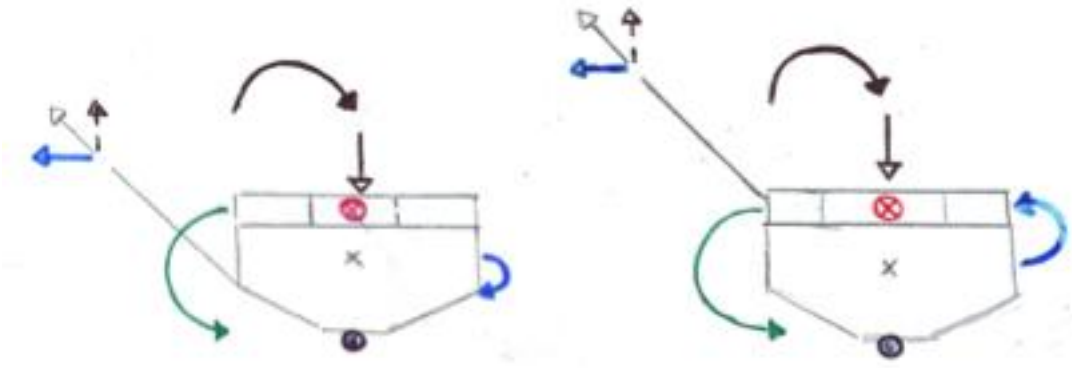

Figure 4.35 Equilibrium of the cross-section depending on the height of the anchorage of the hanger

Figure 4.35 shows the equilibrium in the cross-section with the connection of the hanger located below (on the left) or above the center of gravity (on the right side). The horizontal components of the hanger force (blue), the radial forces from the prestressing system (green), together with the torsional moment caused by vertical forces (black) create a system in equilibrium. The additional horizontal force (blue arrow) can be taken through compression by the stiffening girder (*INFORMATIONSDIENST HOLZ 2000 (a)*), here probably by the timber deck.

It seems as if it is worthwhile to connect the hangers above the center of gravity. Figure 4.35 visualizes on the right side how the horizontal force of the hanger (blue) could help to counteract the torsional moment (black). This could mean to anchor the hangers near the compression timber deck. But it did not appear to be such a good idea. Connections near the timber deck could cause stresses perpendicular to grain and elaborate steel constructions could be needed to take the forces instead.

That is the reason why it has been decided to connect the hangers with the deck structure underneath the timber deck. However, simply from the point of view of durability it seems the better decision to situate this important connection point underneath the timber deck and to leave the timber deck alone.

Figure 4.36 3D-simulation of the two-curved suspension bridge (by Daniel Asp)

Finally, the statics of the thesis' bridge have been outlined from the very beginning to the conditions of the actual related project (Fig. 4.36). Having understood these basics it has to be made a start to the process of modeling the actual structure.

5. Development of the “A Pilgrim’s Walk” Bridge’s model

In chapter 3 it has been outlined how Daniel Asp had developed his final concept of a two-curved suspension bridge. Starting right from the beginning with the two-curved system would entail the risk of complicating the initial situation of the model. Instead it will be taken a look on half of the bridge, on other words, on one curvature of the system.

Therefore, more information about the system lines and dimensions was needed. Daniel Asp helped out by providing AutoCAD files which show the most important assumptions he had decided until then.

5.1 Assumptions and limitations of the model

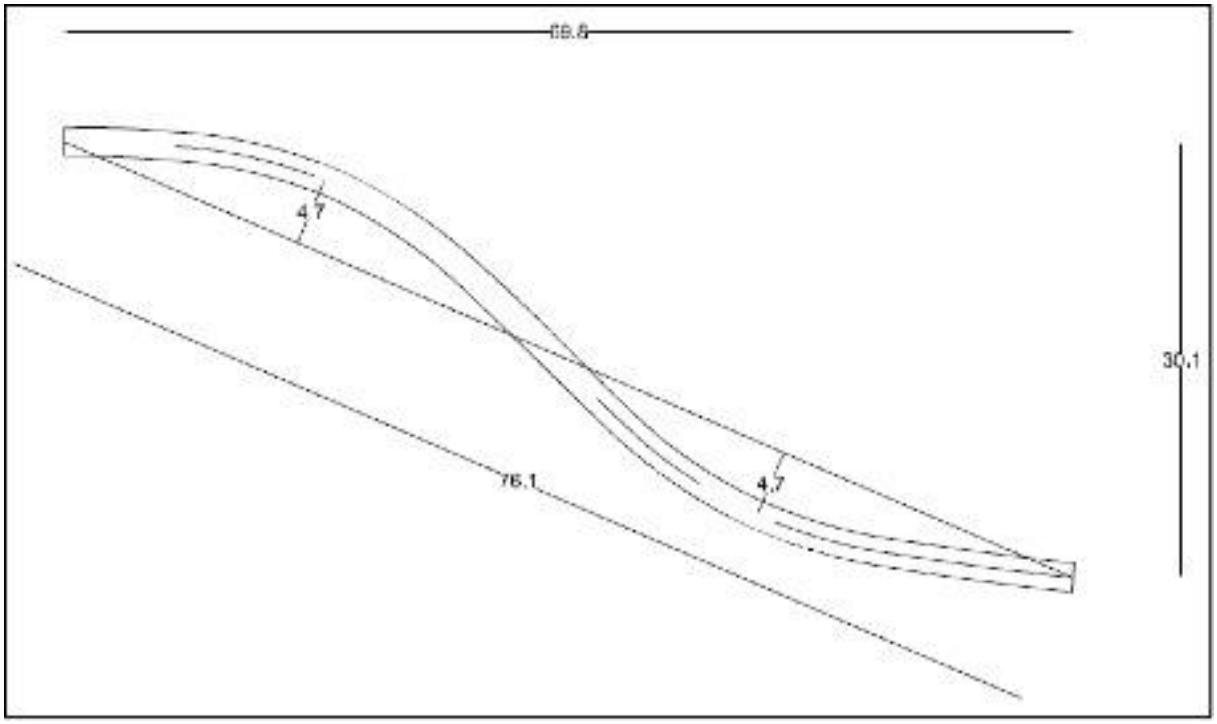

Figure 5.1 System lines of the two-curved structure (taken out of Daniel Asp’s AutoCAD file)

Figure 5.1 demonstrates the general system lines in planar view. The total span length of 76m is much higher than the in chapter 3 discussed lengths of 45 up to 70m of the different location alternatives. But since the development of the model has to accelerate, the data were just used as orientation to model an equivalent shape.

In that way, it can be said that it will be dealt with a double-curved structure of approximately 80m length and with curve of 4,70m. In the AutoCAD file it could be read out that the height difference of the bridge ends amount to 5m and that Daniel Asp chose a deck width of 2,00m.

In this thesis it will be worked on one curvature, which means, with a length of 40m. The height difference halfway of 2,50m causes a slop of only 1:20, which is negligibly small. The inclination will be discounted in the model. The width of the deck is enlarged up to 2,50m. Decks have in general a width around 2,50 or 3,00m (*Crocetti 2012*) . The upper mentioned 2,00m width seemed too slender for such a long pedestrian bridge.

Like in the plans of Daniel Asp, the diaphragms and the anchored hangers will be located every 1,80m along the bridge's length.

5.2 Basic structure of the model

Again, the Bridge of the "Deutsches Museum" was used as example. In Figure 5.2 it can be seen how the separation of the longitudinal forces has been realized in the model of this case. Two arches, one below the other, form the main part of the structure. The diaphragms mentioned in subchapter 4.6 are modeled as radial cantilevers and represent the width of the deck.

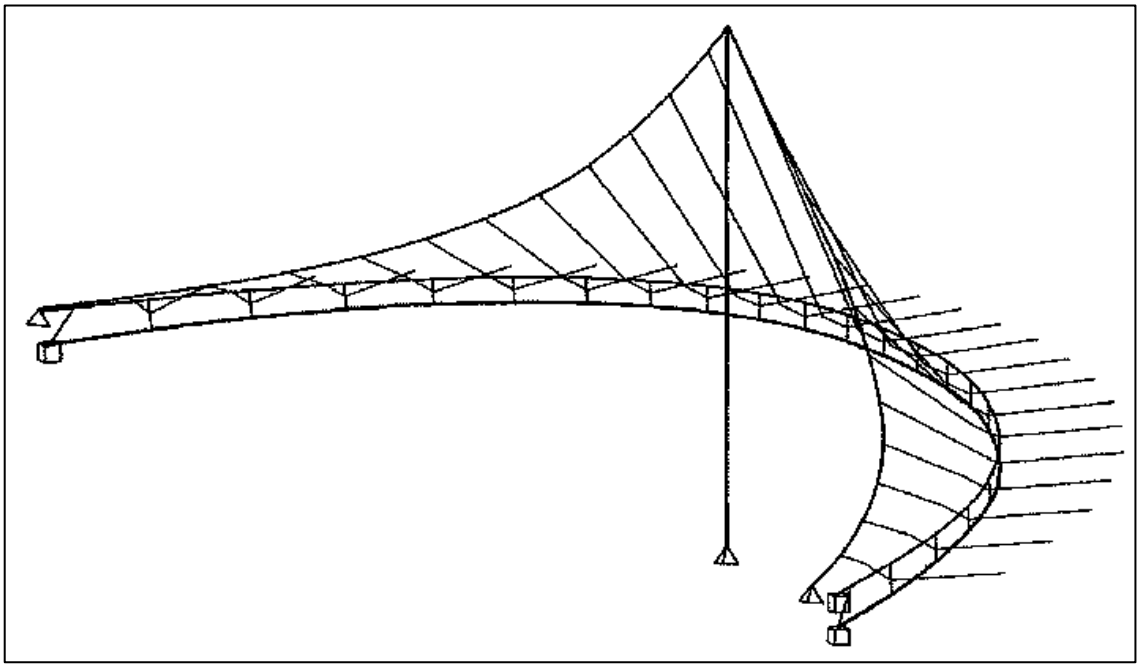

Figure 5.2 Museum Bridge - Calculation model

The arches have fixed restraints at the end to guarantee the stabilization. Hangers run from the connection between upper and lower arch to the main cables. Those are spanned between own fixed restraints and the pin-ended pylon.

In subchapter 4.4.1 it was presented how the basic geometry for all the models in SAP looks like. Just the same, the final model will base on the geometry of a circular segment (Fig.5.3).

Unlike the former examples, this model's circular segment lies in the system line of the system, in other words, in the longitudinal axis of the deck.

Again, the following sketches are made by hand and serve to emphasis the assumptions of subchapter 5.1.

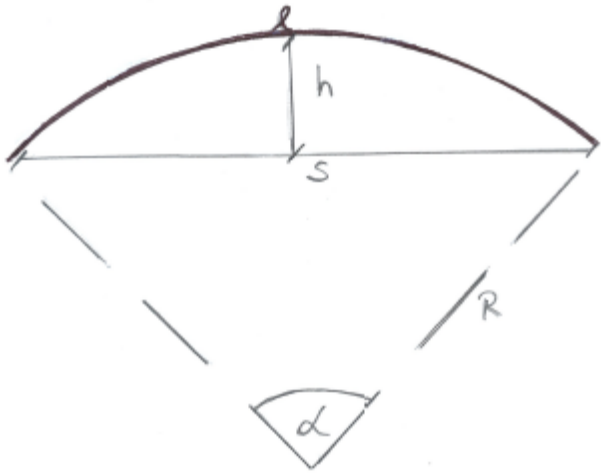

Figure 5.3 Draft of the basic circular segment

- The chord of the circular segment: s = 40m → The radius: R = 44,90m
- The height of the circular segment: h = 4,7m → The angle α = 52,90°
- The width of the deck: b = 2,50m → The length of the deck: l = 41,46m
- The thickness of the deck: d = 0,27m

During the modeling procedure attempts have been made to realize the separation of compression and tension in the deck structure as good as possible.

Compared to the exhibition bridge of the museum in Munich the compression part won't be taken by a single, bar-shaped arch but by a three-dimensional deck with a rectangular cross-section. This deck modeled with beam elements, the so-called compression beam, lies in the system line of the deck structure. That is why the compression timber beam (black) and the tension steel arch (grey) are not directly one below the other if not the tension arch is located in the middle axis like shown in Figure 5.4. A sufficient gap e between the two arches is needed.

The diaphragms are modeled as beam frames (blue), consisting of a timber beam below the timber deck and struts connecting the two arches with each other. As it makes no difference for the analysis, the fact that the deck beam and the strut beam are in reality not on the same level is neglected in the model (Fig. 5.5). As mentioned before, these timber beam frames are situated along the curve every 1,80m and divide the deck into 23 parts. This means that there

are in total 22 beam frames, in other words, 11 hangers to the right and 11 to the left of the pylon.

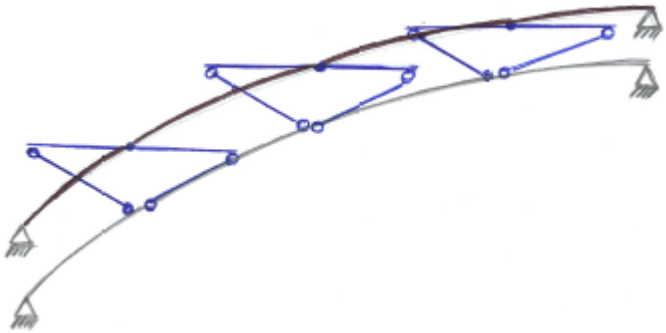

Figure 5.4 Example of system of arches and 3 diaphragms

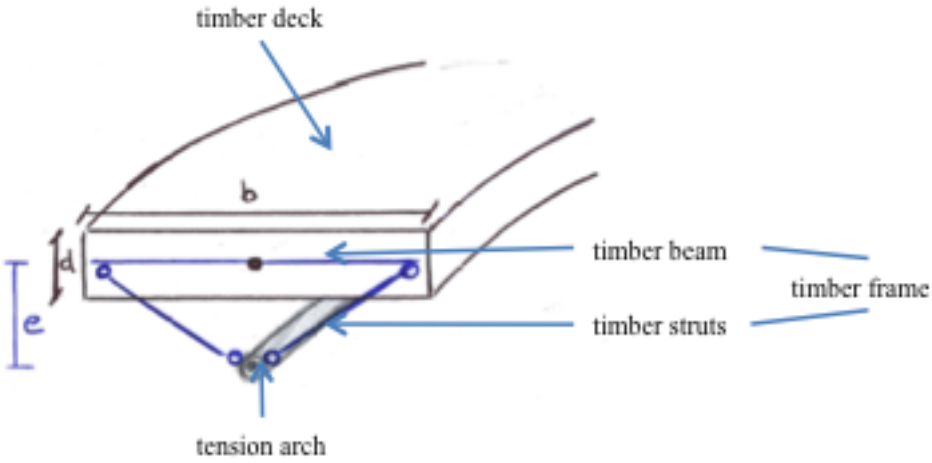

Figure 5.5 Extrude view of the deck system's cross-section

The pylon is basically used under compressive stresses. It is inclined and restrained by a cable which is fixed to the ground in order to stabilize (Fig. 5.6). The pylon is positioned at a distance k from the deck's axis and has a height h.

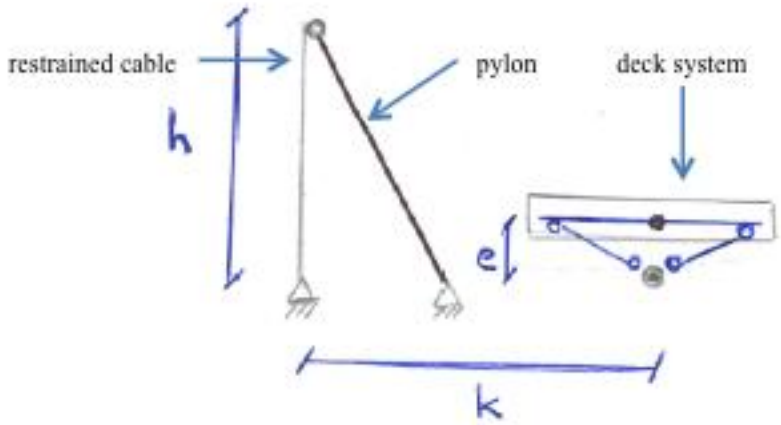

Figure 5.6 Cross-section at the level of the inclined pylon

The main cables determine the space arrangement of the cables. They are spanned with a maximal vertical sag f (Fig. 5.7 and 5.8).

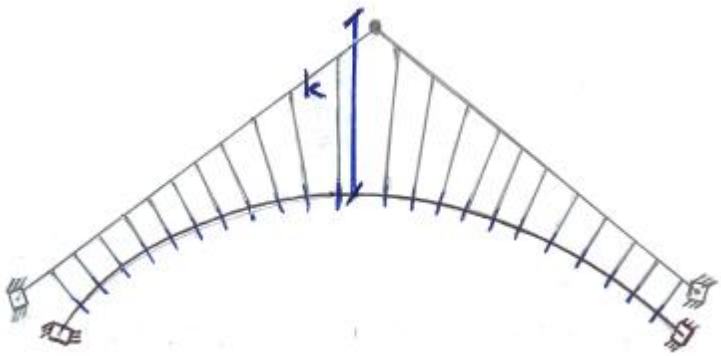

Figure 5.7 Top view of cables' space arrangement ***Figure 5.8 Sectional view of one main cable***

The hangers suspend the deck structure by being anchored below the timber deck in the connection point of beam struts and steel arch. The position of this connection point will be discussed further in the parameter study in subchapter 5.4. It should be just mentioned for now that, principally, it will be analyzed which effects occur with an inner node and an outer node position. This position relates to the outer edge of the timber deck.

5.3 Defining procedure

5.3.1 Section properties

The wooden structural elements are made out of glued laminated timber, in short, glulam. Especially the timber deck needs the advantages of this timber material. Curved shapes can easily be produced. The resulting elements have larger section sizes and longer lengths than solid timber and act as single, completely homogeneous structural units. (*METTEM, C.J. 2011*)

Section properties of Scandinavian glulam have certain cross-section dimensions. As it is explained on *SWEDISH WOOD 16/07/2012*: "Straight glulam components of rectangular cross-sectional dimensions are normally made of 45 mm thick laminates in widths corresponding to the sawmills' standard range."

Therefore, general properties are:

- The height of the cross-section: $h = x \cdot 45$ mm
- The width of the cross-section: $b = 90/115/140/165/190/215$ mm
  Where: $x \geq 1$

In the case of the entire cross-section of the timber deck being out of glulam big dimensions are needed. In Scandinavian bridge constructions stress-laminated glulam decks have successfully been used. Especially in Sweden it is a common technique to assure the increase of load-bearing capacity. The stress laminated glulam deck consists out of several glulam beams placed side by side and then stressed together by high-strength steel stressing rods (Fig. 5.9).

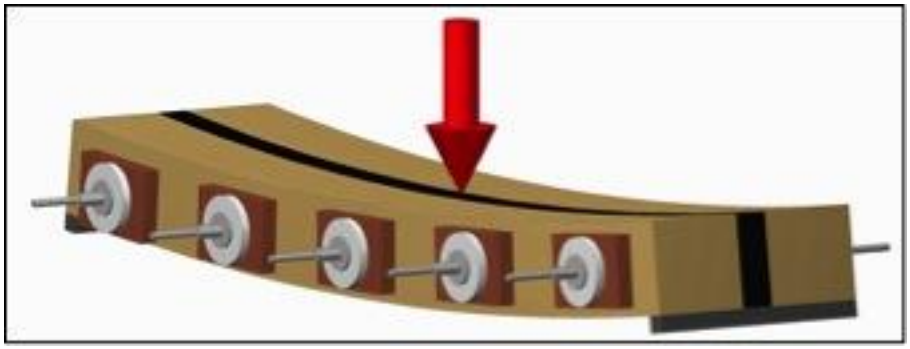

Figure 5.9 Load distribution between laminations as an effect of pre-stressing (EKHOLM, K. 2011)

The basic idea of this concept is that several laminations help carrying a concentrated load. The prestress in transverse direction transmits the load into the adjacent beams. The plate effect of the whole structure results from this transmittion. As a result, the transversely prestressed timber deck fulfills several functions: it distributes and transfers the loads, its plate effect serves as wind bracing and it protects the substructure. In addition, it has a simple manufacture process and a short assembly time. (*SCHICKHOFER, G. 2000*)

Figure 5.10 demonstrates how simple and fast elements of several glulam beams can be joined together element by element by applying the pre-stressing system.

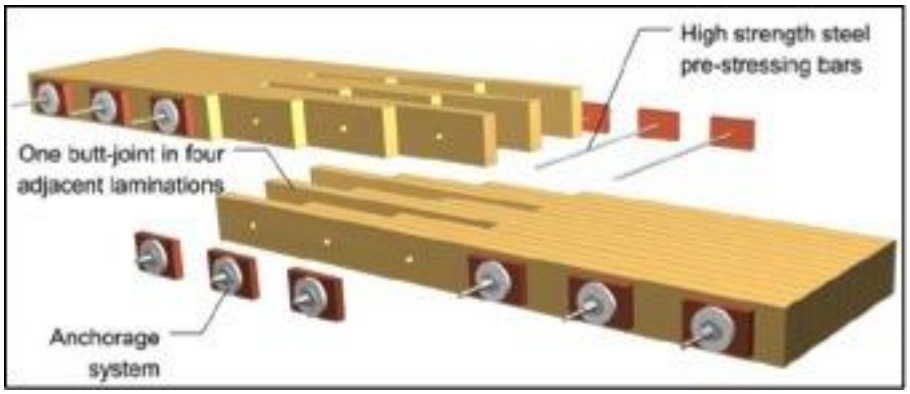

Figure 5.10 System of stress laminated glulam deck (EKHOLM, K. 2011)

The stress laminated technique was capable of asserting itself in the field of not oly large and almost homogenous but also curved structures. Figure 5.11 shows an example of a bridge in Norway, the Tomasjordnes Bridge.

Figure 5.11 Tomasjordnes Bridge, Norway: Example of a curved bridge with a stress-laminated glulam deck (CROCETTI, R. 2012)

The following section properties have been defined thanks to the information of the informative brochure "Die Bruecke im Raum" (*DEUTSCHES MUSEUM et al. 1999*) and with the help of Professor Crocetti.

Compression beam: In SAP the **stress laminated glulam deck** is assigned as one solid timber beam with the same material properties as its equivalent glulam deck. The total cross-section has a width b of **2,50m** and a thickness d of **270**mm.

Tension arch: In the final model a steel pipe of 150mm diameter and 15mm thickness has been replaced by a number of tension rods (Fig. 5.12). These tension rods will be anchored from one timber frame to another over the length of 1,80m. In the end, **three bars** of a diameter of **36mm** have been chosen. In SAP they are assigned as one full cross-section of **62mm** diameter.

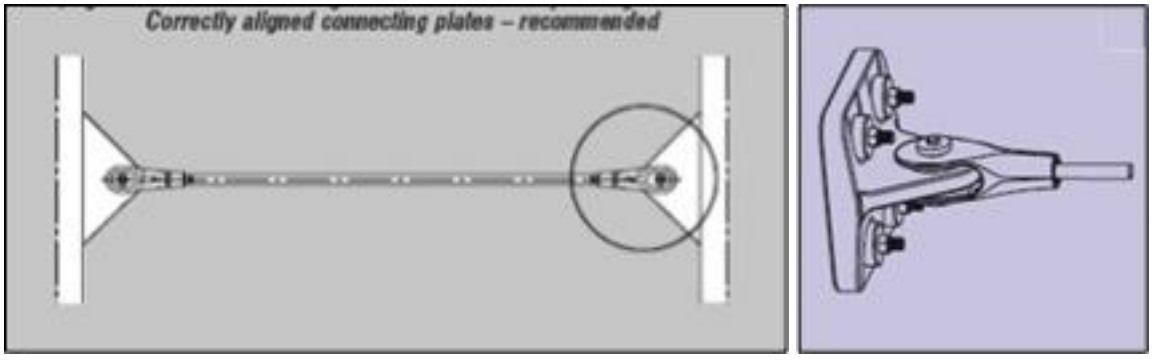

Figure 5.12 Connection of tension rods: tension rod system (left), connection at bridge end (right) (PFEIFER 05/08/2012)

Timber frame: The timber frame consists of one **beam** and **two struts every 1,80m**. After the calculations it has been chosen glulam cross-sections of **215x225mm** for the timber struts and **215x270mm** were chosen for most of the timber beams (more on this topic in chapter 6). During the load-bearing design, the **gap e** between the two arches has been increased from 0,50m to **1,00m**.

Main cable / Restrained cable: For the main or suspension cables and the cable restraining the timber pylon it has been chosen a cable of **40mm** diameter. The main cables are drawn with maximal vertical sag of 80cm. The restrained cable has a length of 4m.

Hanger: The hanger cables suspending the deck along its big curvature have a diameter of **20mm**. They are connected to the main cable of the suspension arrangement (Fig 5.13).

Pylon: Since the pylon takes mostly compression, it will also be designed in **timber**. Therefore, it has been assigned in SAP with one solid wood cross-section of **400mm** diameter. The pylon is drawn with an inclination of $\frac{4}{3}$ (cf. Fig. 5.6).

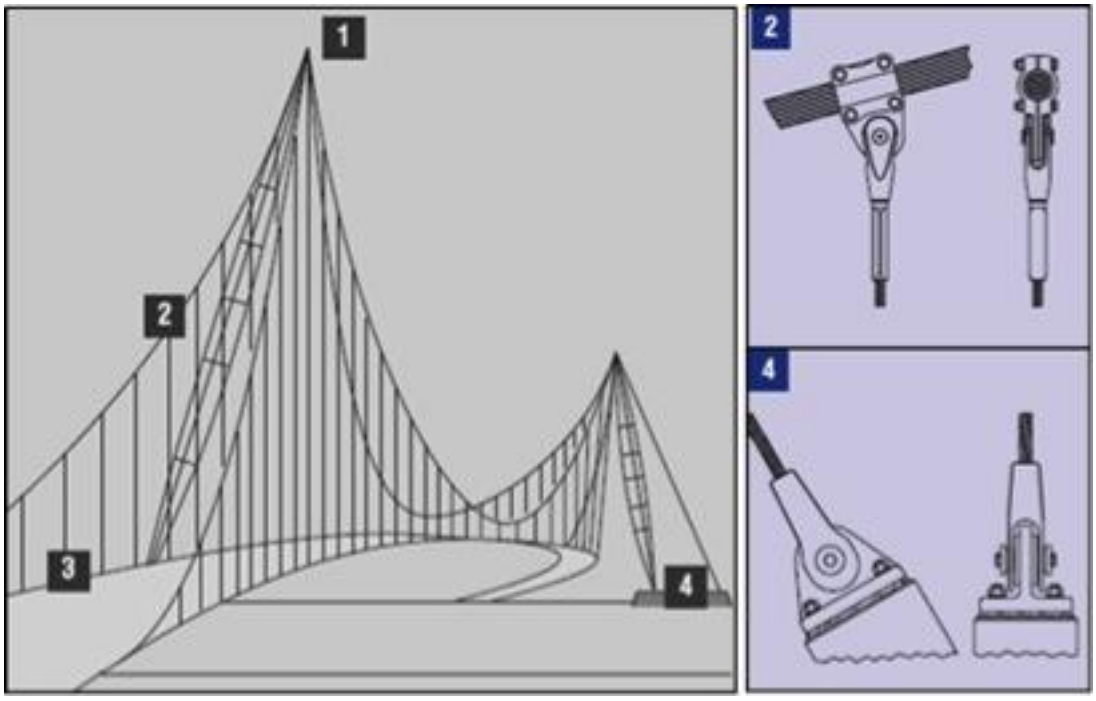

Figure 5.13 Cable system supports the curved bridge deck; (2)Connection of hanger cable to suspension cable, (4)Connection of restrained cable with foundation (PFEIFER 05/08/2012)

5.3.2 Materials

Helpful information about the steel of the tension bars has been found in the brochure and catalogue "Tension members" of the German company Pfeifer. Data sheets helped to find the proper tension members. All following material details (see Table 5.1) have been chosen with the help of Professor Crocetti. The abutments out of concrete are drawn in SAP as single restraints without any material properties.

Property	Timber	Steel (Rod)	Cable
Strength	*Gl 32c*	*S460*	$f_u = 1600 \frac{N}{mm^2}$ $f_y = 0{,}80 \cdot f_u$
Modulus of elasticity	$E_{0,mean} = 13000 \frac{N}{mm^2}$	$E = 210000 \frac{N}{mm^2}$	$E = 210000 \frac{N}{mm^2}$
Density	$\gamma = 4{,}5 \frac{kN}{m^3}$	$\gamma = 78{,}6 \frac{kN}{m^3}$ M36 Type 860	$\gamma = 76{,}9 \frac{kN}{m^3}$ PG20 Type 980

Table 5.1 Summary of materials

5.3.3 Loads

The pedestrian bridge will be subjected to dead and live loads. No other loads are relevant for this study. The snow load is much smaller than the considered live load. The wind load has no significant contact surface. There are no traffic loads under or near the bridge which have to be considered as accidental actions.

Dead load: The dead or permanent load consists of the self-weight of the system, which can be automatically added in the load patterns of SAP.

Live load: As live load was chosen the typical area load $q_k = 5 \frac{kN}{m^2}$ (EN 1991-2:2010-03, 5.3.2.1). This load is applied on the compression beam with width b as uniformly distributed line load:

$$q_k = 5 \frac{kN}{m^2} \cdot b = 5 \frac{kN}{m^2} \cdot 2{,}50m = 12{,}50 \frac{kN}{m}.$$

Load combination:

Ultimate Limit State (ULS): DIN EN 1990/NA:2010-12, 6.4.3.2(3)

Fundamental combination $E_d = \gamma_G \cdot E_{Gk} + \gamma_Q \cdot E_{Qk}$ (5.3.1)

Where: DIN EN 1990/NA:2010-12, Table NA.A.1.2(A)

$\gamma_G = 1{,}35$ the partial factor for unfavorable permanent actions

$\gamma_Q = 1{,}50$ the partial factor for variable action

→ $\boxed{p_d = \gamma_G \cdot g_k + \gamma_Q \cdot q_k = 1{,}35 \cdot g_k + 1{,}50 \cdot 12{,}50}$ $[\frac{kN}{m}]$

Serviceability Limit State (SLS): DIN EN 1990/NA:2010-12, 6.5.3(2)c

Quasi-permanent combination $E_{d,perm} = E_{Gk} + \psi_2 \cdot E_{Qk}$ (5.3.2)

Where: DIN EN 1990/NA:2010-12, Table NA.A.1.1

$\psi_2 = 0{,}60$ the combination factor (category F)

5.4 Parametric study

One important step of this thesis is going to be the load-bearing design of the connections and, for it, the most important parts of the bridge. Therefore, a final model has to be found in order to be able to prove which elements carry the necessary forces and stresses.

During the following parameter study, it is still worked with initial assumptions concerning the section properties. Considerable divergences are: the tensions arch is defined as steel pipe of 150mm diameter and 15mm thickness; the beam elements of the frame are defined as steel profile HEA200 and also the strut elements are defined as steel pipes of 100mm diameter and 10mm thickness. The strong orientation on the Museum's Bridge in Munich leads to these initial cross sections out of steel.

An interesting topic is the position of the connection point between beam struts and steel arch. The distance k and the height h of the pylon are also attractive components for analyzing the effects on the connections. Since both aspects influence the angle of the suspension cables, the hangers, the magnitude of this angle is going to be the third interesting topic.

Basically, two positions of the connection point will be analyzed further. In the first case, the connection point is 0,25m from the outer edge of the deck. The point is located below the timber deck. That means, the distance x from the system's longitudinal axis is 1,00m (Fig. 5.14). In the second case, the connection point is also 0,25m away from the outer edge of the deck, but in this case the point is located outside the timber deck. That means, that the distance x is 1,50m (Fig. 5.15).

These distances are random assumptions just to analyze the differences between the two cases of inner node and outer node position. A noticeable detail of the inner node case is the angle φ_{actual}, which limits the possible angle φ of the hangers.

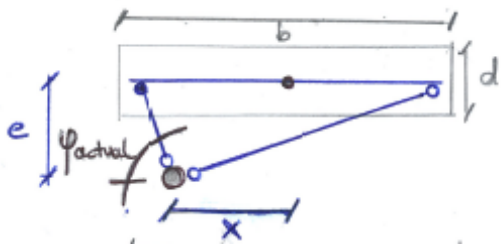

Figure 5.14 Cross-section of inner node case (x=1,00m)

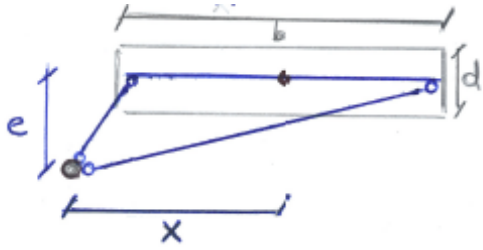

Figure 5.15 Cross-section of outer node case (x=1,50m)

For the parameter study a basic system of the bridge has been modeled. Only the position of the tension arch, the connected struts and hangers will change their positions with respect to

the inner node or the outer node case. In order to simplify the drawing and the system the space arrangement of the cables are left out and replaced by hangers simply restrained at the end instead of being connected to the main cables. The position of these restraints is equivalent to the point where main cables would be connected to the top of the pylon (cf. Fig. 5.6). Furthermore, this position will be varying in its height h (but constant distance k). In this way, the result evaluation of the hangers' angle is included.

The following Figures 5.16 and 5.17 demonstrate the basic systems of the two cases.

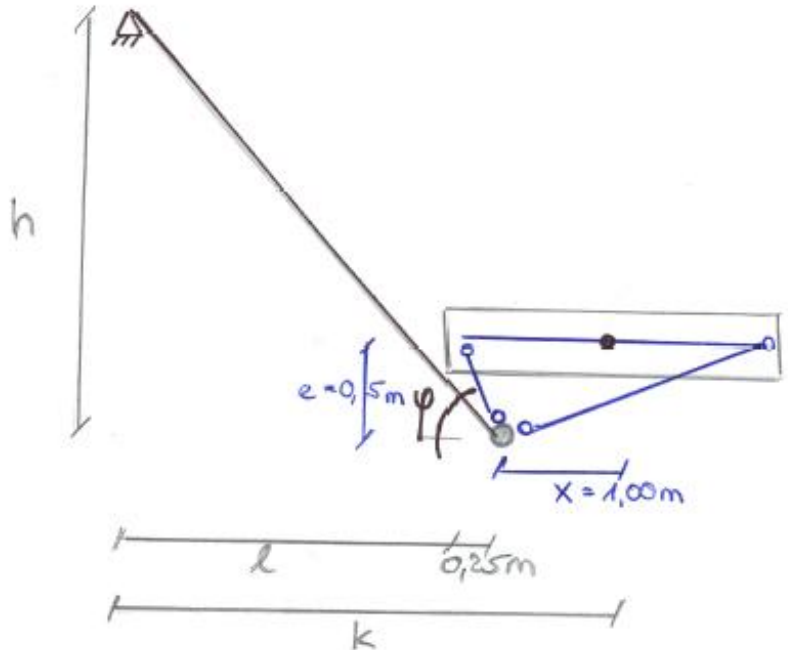

Figure 5.16 Cross-section of inner node basic system

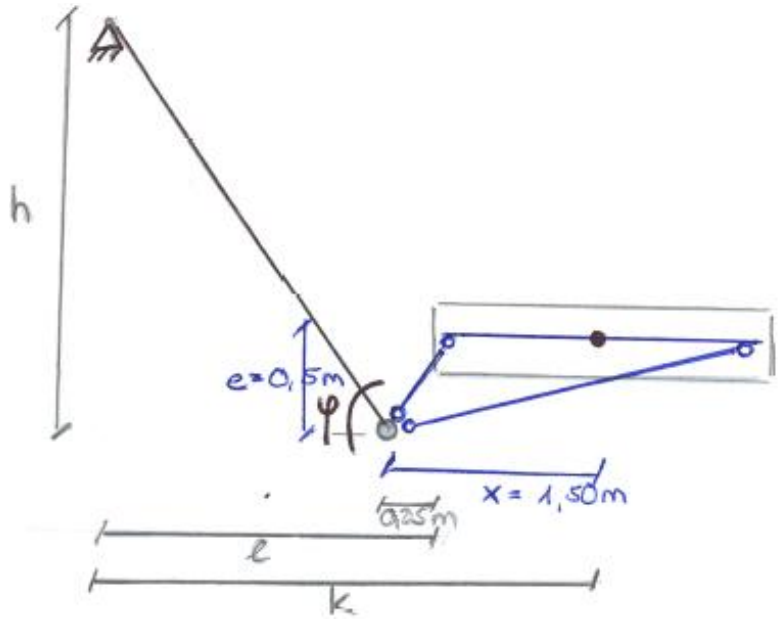

Figure 5.17 Cross-section of outer node basic system

The position of the restraints along the outer edge of the bridge will be varying in its height. So by choosing a fix length k, the distance l of the restraints from the outer edge of the timber deck remains constant. To have enough space for the drawing it has been chosen a distance l of 2,00m.

That means for the varying height h:

- In the System of inner node case (Fig. 5.16):

$$h = (l + 0{,}25m)\, tan\, \varphi \quad [m] \tag{5.4.1}$$

- In the System of outer node case (Fig. 5.17):

$$h = (l - 0{,}25m)\, tan\, \varphi \quad [m] \tag{5.4.2}$$

The aim of this parameter study is to vary the angle φ in both systems to make a statement about the favorable quantity of this angle and to compare the position of the inside node with the node outside the deck system. For this aim, the axial forces of the deck arches and, especially, the amount of tensions in the hangers have to be analyzed in order to observe the general behavior as well as to focus later on the connections. For this study a linear distributed load of $q = 1\frac{kN}{m}$ has been assigned vertically along the compression beam / timber deck.

The software SAP generates the distribution of forces. The results of the hangers should be contrasted with the nominal value of the hangers' tension. The nominal tension F_{aim} in the hangers can be calculated easily through the equilibrium along the length l_E (Fig. 5.18). This influence length l_E corresponds to the distance between the hangers of 1,80m.

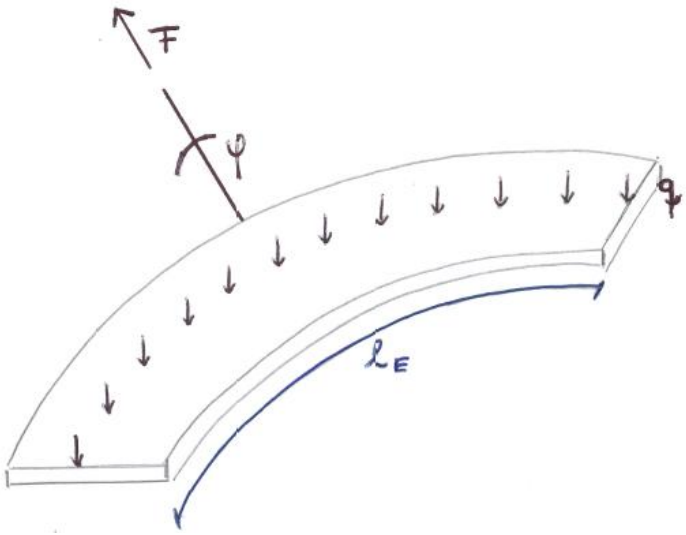

Figure 5.18 Vertical equilibrium of a deck element with the length l_E

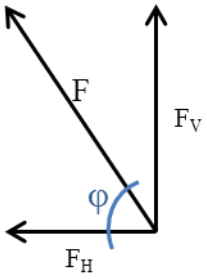

Figure 5.19 Force components of the cable force F depending on the angle φ

The vertical component of the cable force corresponds to the summary of the vertical load q over the length l_E.

$$F_V = Q = q \cdot l_E \tag{5.4.3}$$

As a consequence, the cable force F can be calculated thanks to the angle φ (Fig. 5.19).

$$F_{aim} = \frac{Q}{\sin \varphi} \tag{5.4.4}$$

The horizontal force component is also determined by the angle φ. The more the angle φ increases the smaller is the horizontal component F_H.

With the use of equation (5.4.4):

$$F_H = \cos \varphi \cdot F = \cos \varphi \cdot \frac{Q}{\sin \varphi} = \frac{F_V}{\tan \varphi} \tag{5.4.5}$$

Discussion: inner or outer node case

For both node cases several models have been drawn. The grid points at the end of the hangers which are fixed by the restraints have been moved upwards or downwards to change the height h of the cables (cf. Fig. 5.16 and 5.17). In doing so, the degree of the angle φ changed. It has been started with angles of 10°, 45° and 80°. A model with an angle of 90° would match with the models of chapter 4 which have all fixed restraints along one deck edge.

What became immediately apparent is the fact that for angles φ smaller than a certain value, both the tension steel as well as the compression timber arch are subjected to tension. Since it is not recommendable to have both steel and timber arch charged in tension, it has been investigated under which angle φ_{crit} the forces in the compression beam switch into compression. The uninteresting angles, which are below the angle φ_{crit}, haven't been analyzed further. In the following Excel tables (Fig. 5.20 and 5.21) this change of forces is highlighted in red.

At the same time, the tables show the tension in the hangers from the exterior (‘1’) to the middle cable (‘11’) of half the bridge. Their average value can be checked with the nominal tension force F_{aim}. Of most interest is the maximal value of all cables.

inner node x=1,00m

φ	F_{aim}	tensions in the hangers [kN]													axial forces [kN]		
[°]	[kN]	1	2	3	4	5	6	7	8	9	10	11	average	max	steel	timber	difference
10	10														150	50	100
15	7														125	20	105
20	5														110	1,5	108,5
25	4	0	0	0	1,93	4,43	5,17	5,14	4,83	4,51	4,29	4,17	3,13	5,17	100	-10	90
30	3,7	0	0	0	1,98	4	4,48	4,35	4,04	3,78	3,58	3,5	2,70	4,48	90	-20	70
45	2,5	0	0	0,17	2,84	3,34	3,22	2,94	2,69	2,55	2,48	2,45	2,06	3,34	70	-30	40
...																	
80	1,8	0	0	0,8	1,78	2,1	2,14	2,1	1,95	1,87	1,81	1,79	1,49	2,14	55	-45	10

Figure 5.20 Excel table – axial forces of the inner node models; x=1,00m; φ_{crit}=25°; φ_{actual}=63°

outer node x=1,50m

φ	F_{aim}	tensions in the hangers [kN]													axial forces [kN]		
[°]	[kN]	1	2	3	4	5	6	7	8	9	10	11	average	max	steel	timber	difference
10	10														155	40	115
15	7														130	10	120
20	5	0	0	0	0,42	4,76	6,04	6,25	5,98	5,62	5,32	5,17	3,60	6,25	120	-10	110
25	4	0	0	0	0,54	4,27	5,16	5,18	4,87	4,52	4,27	4,15	3,00	5,18	110	-20	90
30	3,7	0	0	0	0,64	3,91	4,55	4,47	4,15	3,84	3,63	3,53	2,61	4,55	100	-30	70
45	2,5	0	0	0	0,87	3,08	3,3	3,12	2,85	2,63	2,5	2,46	1,89	3,3	90	-45	45
...																	
80	1,8	0	0	0	1,49	2,15	2,25	2,15	2	1,88	1,8	1,77	1,41	2,25	70	-60	10

Figure 5.21 Excel table – axial forces of the outer node models; x=1,50m; φ_{crit}=20°

It is obvious that with increasing angle φ the tension in the hangers decrease. Remembering the distribution of the cable force into its components (cf. Fig. 5.19) it is clear how much higher the hangers’ value becomes if the angle φ decreases. The reason therefore is the increasing influence of the horizontal force component F_H (eq. 5.4.5).

The jump from 45° to 80° does not make such a big difference any more. The results of angles smaller than 45°, on the other hand, vary a lot. That is the reason for having taken a closer look on the systems with angles from the critical angle φ_{crit} = 45°.

Not only the tension in the hangers but also the axial forces in the tension arch (“steel”) and the compression beam (“timber” deck) are decreasing with an increasing angle φ. In fact, the values decrease and the value difference between these two axial forces becomes less.

What could be the reason for this effect?

Again, equilibrium along the length l_E is used to explain the distribution of forces (Fig. 5.22). The influence length l_E corresponds the distance between the hangers of 1,80m.

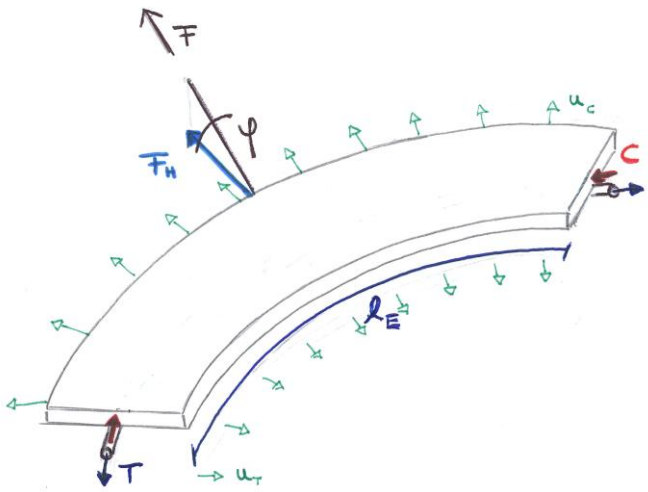

Figure 5.22 Horizontal equilibrium of a deck element with the length l_E

The horizontal component of the cable force F_H is in a balance with the radial deviation forces u_C and u_T.

As a summary over the length l_E:

$$F_H + u_C \cdot l_E - u_T \cdot l_E = 0 \tag{5.4.6}$$

$$\rightarrow\ u_C \cdot l_E = u_T \cdot l_E - F_H$$

The conclusion of the equation (5.4.6) is: If the horizontal cable force component F_H becomes relatively small, the radial forces u_C and u_T converge towards the same value. As already mentioned, the horizontal cable force component F_H decreases if the angle φ is increasing.

In the case of $90° > \varphi \geq 80°$ is $F_H \approx 0$. As a consequence:

$$u_C \cdot l_E \approx u_T \cdot l_E \tag{5.4.7}$$

The horizontal force components of the hangers have a less strong impact on the system. That is the reason why the value difference between the two axial forces C and T also becomes less.

All in all, it can be said that it is desirable to choose an angle φ as close to 90° as possible.

This result was predictable from the beginning. More interesting is the question which case is more favorable: the case where the connection point of tension arch, timber frame and hanger is located just below the deck with x=1,00m or the case where this connection point is located outside the deck structure with x=1,50m.

In order to understand the SAP results it should be understood the consequence of situating the connection point farer away from the longitudinal deck axis. Taking a look on the equilibriums of the cross-sections makes it more obvious.

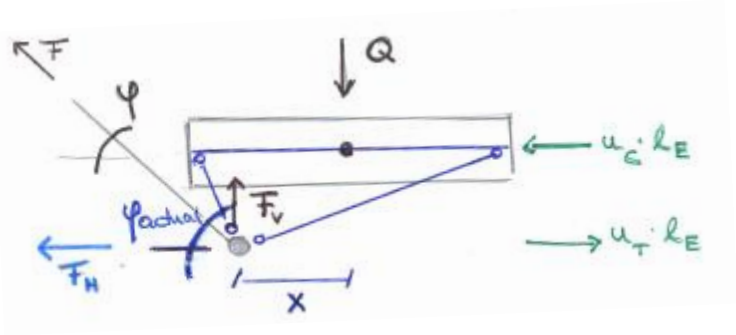

Figure 5.23 Equilibrium in cross-section of inner node case (x=1,00m) over the length l_E

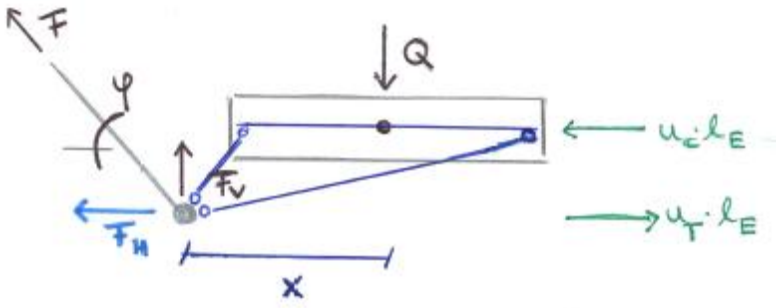

Figure 5.24 Equilibrium in cross-section of outer node case (x=1,50m) over the length l_E

Figures 5.23 and 5.24 demonstrate how the inner pair of radial forces counteracts the torsional moment created by vertical load Q and horizontal cable force F_H. Moving the position of the connection point outward increases the distance x from the longitudinal deck axis which, at the same time, represents the lever arm of the vertical load Q about the connection point. In other words, by increasing the lever arm x the deck structure suffers a higher loading.

Now it can be looked back on the Excel tables of Figures 5.20 and 5.21. The tables demonstrate clearly that the axial forces for the same hanger angle are in the case of the outer node always higher than in the case of the inner node. Even for φ=80° are higher: 70 and −60kN compared to 55 and −45kN.

In the end, a conclusion is found concerning the position of the node. Besides the target of choosing an angle φ as close to 90° as possible, it will be continued with the case of the inner node. All together provides smaller values along the deck structure as well as minor tension in the hangers.

There is just one more point that should be mentioned here. Changing the position of the connection point goes along with moving the position of the tension arch underneath the compression frame and increasing or decreasing the aperture angle φ_{actual}. The decision of the inner node case also means to accept the fact that an aperture angle φ_{actual} limits the possible angle φ of the hangers (cf. Fig. 5.23). But the jump from 45° to 80° does not make such a big difference any more. That means it could be handled with an angle φ of around 45°. In the case of x=1,00m the aperture angle φ_{actual} is 63°. Consequently, the aperture angle φ_{actual} would be big enough for the angle φ of the anchored hangers.

Discussion: variety of inner node position

The investigation whether a minor distance of the lever arm x could improve the distribution of forces even more, did not achieve better results.

As the following tables (Fig. 5.25 and 5.26) illustrate, the critical angle φ_{crit} increases when the lever arm x is chosen smaller to random examples like x=0,75m or 0,25m. This fact is totally counterproductive since the possible angle φ is already determined more by the decreasing aperture angle φ_{actual}. Hence, the inner node case with x=0,25m is excluded from further proceeding (Fig. 5.26).

inner node x=0,75m

α	F_{target}	tension in the hangers [kN]													axial forces [kN]		
[°]	[kN]	1	2	3	4	5	6	7	8	9	10	11	average	max	steel	timber	difference
10	10																
15	7																
20	5														105	10	
25	4	0	0	0	2,68	4,59	5,14	5,06	4,77	4,47	4,26	4,16	3,19	5,14	90	-3	87
30	3,7	0	0	0	2,7	4,15	4,56	4,29	3,99	3,74	3,58	3,51	2,77	4,56	85	-10	75
45	2,5	0	0	0,21	2,57	3,18	3,15	2,92	2,7	2,57	2,5	2,47	2,02	3,18	70	-25	45
...																	
80	1,8																

Figure 5.25 Excel table – axial forces of the inner node models; x=0,75m; φ_{crit}=25°; φ_{actual}=45°

inner node x=0,25m

α	F_{target}	tension in the hangers [kN]													axial forces [kN]		
[°]	[kN]	1	2	3	4	5	6	7	8	9	10	11	average	max	steel	timber	difference
10	10																
15	7																
20	5																
25	4																
30	3,7														65	10	
45	2,5	0	0	2	2,84	2,99	2,89	2,73	2,61	2,54	2,51	2,5	2,15	2,99	45	-2	43
...																	
80	1,8																

Figure 5.26 Excel table – axial forces of the inner node models; x=0,25m; φ_{crit}=45°; φ_{actual}=27°

Figure 5.25 shows no big differences compared to Figure 5.20. In the case of an angle φ of 45° the results for the tension in the hangers are in the two inner node positions nearly the same (Fig. 5.27).

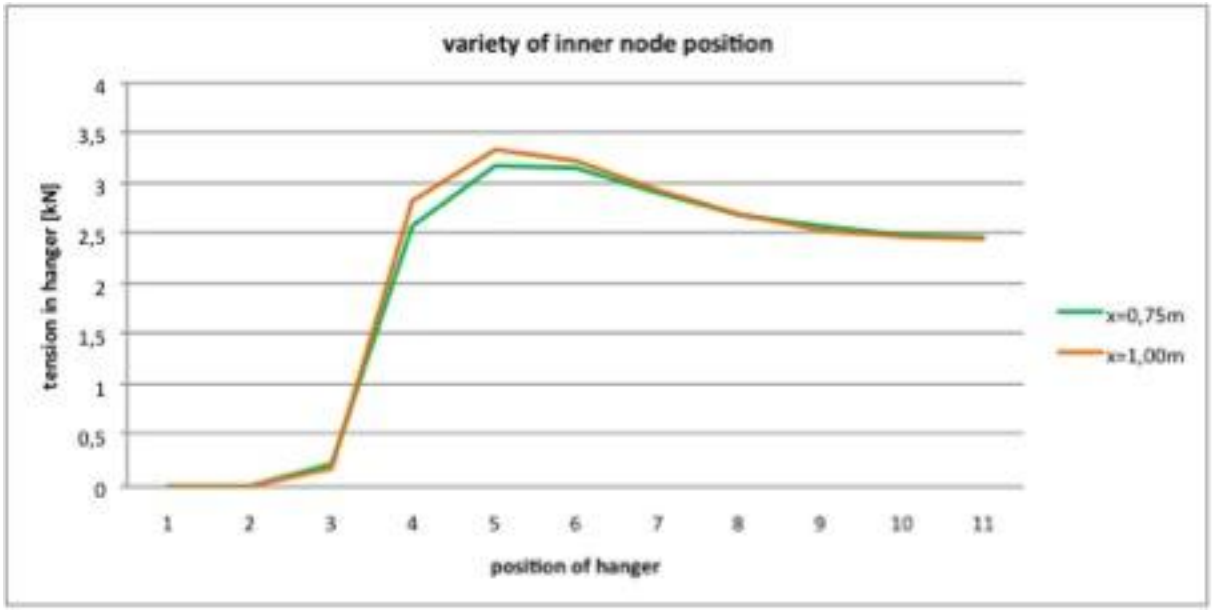

Figure 5.27 Tension in the hangers: inner node case x=0,75m compared to inner node case x=1,00m; $\varphi = 45^{\circ}$

Consequentially, it seems as if it is not worthwhile to continue with an inner node case model where the distance x is smaller than 1,00m.

Derivation of the correlation between critical angle φ_{crit} and distance x

It has already been mentioned that a certain angle φ_{crit} arouses interest. All angles being smaller than this angle cause tension not only in the tension steel arch but also in the compression timber beam. In the case of smaller distances x, this angle φ_{crit} even increases in value. Since this is an obvious fact of the data's results, the reason for this correlation should be figured out in the following step.

Again, equilibrium along the length l_E (distance between the hangers of 1,80m) is used to explain the distribution of forces (Fig. 5.28).

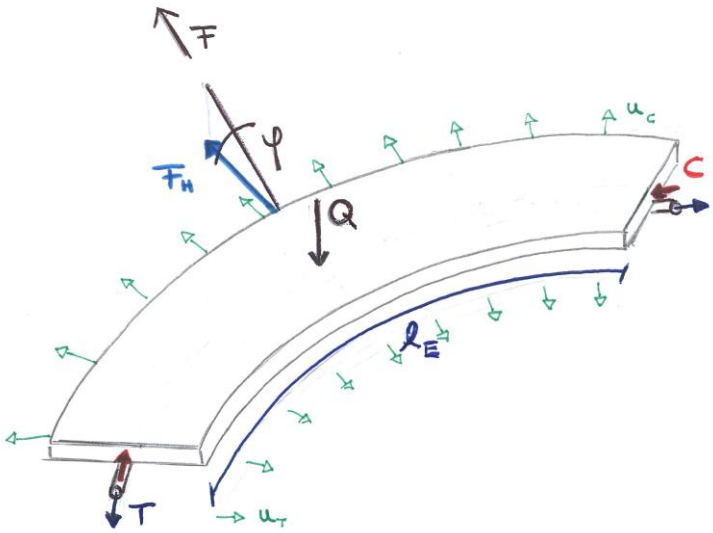

Figure 5.28 Total equilibrium of a deck element with the length l_E

$$\sum V = 0: \qquad Q = q \cdot l_E = F_v \tag{5.4.8}$$

$$\sum H = 0: \qquad F_H + u_C \cdot l_E - u_T \cdot l_E = 0 \tag{5.4.9}$$

Considering equation (5.4.5) with equation (5.4.9):

$$F_H = \frac{F_V}{\tan\varphi} = \frac{Q}{\tan\varphi} = \frac{q \cdot l_E}{\tan\varphi} \tag{5.4.10}$$

Just to remind, equation (4.1.9) says:

$$q_R = \frac{C}{R}$$

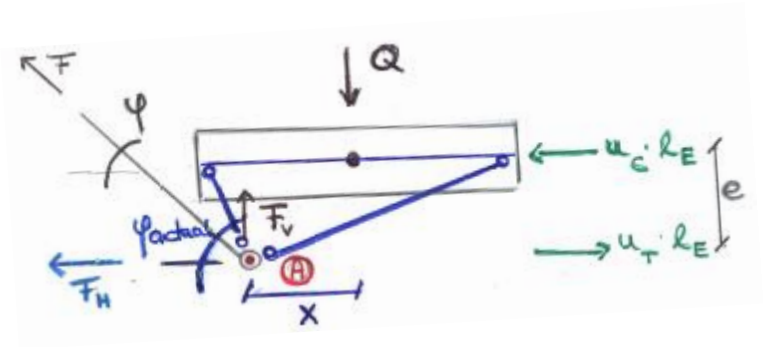

Figure 5.29 Equilibrium in cross-section of inner node case over the length l_E depending on x and e

$$\sum\nolimits_A^+ M = 0: \qquad Q \cdot x - u_C l_E \cdot e = 0 \tag{5.4.11}$$

$$\rightarrow u_C = \frac{Q \cdot x}{l_E \cdot e}$$

Considering equation (5.4.8):

$$\boxed{u_C = q \cdot \frac{x}{e}} \tag{5.4.12}$$

The conclusions are as follows:

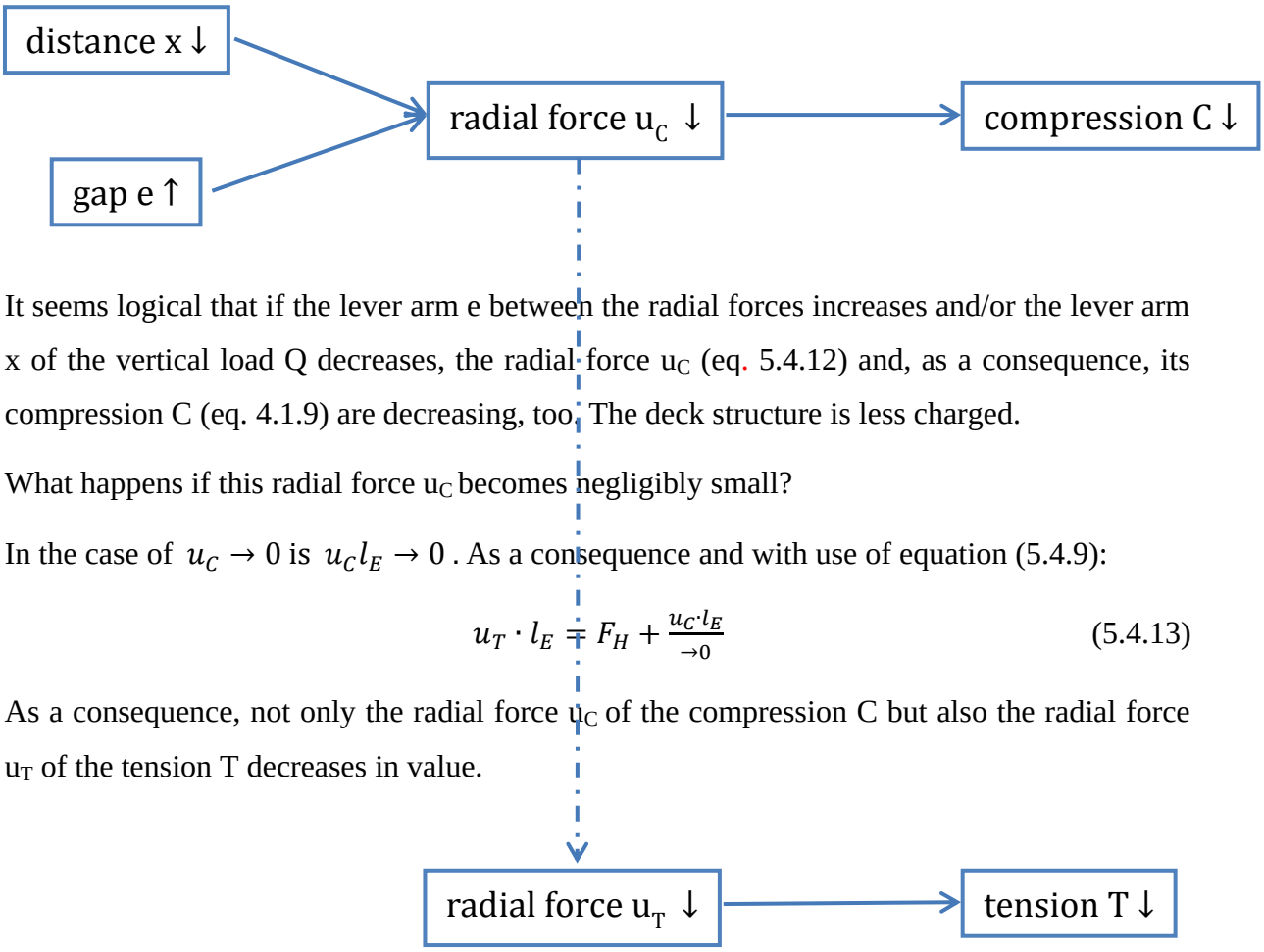

It seems logical that if the lever arm e between the radial forces increases and/or the lever arm x of the vertical load Q decreases, the radial force u_C (eq. 5.4.12) and, as a consequence, its compression C (eq. 4.1.9) are decreasing, too. The deck structure is less charged.

What happens if this radial force u_C becomes negligibly small?

In the case of $u_C \to 0$ is $u_C l_E \to 0$. As a consequence and with use of equation (5.4.9):

$$u_T \cdot l_E = F_H + \underbrace{u_C \cdot l_E}_{\to 0} \tag{5.4.13}$$

As a consequence, not only the radial force u_C of the compression C but also the radial force u_T of the tension T decreases in value.

But where is the correlation between critical angle φ_{crit} and distance x? Why or when does the radial force u_C become negative, in other words, act in precisely the opposite direction to cause tension instead of compression in the compression timber beam?

Solving equation (5.4.9) for the radial force u_C:

$$u_C \cdot l_E = u_T \cdot l_E - F_H \tag{5.4.14}$$

With use of equation (5.4.10):

$$u_C \cdot l_E = u_T \cdot l_E - \frac{q \cdot l_E}{\tan \varphi} \tag{5.4.15}$$

$$\rightarrow u_C = u_T - \frac{q}{\tan \varphi}$$

In the case of $u_C < 0$ is $(u_T - \frac{q}{\tan \varphi}) < 0$. As a consequence:

$$\boxed{u_T < \frac{q}{\tan \varphi}} \tag{5.4.16}$$

It is obvious that we are getting closer to the explanation. The angle φ has to be brought in addition. The following graph (Fig. 5.30) shows a part of the tangent function. The interesting part of the angle φ between 0° to 45° is highlighted in red.

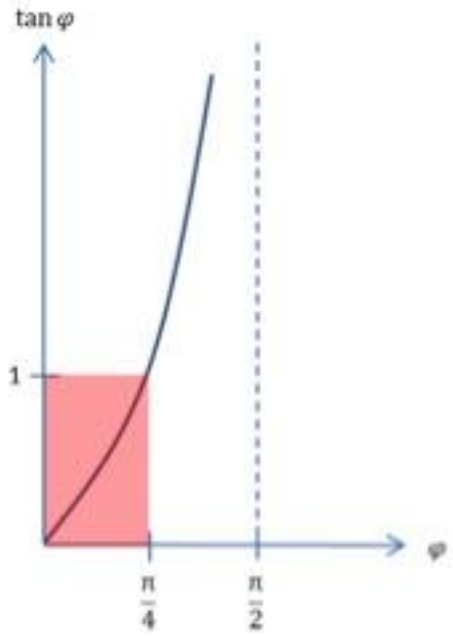

Figure 5.30 Sketched illustration of the tangent function

The conclusion is as follows:

Equation (5.4.16) can be discussed as follows:

The smaller the angle φ becomes the bigger is the ratio $\frac{q}{\tan\varphi}$ (Fig. 5.30) and, as a consequence, it is easier for the radial force u_T to be smaller than this ratio $\frac{q}{\tan\varphi}$ (eq. 5.4.16). It is valid $u_C < 0$. The radial force u_C acts in precisely the opposite direction and causes tension instead of compression in the compression timber beam. Otherwise, it can be observed that under a certain big critical angle φ_{crit} the tension in the compression timber beam switches again into compression. That means the radial force u_C of the compression C acts again in the right direction and it is valid $u_C > 0$. In Figure 5.31 this switch can be observed as zero point of the φ-C-function (data of the case x=1,00m). It should be recalled that for reasons of simplification a linear distributed load of $q = 1\frac{kN}{m}$ has been assigned vertically along the compression beam / timber deck.

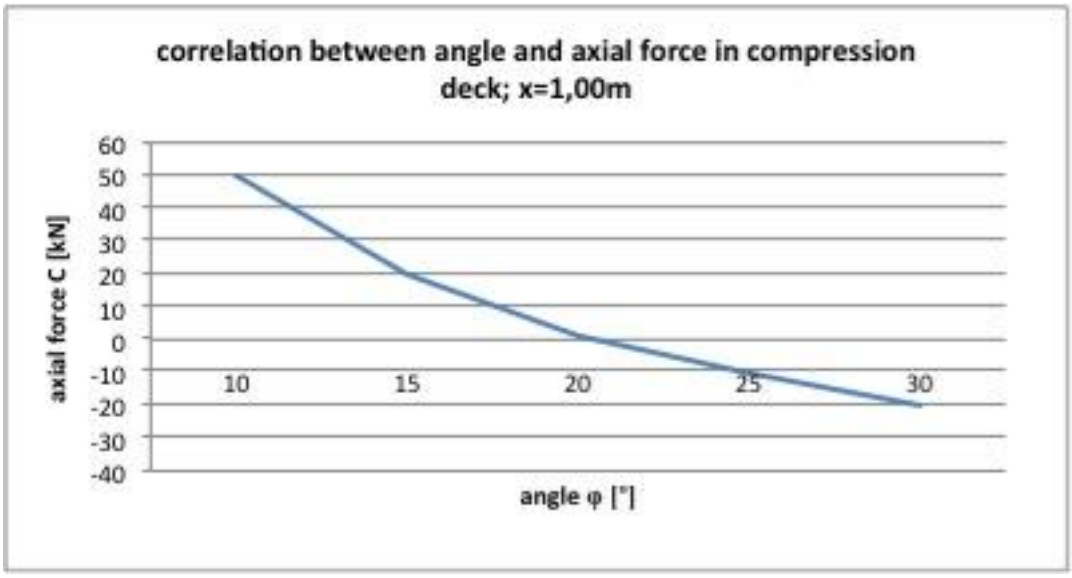

Figure 5.31 Demonstration of the correlation between angle φ and axial force C with the data of the inner node case x=1,00m; $\varphi_{crit} \approx 28^{\circ}$ (cf. Fig. 5.20)

Adding the conclusions of page 73, it can be said that the probability of the radial force u_T to be smaller than the ratio $\frac{q}{\tan \varphi}$ is even higher if the distance x decreases in value.

In order to have a tolerably high value of the radial force u_T and in order to have a positive radial force u_C it is worthwhile to choose a bigger distance x. An increased distance x causes higher stresses in the deck structure, in other words, higher values of radial forces u_C and u_T and decreases the probability of the radial force u_T to be smaller than the ratio $\frac{q}{\tan \varphi}$ (eq. 5.4.16). In turn, the angle φ does not need to have such a high value any more to assure the switch from tension into compression in the compression timber beam. Increasing the distance x causes even smaller critical angles.

During the modeling process of the parameter study the values of the critical angles have been estimated roughly (cf. Fig. 5.20, 5.21, 5.25 and 5.26). For the case x=1,00m it can more accurately be read out from Figure 5.31 under which angle φ the axial load in the compression deck is equal to zero. This critical angle φ_{crit} has a value around 21° (estimated value: 25°).

A graph about the correlation between distance x and critical angle φ_{crit} would be able to demonstrate the progression of the angle more vivid. So as to gain this visualization, graphs about correlations between angle φ and axial forces have been made with the data of the other distances x (cf. Appendix A). As a result, the more accurate values of the critical angles could be read out. The progression is shown in Figure 5.32. What is important here is not the quantity of the results but the regressive tendency.

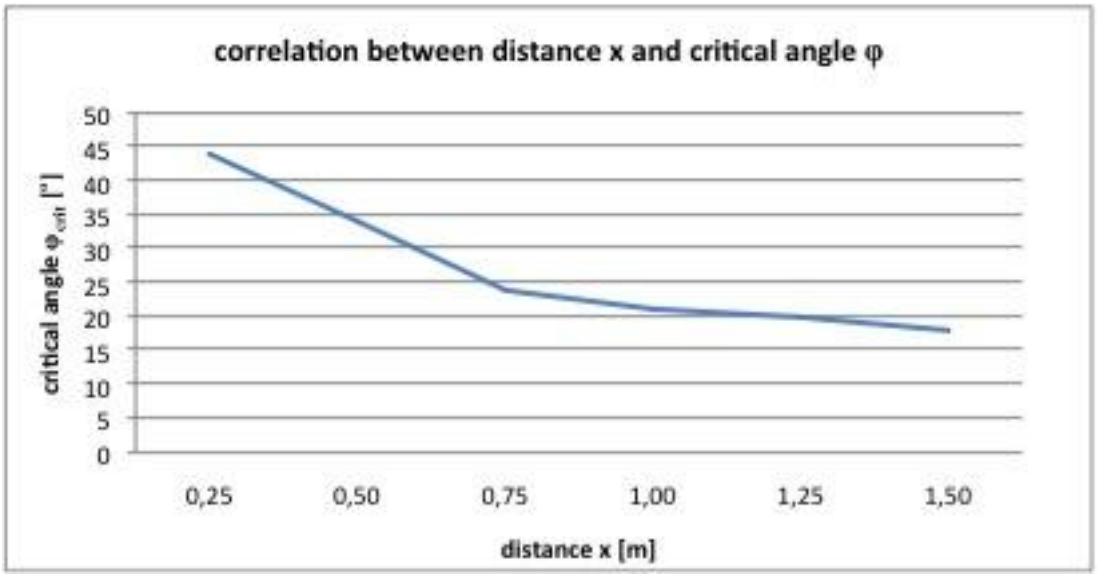

Figure 5.32 Demonstration of the correlation between distance x and critical angle φ_{crit}

In summary, the following became clear: In order to prevent the situation $u_C < 0$ the angle φ has to be bigger than the critical angle φ_{crit}. The structure is able to counteract this switch of forces from compression to tension in a better way if the distance x is kept relatively big.

5.5 Final model

It will be continued with an inner node position of x=1,00m. The outer node position of x=1,50m had clearly higher axial forces in the whole structure. This result is highly advantageous for the durability of the timber frame structure. In the case of the inner node position, the whole timber frame along with its connections lies below the timber deck. The massive timber deck protects beam, struts and especially the important connection point between struts, tension arch and hanger against rainfall, similar to a roof.

An inner node position of less than x=1,00m (the examples were x=0,75m and 0,25m) had obvious disadvantages concerning an increasing critical angle φ_{crit} and a decreasing aperture angle φ_{actual}. Since the results did not noticeably improve in value, it does not seem worthwhile to minimize the distance x further.

A hangers' angle φ of 45° is chosen. The tension and deck structure's axial forces of higher angles showed no significant difference. In the inner node case of x=1,00m, the aperture angle φ_{actual} limited by the beam frame has 63 degrees. An angle φ of about 45° is small enough to be able to connect the hangers with the steel tension arch.

At the beginning, the height h of the pylon as well as its distance k from the deck's axis has been 4m. Drawing the hangers for the final model in SAP made it clear that the external hangers could not be connected to the main cables without "passing through" the timber deck. That is why the distance k was enlarged to 5m and the final restraints of the main cables are moved 0,50m away from the outer edge of the timber deck. The idea was to displace the restraints of the main cables about the space the external hangers need to pass the timber deck without difficulties and to give them an additional buffer space of around 400cm (*Crocetti 2012*).

Figures 5.33 and 5.34 aim to outline the actual system dimensions (scale 1:500).

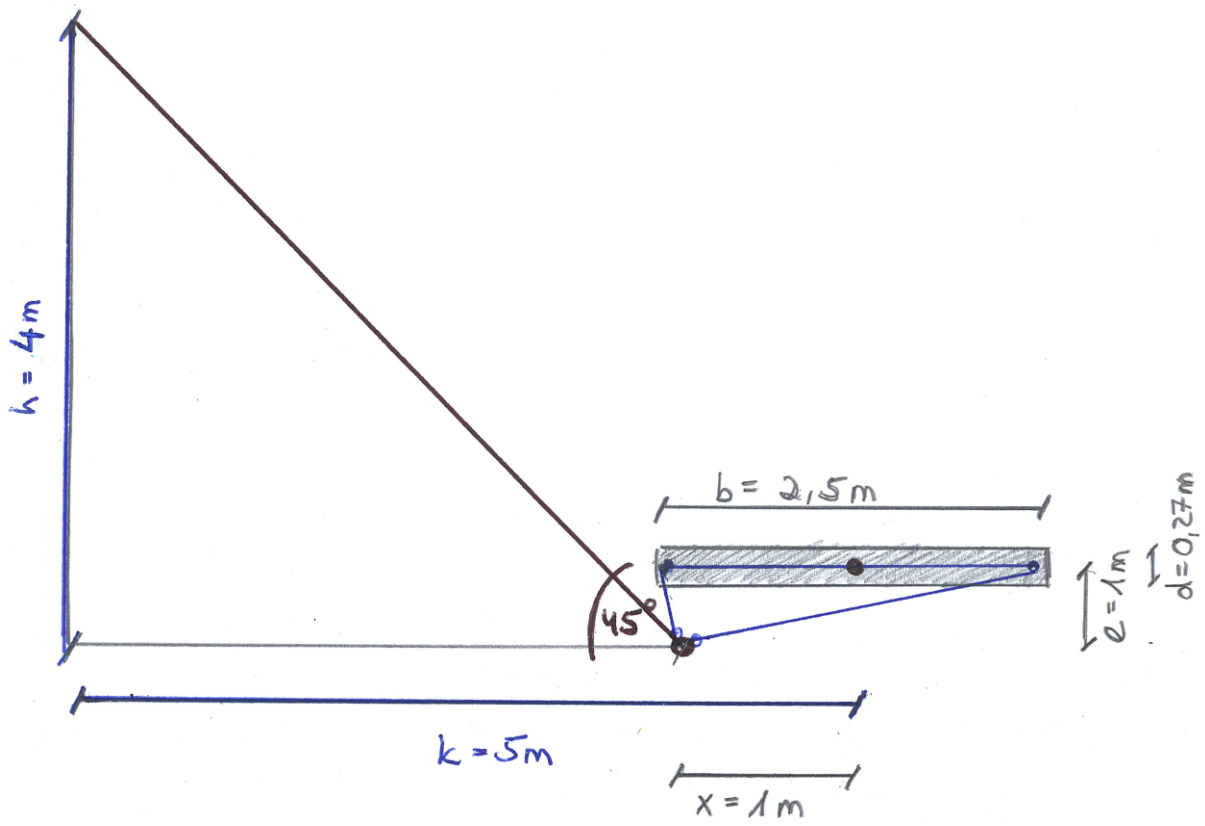

Figure 5.33 Draft: Cross-section at the height of the innermost hanger near the pylon

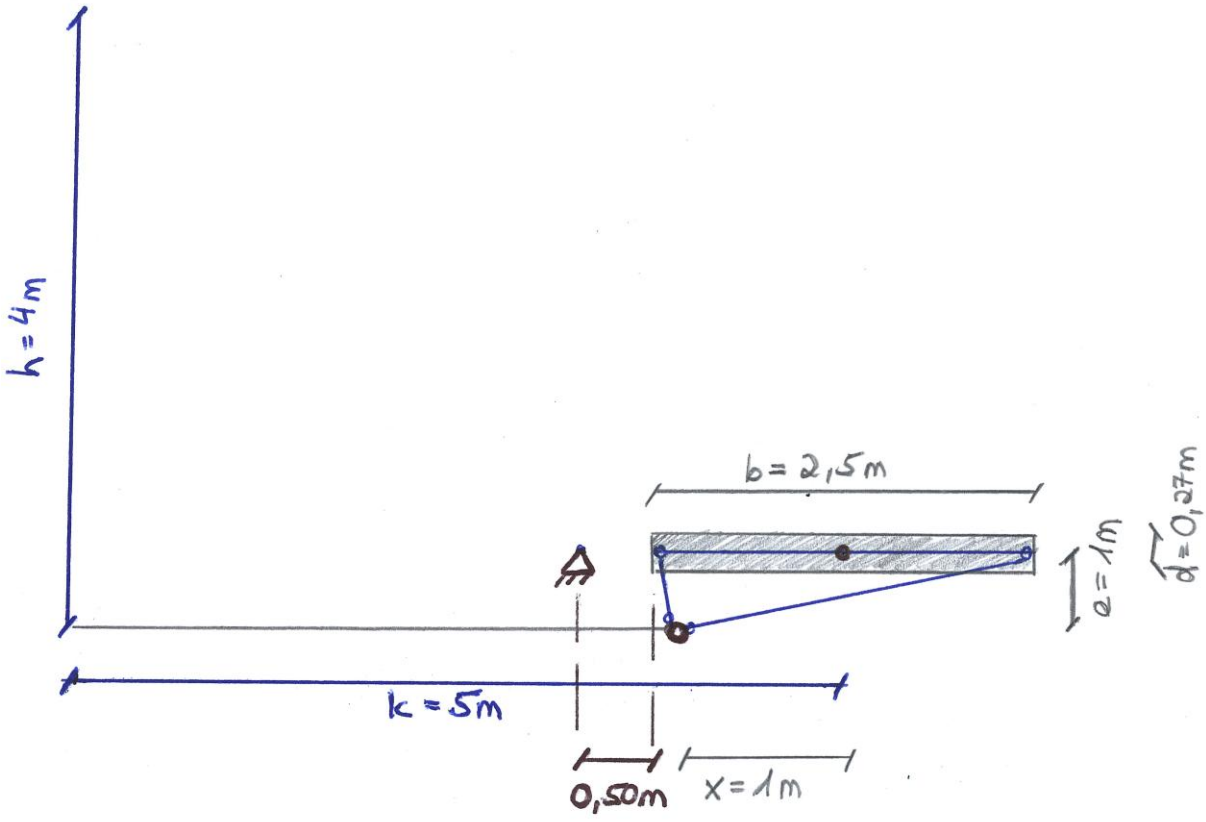

Figure 5.34 Draft: Cross-section with the restraint of one main cable at the end of the bridge

6. Load-bearing design of parts of the "A Pilgrim's Walk" Bridge

During the load-bearing design process it has been worked with European standards. Common rules for the design of timber structures and rules for the design of timber bridges are summarized in the newest version of Eurocode 5: **DIN EN 1995-1-1:2012-10** and **DIN EN 1995-2:2010-12**. Unless specified in the text, the requirements are taken out from this Eurocode 5 (EC5). Since the thesis will be presented in Germany, the **National Annex of Germany** is used in addition: **DIN EN 1995-1-1/NA:2012-12** and **DIN EN 1995-2/NA:2011-08**.

First, it seems useful to define the basics of the calculations. The design values of the loads and load combinations are defined in subchapter 5.3.3. Unless specified in the text, the SAP-results of the Ultimate Limit State (ULS) are used. The design values of material properties are defined by the partial factor method, as well.

According to EC5-1-1, 2.4.3(1), the design value R_d of a resistance (load-carrying capacity) shall be calculated as:

$$R_d = k_{mod} \cdot \frac{R_k}{\gamma_M} \quad (6.0.1)$$

Where: R_k characteristic values of a resistance property

γ_M=1,30 partial factor for glulam — EC5-1-1/NA, Table NA.2

k_{mod}=0,90 modification factor — EC5-1-1, Table 3.1

service class 2 "protected" — EC5-2/NA, NCL NA.2.3.1.3

load-duration class "short term action" — EC5-2/NA, Table NA.1

Values for strength properties of GL 32c are taken from EN 1194:1999-10, Table 2:

Flexural strength $f_{m,g,k} = 32{,}0 \frac{N}{mm^2}$ (6.0.2)

Tensile strength $f_{t,0,g,k} = 19{,}5 \frac{N}{mm^2}$ (6.0.3)

$f_{t,90,g,k} = 0{,}45 \frac{N}{mm^2}$ (6.0.4)

Compressive strength $f_{c,0,g,k} = 26{,}5 \frac{N}{mm^2}$ (6.0.5)

$f_{c,90,g,k} = 3{,}0 \frac{N}{mm^2}$ (6.0.6)

Shear strength $f_{v,g,k} = 3{,}2 \frac{N}{mm^2}$ (6.0.7)

6.1. Distribution of loads in the timber frame

As demonstrated in chapter 5, timber beam frames are situated along the curve every 1,80m (Fig. 6.1). This means that there are in total 22 timber frames; in other words, 11 frames to the right and 11 to the left of the pylon. Since the two halves of the one curved structure are symmetric to each other, it will be focused on one half of the bridge. Therefore, the results are compared from the exterior frame (‘1’) to the middle frame (‘11’).

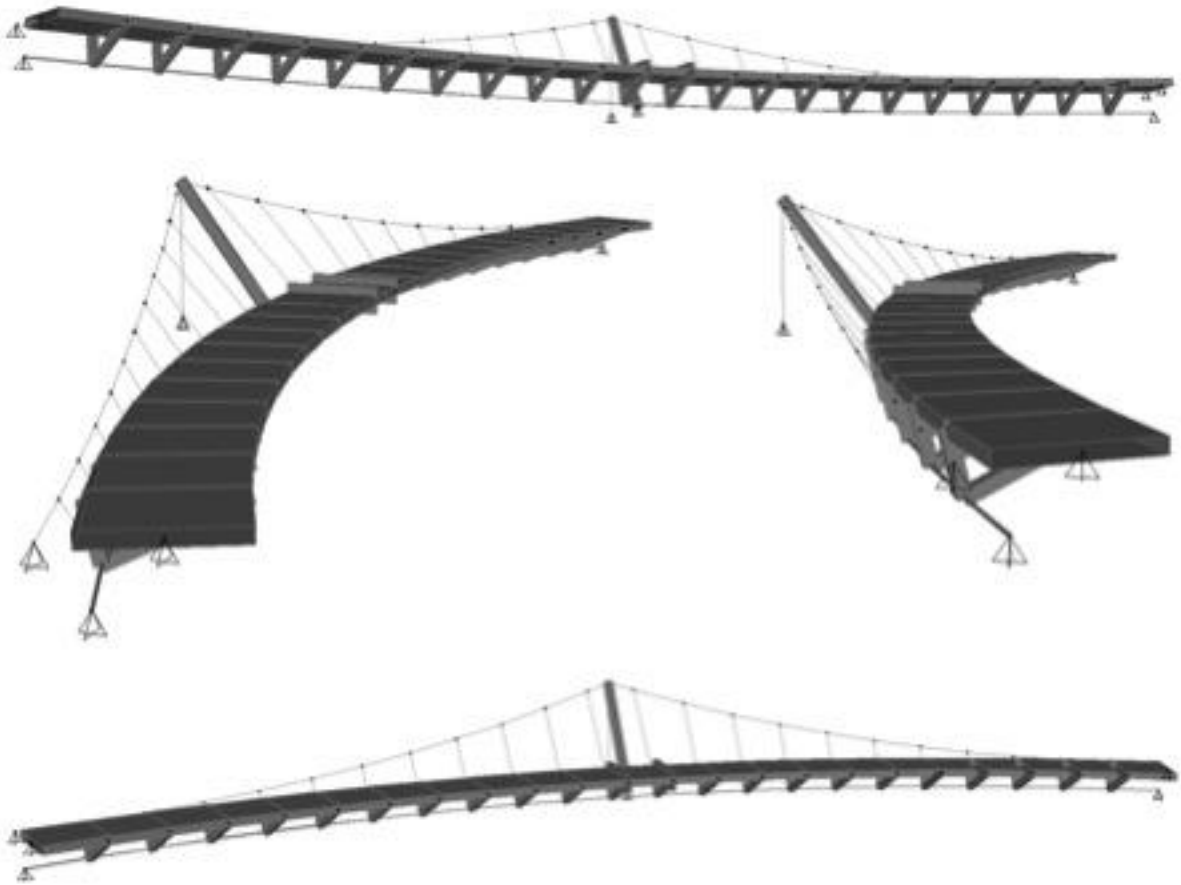

Figure 6.1 SAP-model from various perspectives: extrude view

The bridge is loaded homogenously over the timber deck by dead and live load (cf. subchapter 5.3.3). It turned out that the most loaded frame of the half curve is the middle frame (‘11’) which lies directly by the pylon. The forces seem to accumulate in the middle of this one curved bridge. The second most loaded frame is the exterior frame. A stiffening effect near fixed restraints seems to lead to higher forces in parts of the bridge structure.

The distribution of loads is more complicated than expected. As examined in chapter 4, the statics have always to be considered in a three-dimensional way. In that way, the beam of the

timber frame is not just a simply supported beam but is influenced by the connected timber deck, as well.

At first, Figure 6.2 simulates just the triangle of the timber frame. It is expected to see tensile forces as axial forces in the timber beam. The pinned timber struts are mostly loaded in compression.

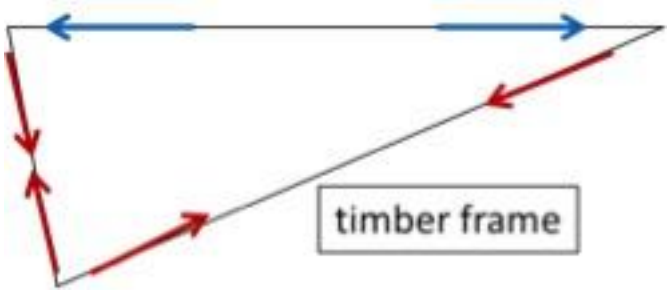

Figure 6.2 Axial forces in timber frame

Figure 6.3 shows the timber frame as triangle, the timber deck as beam element (like modeled in SAP) and the cable of the hanger connected to the struts of the timber frame.

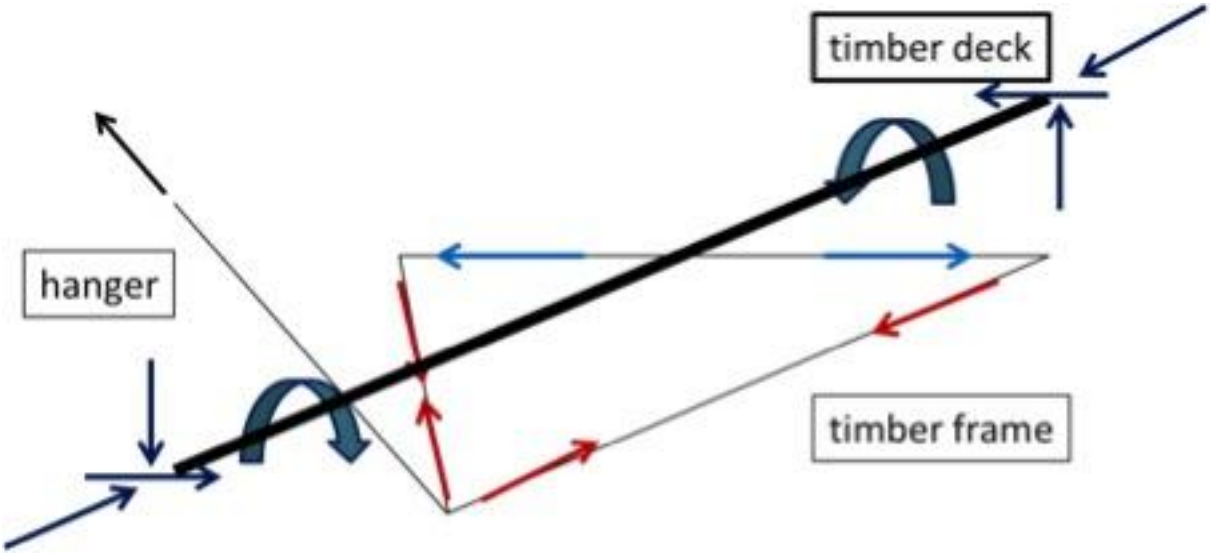

Figure 6.3 Influence of the timber deck's section forces on the timber beam

Taking the three-dimensional effect into account, it is clear that the torsion and the forces in the deck influence the distribution of loads in the beam of the timber frame. That is the reason why the distribution of tension, shear and bending is changing over the whole half curve of the bridge. While the struts of the other frames are in compression, in the cases of most and second most loaded frame always one strut is in tension. The static systems of these two frames differ even more from the classical system of a simply supported beam.

The section forces of the most and second most loaded timber beam are as follows (Fig. 6.4).

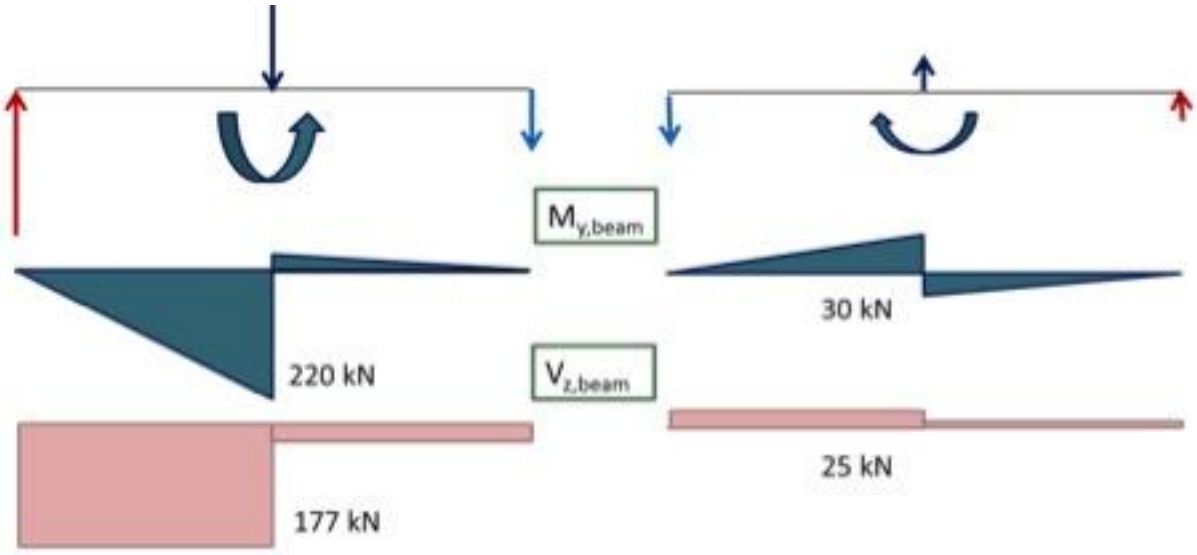

Figure 6.4 Contribution of forces of the middle (left) and the exterior (right) timber beam

By comparing these two most loaded beams, it becomes obvious how most of the forces are cumulated in the center of the bridge. Figure 6.4 demonstrates how the section forces' values of the exterior beam are about 1/7 of the values of the middle beam. In both cases, the torsion of the timber deck causes a jump in the bending moment diagram. Vertical forces cause a jump in the shear force diagram. In total, the systems are in equilibrium.

It must be considered that in this SAP-model the timber deck is modeled with beam elements along the system line. The timber deck is located in one point of the timber beam. As a consequence, SAP shows its influence as a jump just in one point. In reality the timber deck is connected to the beam over the whole width of the deck. The timber deck influences the distribution of loads in the timber beam evenly over the whole width. As a matter of fact, a distributed vertical load as well as a distributed torsional moment would be transmitted from the deck into the beam. The "real" section forces have a slope instead of a jump.

What are the consequences for the load-bearing design process?

For the load-bearing design process the maximal values are of interest and not the real slope of the distribution. Consequently, it is sufficient to use these results (*Crocetti 2012*).

As the struts are subjected to tension always in one timber frame of half bridge structure, during the connection design process it has to be considered that connections and junctions have to take this tension.

6.2. Timber frame

The timber frame is a triangle of beam elements every 1,80m along the curved structure. It is connected to the deck from below and is composed of timber beam and timber struts.

6.2.1 Timber beam

It will be started with the most loaded timber frame. This innermost timber beam is subjected to the following section forces (Table 6.1).

Section force	Symbol	Maximum value
Axial tension	$\mathbf{F_{t,Ed}}$	**44,3 kN**
Shear force	$\mathbf{F_{v,Ed}}$	**176,8 kN**
Bending Moment	$\mathbf{M_{y,Ed}}$	**220,3 kNm**

Table 6.1 Section forces of middle timber beam

A striking aspect is the high shear. Compared to the second most loaded frame, this shear force is 7 time higher (cf. Fig. 6.4).

Quite unusual for a timber structure, this shear force has the highest influence on the structural design. For this reason, it is of interest to compare the necessary cross-section of this timber beam with the cross-section needed by another timber beam of the curved structure.

Therefore, the calculations are also done for the second most loaded timber beam. This outermost timber beam is subjected to the following section forces (Table 6.2).

Section force	Symbol	Maximum value
Axial tension	$\mathbf{F_{t,Ed}}$	**39,5 kN**
Shear force	$\mathbf{F_{v,Ed}}$	**24,6 kN**
Bending Moment	$\mathbf{M_{y,Ed}}$	**30,4 kNm**

Table 6.2 Section forces of exterior timber beam

6.2.1.1 Most loaded timber beam

The design requirements are fulfilled by the following geometrical parameters (Table 6.3). As the necessary dimensions turned out to be bigger than expected, the gap e between compression deck and steel arch has been increased from 0,50 to 1,00m (cf. subchapter 5.3.1).

The fact that the necessary height of the beam is totally unpractical will be discussed in subchapter 6.2.1.3.

Geometrical parameter	Symbol	Value
width	**b**	**215 mm**
height	**h**	**720 mm**
Cross-section area	**A**	**0,15m^2**
Modulus of resistance	**W_y**	**1,86*10^{-2}m^3**

Table 6.3 Section properties of most loaded timber beam

Shear

<u>According to EC5-1, 6.1.7(1):</u> $\boxed{\tau_d \leq f_{v,d}}$ (6.2.1)

Design stress: $\tau_d = 1{,}5 \cdot \frac{F_{v,Ed}}{A_{ef}} = 1{,}5 \cdot \frac{0{,}1768MN}{0{,}12m^2} = 2{,}19\,\frac{N}{mm^2}$ (6.2.2)

With: $b_{ef} = k_{cr} \cdot b = 0{,}781 \cdot 215mm = 168\,mm$ (6.2.3)

$A_{ef} = b_{ef} \cdot h = 0{,}168m \cdot 0{,}720m = 0{,}12\,m^2$ (6.2.4)

Where: k_{cr} $k_{cr} = \frac{2{,}5}{f_{v,k}} = \frac{2{,}5}{3{,}2} = 0{,}781$ EC5-1-1/NA, NDP 6.1.7(2)

b_{ef} effective width EC5-1-1, 6.1.7(2)

Design strength: $f_{v,d} = k_{mod} \cdot \frac{f_{v,k}}{\gamma_M} = 0{,}9 \cdot \frac{3{,}20}{1{,}3} = 2{,}22\,\frac{N}{mm^2}$ (6.2.5)

According to (6.2.1): $\mathbf{2{,}19\,\frac{N}{mm^2} \leq 2{,}22\,\frac{N}{mm^2}}$ **OK**

Combined bending and axial tension

<u>According to EC5-1-1, 6.2.3(1):</u> $\boxed{\frac{\sigma_{t,0,d}}{f_{t,0,d}} + \frac{\sigma_{m,y,d}}{f_{m,y,d}} \leq 1}$ (6.2.6)

Design stress: $\sigma_{t,0,d} = \frac{F_{t,Ed}}{A} = \frac{0{,}0443MN}{0{,}15m^2} = 0{,}29\,\frac{N}{mm^2}$ (6.2.7)

$\sigma_{m,y,d} = \frac{M_{y,Ed}}{W_y} = \frac{0{,}2203MNm}{0{,}0186m^3} = 11{,}86\,\frac{N}{mm^2}$ (6.2.8)

Design strength: $f_{t,0,d} = k_{mod} \cdot \frac{f_{t,0,k}}{\gamma_M} = 0{,}9 \cdot \frac{19{,}50}{1{,}3} = 13{,}50\,\frac{N}{mm^2}$ (6.2.9)

$$f_{m,y,d} = k_{mod} \cdot \frac{f_{m,y,k}}{\gamma_M} = 0{,}9 \cdot \frac{32{,}00}{1{,}3} = 22{,}15 \frac{N}{mm^2} \quad (6.2.10)$$

According to (6.2.6): $\mathbf{\frac{0{,}29}{13{,}50} + \frac{11{,}86}{22{,}15} = 0{,}56 \leq 1}$ **OK**

Limit values for deflection of beams

According to EC5-1-1, 2.2.3(2), the instantaneous deformation w_{inst}, (cf. Fig. 6.5) should be calculated for the characteristic combination of actions.

According to EC5-1-1, 2.2.3(3), the final deformation w_{fin} (cf. Fig. 6.5) should be calculated for the quasi-permanent combination of actions.

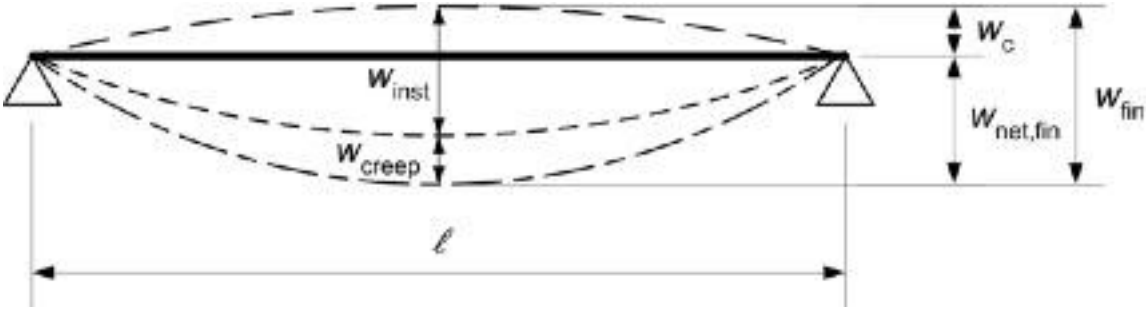

Figure 6.5 Components of deflection (EC5-1-1, Figure 7.1)

<u>According to EC5-2, Table 7.1:</u> $\boxed{w_{inst,Q} \leq \frac{L}{400}}$ (6.2.11)

With: SAP-result $w_{inst,Q} = 0{,}38\ mm$

Where: $w_{inst,Q}$ the instantaneous deflection due to live load EC5-2/NA, NDP 7.2

According to (6.2.11): $\mathbf{0{,}38\ mm \leq \frac{2500}{400} = 6{,}25\ mm}$ **OK**

<u>According to EC5-1-1, Table 7.2:</u> $\boxed{w_{fin} = w_{fin,G} + w_{fin,Q} \leq \frac{L}{250} - \frac{L}{350}}$ (6.2.12)

With: SAP-result $w_{inst,G} = 0{,}11\ mm$

SAP-result $w_{inst,Q} = 0{,}38\ mm$

$$w_{fin,G} = w_{inst,G} \cdot (1 + k_{def}) \quad (6.2.13)$$

$$w_{fin,Q} = w_{inst,Q} \cdot (1 + \psi_2 \cdot k_{def}) \quad (6.2.14)$$

Where: $w_{inst,G}$ the instantaneous deflection due to dead load

$w_{inst,Q}$ the instantaneous deflection due to live load

$w_{fin,G}$ the final deflection due to dead load

$w_{fin,Q}$ the final deflection due to live load

$\boldsymbol{k_{def} = 0,80}$ the deformation factor EC5-1-1, Table 3.2

$\boldsymbol{\psi_2 = 0,60}$ the combination factor (category F) cf. equation (5.3.2)

According to (6.2.12): $w_{fin} = (0{,}11 + 0{,}60 \cdot 0{,}38) \cdot (1 + 0{,}80)$

$$\boldsymbol{w_{fin} = 0,61\ mm \leq \frac{2500}{350} = 7,14\ mm} \quad \textbf{OK}$$

6.2.1.2 Second most loaded timber beam

The requirements are fulfilled by the following geometrical parameters (Table 6.4).

Geometrical parameter	Symbol	Value
width	**B**	**215 mm**
height	**H**	**270 mm**
Cross-section area	**A**	**0,06m^2**
Modulus of resistance	**W$_y$**	**2,61*10^{-3}m^3**

Table 6.4 Section properties of second most loaded timber beam

The cross-section is not chosen smaller in order to have enough practical space for the connections.

Shear

<u>According to EC5-1, 6.1.7(1):</u> $\boxed{\tau_d \leq f_{v,d}}$ (6.2.15)

Design stress: $\tau_d = 1{,}5 \cdot \frac{F_{v,Ed}}{A_{ef}} = 1{,}5 \cdot \frac{0{,}0246MN}{0{,}05m^2} = 0{,}81 \frac{N}{mm^2}$ (6.2.16)

With: $b_{ef} = k_{cr} \cdot b = 0{,}781 \cdot 215mm = 168\ mm$ (6.2.17)

$A_{ef} = b_{ef} \cdot h = 0{,}168m \cdot 0{,}270m = 0{,}05\ m^2$ (6.2.18)

Where: k_{cr} $k_{cr} = \frac{2,5}{f_{v,k}} = \frac{2,5}{3,2} = 0,781$ EC5-1-1/NA, NDP 6.1.7(2)

b_{ef} effective width EC5-1-1, 6.1.7(2)

Design strength: $f_{v,d} = k_{mod} \cdot \frac{f_{v,k}}{\gamma_M} = 0,9 \cdot \frac{3,20}{1,3} = 2,22 \frac{N}{mm^2}$ (6.2.19)

According to (6.2.15): $\mathbf{0,81 \frac{N}{mm^2} \leq 2,22 \frac{N}{mm^2}}$ **OK**

Combined bending and axial tension

According to EC5-1-1, 6.2.3(1): $\boxed{\frac{\sigma_{t,0,d}}{f_{t,0,d}} + \frac{\sigma_{m,y,d}}{f_{m,y,d}} \leq 1}$ (6.2.20)

Design stress: $\sigma_{t,0,d} = \frac{F_{t,Ed}}{A} = \frac{0,0395MN}{0,06m^2} = 0,68 \frac{N}{mm^2}$ (6.2.21)

$\sigma_{m,y,d} = \frac{M_{y,Ed}}{W_y} = \frac{0,304MNm}{0,00261m^3} = 11,64 \frac{N}{mm^2}$ (6.2.22)

Design strength: $f_{t,0,d} = k_{mod} \cdot \frac{f_{t,0,k}}{\gamma_M} = 0,9 \cdot \frac{19,50}{1,3} = 13,50 \frac{N}{mm^2}$ (6.2.23)

$f_{m,y,d} = k_{mod} \cdot \frac{f_{m,y,k}}{\gamma_M} = 0,9 \cdot \frac{32,00}{1,3} = 22,15 \frac{N}{mm^2}$ (6.2.24)

According to (6.2.20): $\mathbf{\frac{0,68}{13,50} + \frac{11,64}{22,15} = 0,58 \leq 1}$ **OK**

Limit values for deflection of beams

The exterior beam shows deflections in negative direction which are very small. Taking a look on the deflection, the fourth beam from the outside is authoritative.

According to EC5-1-1, 2.2.3(2), the instantaneous deformation w_{inst}, (cf. Fig. 6.6) should be calculated for the characteristic combination of actions.

According to EC5-1-1, 2.2.3(3), the final deformation w_{fin} (cf. Fig. 6.6) should be calculated for the quasi-permanent combination of actions.

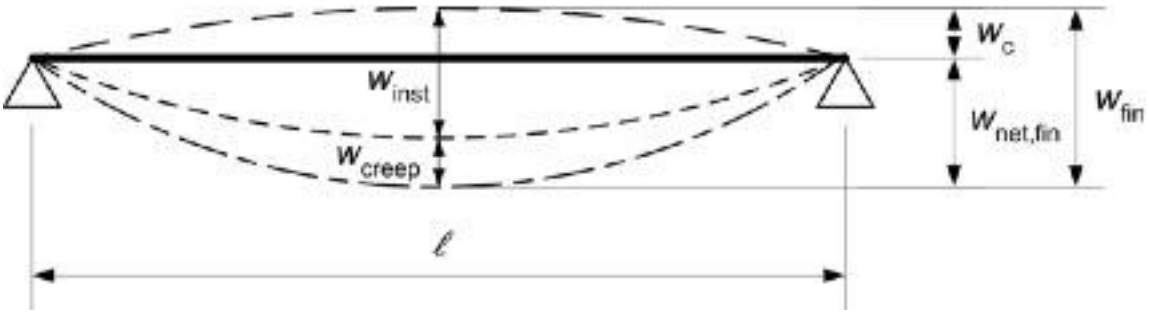

Figure 6.6 Components of deflection (EC5-1-1, Figure 7.1)

<u>According to EC5-2, Table 7.1:</u> $\boxed{w_{inst,Q} \leq \frac{L}{400}}$ (6.2.25)

With: SAP-result $w_{inst,Q} = 1{,}47\ mm$

Where: $w_{inst,Q}$ the instantaneous deflection due to live load EC5-2/NA, NDP 7.2

According to (6.2.25): $\mathbf{1{,}47\ mm \leq \frac{2500}{400} = 6{,}25\ mm}$ **OK**

<u>According to EC5-1-1, Table 7.2:</u> $\boxed{w_{fin} = w_{fin,G} + w_{fin,Q} \leq \frac{L}{250} - \frac{L}{350}}$ (6.2.26)

With: SAP-result $w_{inst,G} = 0{,}41\ mm$

SAP-result $w_{inst,Q} = 1{,}47\ mm$

$w_{fin,G} = w_{inst,G} \cdot (1 + k_{def})$ (6.2.27)

$w_{fin,Q} = w_{inst,Q} \cdot (1 + \psi_2 \cdot k_{def})$ (6.2.28)

Where: $w_{inst,G}$ the instantaneous deflection due to dead load

$w_{inst,Q}$ the instantaneous deflection due to live load

$w_{fin,G}$ the final deflection due to dead load

$w_{fin,Q}$ the final deflection due to live load

$\boldsymbol{k_{def} = 0{,}80}$ the deformation factor EC5-1-1, Table 3.2

$\boldsymbol{\psi_2 = 0{,}60}$ the combination factor (category F) cf. equation (5.3.2)

According to (6.2.26): $w_{fin} = (0{,}41 + 0{,}60 \cdot 1{,}47) \cdot (1 + 0{,}80)$

$\mathbf{w_{fin} = 2{,}33\ mm \leq \frac{2500}{350} = 7{,}14\ mm}$ **OK**

6.2.1.3 Conclusion

The most demanding factor has been the shear force of the most loaded timber beam in the middle of the bridge structure. This shear force value is 7 times higher than the shear force value of the second most loaded timber beam. As a result, a glulam cross-section of 215x720mm would be needed to guarantee the shear resistance of this innermost timber beam.

Besides these in total two timber beams lying in the middle of the whole curvature, a glulam cross-section of 215x270mm fulfilled the requirements sufficiently for the rest of the timber beams.

Putting aside the fact that it seems aesthetically unattractive to design two beams nearly 3 times higher than the rest of the beams, the question can be raised if such a high cross section is still useful (Fig. 6.7).

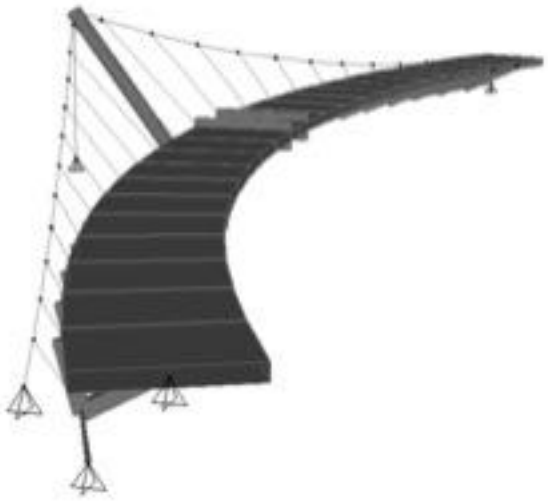

Figure 6.7 Three-dimensional perspective of SAP-model

As a consequence, replacing the two innermost timber beams by smaller steel profiles could be an alternative. By quick hand calculations it can be estimated that a profile HEB 260 could be enough to take the high shear force and the bending moment in the middle of the bridge. The height of 260mm would be similar to the 270mm of the glulam beams.

In order to hide the steel profiles, a possibility could be to cover them with timber planks. By doing so, the aesthetical pleasant experience of the timber bridge could be preserved.

6.2.2 Timber struts

The requirements are calculated for both systems: the left and the right strut. Figure 6.8 visualizes the proportions of the timber frame.

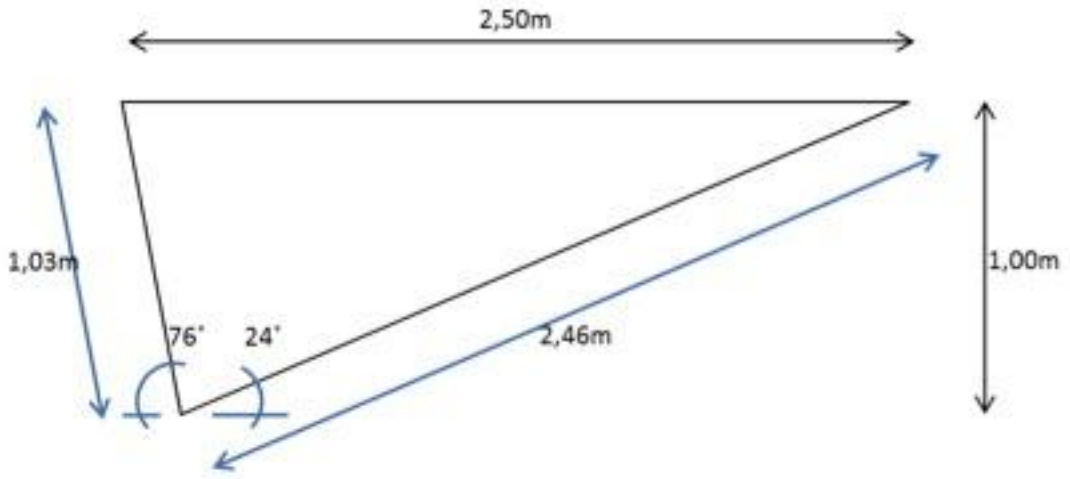

Figure 6.8 Geometrical properties of timber frame

In the interest of simplification, the two timber struts will have the same cross-section properties among themselves and the same width as the timber beam located above them. The cross-section of the struts has to be able to take the maximum compression force. The rare and small tension forces can be taken by the connections.

Table 6.5 shows the maximum value and the position of the compression forces in both struts.

Compression	Symbol	Frame	Maximum value
left strut	$\mathbf{F_{c,Ed,left}}$	**‘11’**	**182,6 kN**
right strut	$\mathbf{F_{c,Ed,right}}$	**‘1’**	**43,4 kN**

Table 6.5 Compressive forces in timber struts

The left strut is shorter but is subjected to the highest compression force. The right strut’s compression force is much lower but, since its length is bigger, the risk of buckling is higher.

6.2.2.1 Left timber strut

The width of the strut is set by the timber beam’s dimension. Again, the height should not be chosen too small in order to have practical space for the connections. This leads to results in which the requirements are fulfilled by the following geometrical parameters without difficulty (Table 6.6).

Geometrical parameter	Symbol	Value
width	**b**	**215 mm**
height	**h**	**225 mm**
Cross-section area	**A**	**4,84*10^{-2} m^2**
Moment of inertia	**I_y** **I_z**	**2,04*10^{-4}m^4** **1,86*10^{-4}m^4**

Table 6.6 Section properties of left timber strut

Compression parallel to the grain

According to EC5-1-1, 6.1.4(1): $\boxed{\sigma_{c,0,d} \leq f_{c,0,d}}$ (6.2.29)

Design stress: $\sigma_{c,0,d,left} = \frac{F_{c,Ed,left}}{A} = \frac{0{,}1826MN}{0{,}0484m^2} = 3{,}77\frac{N}{mm^2}$ (6.2.30)

Design strength: $f_{c,0,d} = k_{mod} \cdot \frac{f_{c,0,k}}{\gamma_M} = 0{,}9 \cdot \frac{26{,}5}{1{,}3} = 18{,}35\frac{N}{mm^2}$ (6.2.31)

According to (6.2.29): $\mathbf{3{,}77\frac{N}{mm^2} \leq\ 18{,}35\frac{N}{mm^2}}$ **OK**

Buckling about the z-axis (weak axis)

According to EC5-1-1, 6.3.2(1): $\boxed{\lambda_{rel,z} = \frac{\lambda_z}{\pi}\sqrt{\frac{f_{c,0,k}}{E_{0,05}}}}$ (6.2.32)

With: $\lambda_z = \frac{l_{ef,z}}{i_z} = \frac{103cm}{6{,}21cm} = 16{,}58$ (6.2.33)

$i_z = \sqrt{\frac{I_z}{A}} = \sqrt{\frac{1{,}86\cdot10^{-4}}{4{,}84\cdot10^{-2}}} = 6{,}21\ cm$ (6.2.34)

$l_{ef,z} = \beta \cdot s = 1{,}00 \cdot 103cm = 103\ cm$ (6.2.35)

Where: $\lambda_{rel,z}, \lambda_z$ slenderness ratios corresponding to bending about the *z*-axis

$E_{0,05}$ the fifth percentile value of the modulus of elasticity parallel to the grain

$E_{0,05} = 10500\frac{N}{mm^2}$ (*SVENSKT TRÄ TM 2012*)

$l_{ef,z}$ buckling length EC5-1-1/NA, NA.13.2(NA.1)

β buckling length coefficient EC5-1-1/NA, Table NA.23

According to (6.2.32): $\lambda_{rel,z} = \frac{16,58}{\pi}\sqrt{\frac{26,50}{10500}} = 0,265$

According to EC5-1-1, 6.3.2(2): $\boldsymbol{\lambda_{rel,z} \leq 0,3}$ **requirement not necessary**

Buckling about the y-axis (strong axis)

The risk of buckling is less than in the case of buckling around the z-axis. The requirement is not necessary.

6.2.2.2 Right timber strut

The two timber struts have the same cross-section properties among themselves. In the case of the right strut, the requirements are fulfilled again without difficulty (Table 6.7).

Geometrical parameter	Symbol	Value
width	**b**	**215 mm**
height	**h**	**225 mm**
Cross-section area	**A**	**4,84*10^{-2} m^2**
Moment of inertia	**I_y**	**2,04*10^{-4}m^4**
	I_z	**1,86*10^{-4}m^4**

Table 6.7 Section properties of right timber strut

Compression parallel to the grain

According to EC5-1-1, 6.1.4(1): $\boxed{\sigma_{c,0,d} \leq f_{c,0,d}}$ (6.2.36)

Design stress: $\sigma_{c,0,d,right} = \frac{F_{c,Ed,right}}{A} = \frac{0,0434MN}{0,0484m^2} = 0,90\frac{N}{mm^2}$ (6.2.37)

Design strength: $f_{c,0,d} = k_{mod} \cdot \frac{f_{c,0,k}}{\gamma_M} = 0,9 \cdot \frac{26,5}{1,3} = 18,35\frac{N}{mm^2}$ (6.2.38)

According to (6.2.36): $\boldsymbol{0,90\frac{N}{mm^2} \leq 18,35\frac{N}{mm^2}}$ **OK**

Buckling about the z-axis (weak axis)

According to EC5-1-1, 6.3.2(1): $\boxed{\lambda_{rel,z} = \frac{\lambda_z}{\pi}\sqrt{\frac{f_{c,0,k}}{E_{0,05}}}}$ (6.2.39)

With: $\lambda_z = \frac{l_{ef,z}}{i_z} = \frac{246cm}{6{,}21cm} = 39{,}59$ (6.2.40)

$i_z = \sqrt{\frac{I_z}{A}} = \sqrt{\frac{1{,}86\cdot10^{-4}}{4{,}84\cdot10^{-2}}} = 6{,}21\ cm$ (6.2.41)

$l_{ef,z} = \beta \cdot s = 1{,}00 \cdot 103cm = 246\ cm$ (6.2.42)

Where: $\lambda_{rel,z}, \lambda_z$ slenderness ratios corresponding to bending about the *z*-axis

$E_{0,05}$ the fifth percentile value of the modulus of elasticity parallel to the grain

$E_{0,05} = 10500\frac{N}{mm^2}$ (*SVENSKT TRÄ TM 2012*)

$l_{ef,z}$ buckling length EC5-1-1/NA, NA.13.2(NA.1)

β buckling length coefficient EC5-1-1/NA, Table NA.23

According to (6.2.39): $\lambda_{rel,z} = \frac{39{,}59}{\pi}\sqrt{\frac{26{,}50}{10500}} = 0{,}633$

According to EC5-1-1, 6.3.2(2): $\boldsymbol{\lambda_{rel,z} > 0{,}3}$ **requirement necessary**

According to EC5-1-1, 6.3.2(3): $\boxed{\frac{\sigma_{c,0,d,rig/t}}{k_{c,z}\cdot f_{c,o,d}} \leq 1}$ (6.2.43)

With: $k_{c,z} = \frac{1}{k_z + \sqrt{{k_z}^2 - \lambda_{rel,z}^2}} = 0{,}949$ (6.2.44)

$k_z = 0{,}5 \cdot [1 + \beta_c \cdot (\lambda_{rel,z} - 0{,}3) + \lambda_{rel,z}^2]$ (6.2.45)

$k_z = 0{,}5 \cdot [1 + 0{,}10 \cdot (0{,}633 - 0{,}3) + 0{,}633^2] = 0{,}717$

Where: $k_{c,z}, k_z$ factors to take in account the increased stress due to the deflection

β_c a factor for members within the straightness limits ($\beta_c = 0{,}10$ glulam)

According to (6.2.43): $\boldsymbol{\frac{0{,}90}{0{,}949\cdot 18{,}35} = 0{,}05 \leq 1}$ **OK**

Buckling about the y-axis (strong axis)

The risk of buckling is less than in the case of buckling around the z-axis. The requirement is not necessary.

6.2.3 Junction: Beam-Strut

The timber struts are connected to the timber beam at angles of 76° and 24°. Since all elements of these junctions have the same material properties, the most striking aspect is the beam's compression perpendicular to the grain. Therefore, the maximum value of axial compression in the struts is of interest.

Every strut is subjected once along the half curved structure to tension instead of compression. This tension will be taken by the connections. At the same time, it affects the beam with connection forces at an angle to the grain. The possibility of splitting has to be taken into account by taking a look on the two cases of tension forces. According to EC5-1-1, 8.1.4(2), the maximum value of the beam's shear force is of interest.

Table 6.8 shows the maximum values and the position of the forces in both struts.

	Symbol	Frame	Maximum value
left strut α=76°	**$F_{c,Ed,left}$** **$F_{v,Ed,left}$**	**'11'** **'1'**	**182,6 kN** **24,6 kN**
right strut α=24°	**$F_{c,Ed,right}$** **$F_{v,Ed,left}$**	**'1'** **'11'**	**43,4 kN** **25,0 kN**

Table 6.8 Compressive and shear forces at junction of beam with left / right timber strut

6.2.3.1 Left timber strut

The requirements are fulfilled by the following geometrical parameters (Table 6.9).

Geometrical parameter	Symbol	Value
width	**b**	**215 mm**
struts	**h_{strut}**	**225 mm**
beam '1'	**$h_{beam,'1'}$**	**270 mm**
beam '11'	**$h_{beam,'11'}$**	**720 mm**

Table 6.9 Geometrical parameters at junction beam – left timber strut

Compression perpendicular to the grain

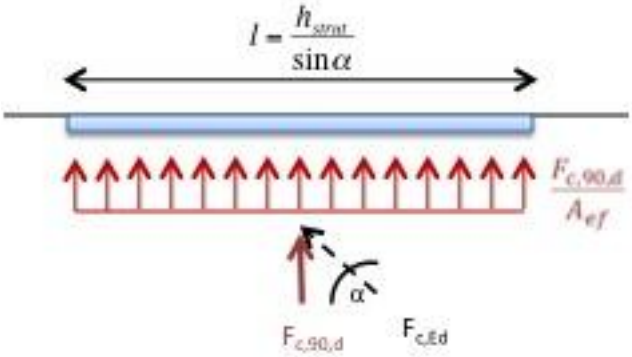

Figure 6.9 Compression perpendicular to the grain at junction beam – left timber strut

According to EC5-1-1, 6.1.5(1): $\boxed{\sigma_{c,90,d} \leq k_{c,90} \cdot f_{c,90,d}}$ (6.2.46)

Design stress: $\sigma_{c,90,d,left} = \frac{F_{c,90,d,left}}{A_{ef}} = \frac{0{,}1772MN}{6{,}28 \cdot 10^{-2} m^2} = 2{,}82 \frac{N}{mm^2}$ (6.2.47)

With: $F_{c,90,d,left} = \sin\alpha \cdot F_{c,ED,left}$ (6.2.48)

$F_{c,90,d,left} = \sin 76^\circ \cdot 182{,}6\ kN = 177{,}2\ kN$

$A_{ef} = b \cdot l_{ef} = 0{,}215 \cdot 0{,}292 = 6{,}28 \cdot 10^{-2}\ m^2$ (6.2.49)

$l_{ef} = l_{left} + 2 \cdot 30mm = 291{,}9\ mm$ (6.2.50)

$l_{left} = \frac{h_{truss}}{sin\,\alpha} = \frac{225mm}{\sin 76^\circ} = 231{,}9$ mm (6.2.51)

Design strength: $f_{c,90,d} = k_{mod} \cdot \frac{f_{c,90,k}}{\gamma_M} = 0{,}9 \cdot \frac{3{,}0}{1{,}3} = 2{,}08 \frac{N}{mm^2}$ (6.2.52)

Where: $k_{c,90}$ a factor taking into account the load configuration, possibility of splitting and degree of compressive deformation

$k_{c,90} = 1{,}75 \qquad l \leq 400\ mm$ EC5-1-1, 6.1.5(4)

A_{ef} the effective contact area of distribution in the case of compression perpendicular to the grain

l_{ef} the effective length of distribution EC5-1-1, 6.1.5(1)

According to (6.2.46): $\mathbf{2,82 \frac{N}{mm^2} \leq 1,75 \cdot 2,08 = 3,63 \frac{N}{mm^2}}$ **OK**

According to EC5-1-1, 6.1.5(1), (4) and EC5-1-1, Figure 6.2:

$$\Delta l_{ef} = 2 \cdot 30mm \leq \begin{cases} a \\ l_{left} = 232mm \\ \frac{l_1}{2} = \frac{L - l_{left} - l_{right}}{2} = \frac{2500-232-553}{2} = 858\,mm \end{cases} \quad (6.2.53)$$

According to EC5-1-1, 6.1.5(3):

$$l_1 \geq 2h \quad (6.2.54)$$

$1716\,mm \geq 2 \cdot 720\,mm = 1440\,mm$ **OK**

Connection forces at an angle to the grain

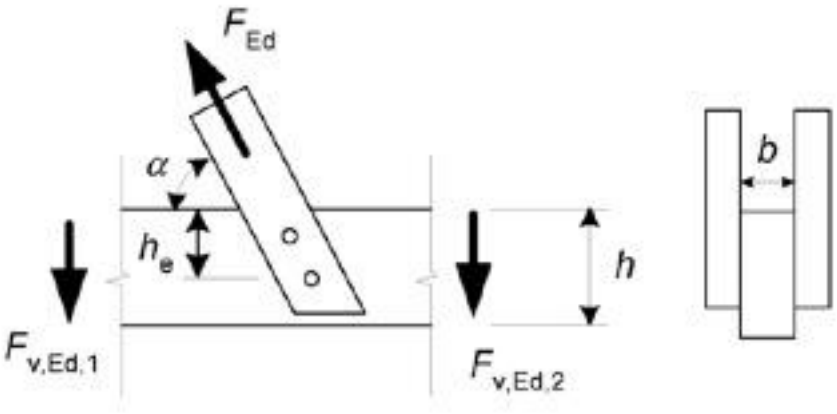

Figure 6.10 Inclined force transmitted by a connection (EC5-1-1, Figure 8.1)

According to EC5-1-1, 8.1.4(2): $\boxed{F_{v,Ed} \leq F_{90,Rd}}$ (6.2.55)

Design force: $F_{v,Ed} = F_{v,Ed,left} = 24{,}6\,kN$

Design splitting capacity: $F_{90,Rk} = 14bw \cdot \sqrt{\frac{h_e}{\left(1-\frac{h_e}{h}\right)}}$ (6.2.56)

$$F_{90,Rk} = 14 \cdot 215 \cdot 1 \cdot \sqrt{\frac{136}{\left(1-\frac{136}{270}\right)}} = 49{,}8\,kN$$

$$F_{90,Rd} = k_{mod} \cdot \frac{F_{90,Rk}}{\gamma_M} = 0{,}9 \cdot \frac{67}{1{,}3} = 34{,}5\,kN \quad (6.2.57)$$

With: $h_e = a_2 + a_{4t} = 87{,}3 + 48{,}5 = 135{,}8\,mm$ (6.2.58)

Where: w a modification factor ($w = 1$ for not punchedmetalplate fasteners)

h_e the loaded edge distance to the center of the most distant fastener or to the edge of the punched metal plate fastener cf. Figure 6.16

h the timber member height (here: $h = h_{beam} = 270\ mm$)

According to (6.2.55): $\mathbf{24,6\ kN \leq 34,5\ kN}$ **OK**

6.2.3.2 Right timber strut

It has been continued with the same geometrical parameters (Table 6.10).

Geometrical parameter	Symbol	Value
width	**b**	**215 mm**
struts	$\mathbf{h_{strut}}$	**225 mm**
beam '1'	$\mathbf{h_{beam,'1'}}$	**270 mm**
beam '11'	$\mathbf{h_{beam,'11'}}$	**720 mm**

Table 6.10 Geometrical parameters at junction beam – right timber strut

Compression perpendicular to the grain

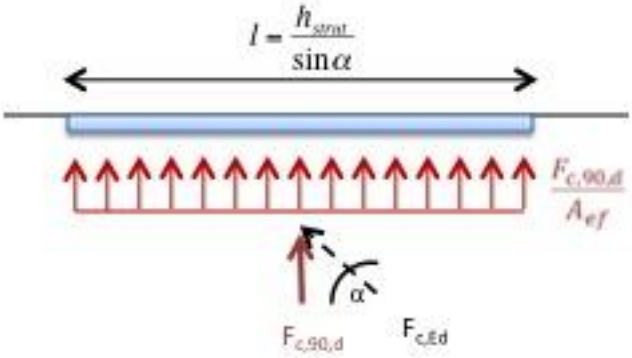

Figure 6.11 Compression perpendicular to the grain

According to EC5-1-1, 6.1.5(1): $\boxed{\sigma_{c,90,d} \leq k_{c,90} \cdot f_{c,90,d}}$ (6.2.59)

Design stress: $\sigma_{c,90,d,right} = \frac{F_{c,90,d,right}}{A_{ef}} = \frac{0{,}0177MN}{0{,}13\ m^2} = 0{,}13\ \frac{N}{mm^2}$ (6.2.60)

With: $F_{c,90,d,right} = \sin\alpha \cdot F_{c,ED,right}$ (6.2.61)

$F_{c,90,d,right} = \sin 24^\circ \cdot 43{,}40\ kN = 17{,}65\ kN$

$A_{ef} = b \cdot l_{ef} = 0{,}215 \cdot 0{,}613 = 0{,}13\ m^2$ (6.2.62)

$l_{ef} = l_{right} + 2 \cdot 30mm = 613\ mm$ (6.2.63)

$l_{right} = \frac{h_{truss}}{\sin\alpha} = \frac{225mm}{\sin 24^\circ} = 553\ \text{mm}$ (6.2.64)

Design strength: $$f_{c,90,d} = k_{mod} \cdot \frac{f_{c,90,k}}{\gamma_M} = 0{,}9 \cdot \frac{3{,}0}{1{,}3} = 2{,}08 \frac{N}{mm^2} \quad (6.2.65)$$

Where: $k_{c,90}$ a factor taking into account the load configuration, possibility of splitting and degree of compressive deformation

$k_{c,90} = 1{,}75 \qquad l \leq 400\ mm$ EC5-1-1, 6.1.5(4)

A_{ef} the effective contact area of distribution in the case of compression perpendicular to the grain

l_{ef} the effective length of distribution EC5-1-1, 6.1.5(1)

According to (6.2.46): $\mathbf{0{,}13 \frac{N}{mm^2} \leq 1{,}75 \cdot 2{,}08 = 3{,}63 \frac{N}{mm^2}}$ **OK**

<u>According to EC5-1-1, 6.1.5(1), (4) and EC5-1-1, Figure 6.2:</u>

$$\Delta l_{ef} = 2 \cdot 30mm \leq \begin{cases} a \\ l_{right} = 553\ mm \\ \frac{l_1}{2} = \frac{L - l_{left} - l_{right}}{2} = \frac{2500 - 232 - 553}{2} = 858\ mm \end{cases} \quad (6.2.66)$$

<u>According to EC5-1-1, 6.1.5(3):</u>

$l_1 \geq 2h$ (6.2.67)

$1716\ mm \geq 2 \cdot 270\ mm = 540\ mm$ **OK**

Connection forces at an angle to the grain

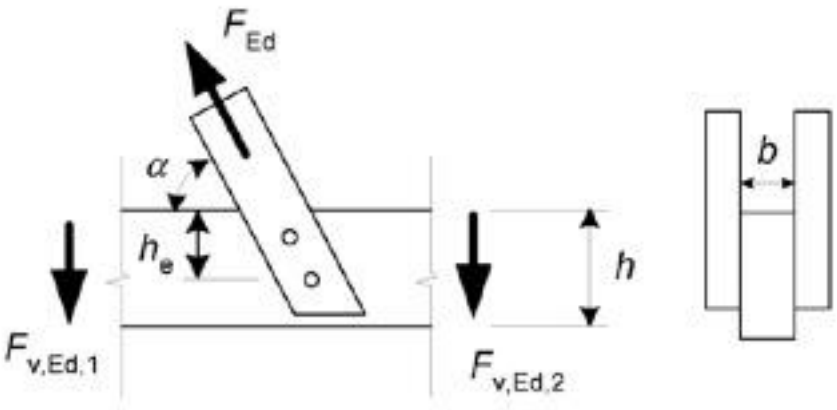

Figure 6.12 Inclined force transmitted by a connection (EC5-1-1, Figure 8.1)

<u>According to EC5-1-1, 8.1.4(2):</u> $\boxed{F_{v,Ed} \leq F_{90,Rd}}$ (6.2.68)

Design force: $F_{v,Ed} = F_{v,Ed,right} = 25{,}0\ kN$

Design splitting capacity: $F_{90,Rk} = 14bw \cdot \sqrt{\frac{h_e}{(1-\frac{h_e}{h})}}$ (6.2.69)

$$F_{90,Rk} = 14 \cdot 215 \cdot 1 \cdot \sqrt{\frac{119}{\left(1-\frac{119}{720}\right)}} = 35{,}9\ kN$$

$$F_{90,Rd} = k_{mod} \cdot \frac{F_{90,Rk}}{\gamma_M} = 0{,}9 \cdot \frac{34{,}3}{1{,}3} = 24{,}9\ kN \qquad (6.2.70)$$

With: $h_e = a_2 + a_{4t} = 82{,}2\ mm + 36{,}6\ mm = 118{,}8\ mm$

Where: w a modification factor ($w = 1$ for not punchedmetalplate fasteners)

h_e the loaded edge distance to the center of the most distant fastener or to the edge of the punched metal plate fastener cf. Figure 6.18

h the timber member height (here: $h = h_{beam} = 720\ mm$)

According to (6.2.55): $\mathbf{25{,}0\ kN \geq 24{,}9\ kN}$ **FAILED**

The ratio between the loaded edge distance and the timber member height $\frac{h_e}{h}$ is too small. This increases the possibility of splitting caused by the tension force component perpendicular to the grain. The connection between beam and right strut is located too low in proportion to the total height of the horizontal timber member, the timber beam.

Since the only tension in the right timber strut can be observed in the innermost timber frame with the position ‘11’, it does not surprise that the needed height of 720 mm causes difficulties in designing the connection.

In order to fulfill the requirement, distances between the bolts of 100 mm instead of 90 mm could be already enough. The spacing a_2 and the distance a_{4t} could be increased sufficiently.

With regard to (6.2.56): $F_{90,Rk} = 14 \cdot 215 \cdot 1 \cdot \sqrt{\frac{122}{\left(1-\frac{122}{720}\right)}} = 36{,}5\ kN$

With: $h_e = 2 \cdot a_2 + a_{4t} = 2 \cdot 40{,}7\ mm + 40{,}7\ mm = 122\ mm$

With regard to (6.2.57) $F_{90,Rd} = k_{mod} \cdot \frac{F_{90,Rk}}{\gamma_M} = 0{,}9 \cdot \frac{36{,}5}{1{,}3} = 25{,}3\ kN$

According to (6.2.55): $\mathbf{25{,}0\ kN \leq 25{,}3\ kN}$ **OK**

On the other hand, the question should be raised if this step of increasing the distances is useful. In subchapter 6.2.1.3, the conclusion is drawn that replacing the two innermost timber

beams by two steel profiles could be much more practical. In this way, the problem about the connection forces at an angle to the grain in the beam would be solved and there is no need to design the connection between timber beam and right strut differently from the other connections.

6.2.4 Junction: Strut-Strut

The timber struts have angles of inclination of 76˚ and 24˚. Underneath the timber deck the two struts meet in the connection point with hangers and tension arch. The position of this point has been discussed in the parameter study in subchapter 5.4.

In Figure 6.13 the most important geometrical properties of this connection point are shown.

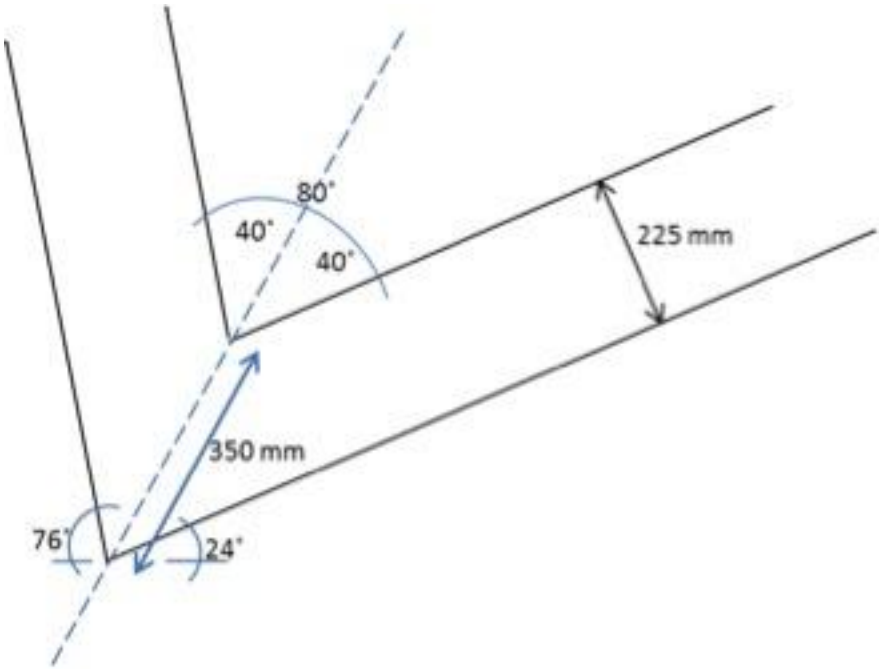

Figure 6.13 Geometrical properties of connection point

Both struts are equally in material and section properties. They are connected to each other under an angle of 80˚. As a consequence, compression stresses at an angle to the grain are caused. Therefore, the maximum value of axial compression in the struts is of interest.

In subchapter 6.3 the design of this connection point will be presented in detail. It should be mentioned at this point that in order to prevent direct contact of the glulam struts and to transmit the tensional forces along the tension arch a steel plate separates the struts in the section area.

Table 6.11 shows value and the position of the maximum compression force.

Compression	Symbol	Frame	Maximum value
left strut	$\mathbf{F_{c,Ed,left}}$	**'11'**	**182,6 kN**

Table 6.11 Maximum compressive force in struts

Compression stresses at an angle to the grain

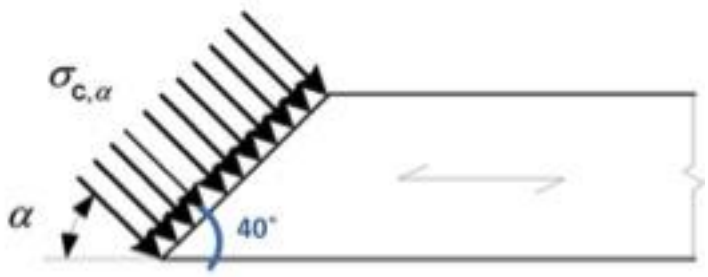

Figure 6.14 Compressive stresses at an angle to the grain (EC5-1-1, Figure 6.7)

The angle α to the grain corresponds with the angle which forms a right angle with the section angle of 40˚. $\alpha = 50^{\circ}$ cf. Fig. 6.13 and 6.14

According to EC5-1-1, 6.2.2(2): $$\sigma_{c,\alpha,d} \leq \frac{f_{c,0,d}}{\frac{f_{c,0,d}}{k_{c,90} \cdot f_{c,90,d}}(sin\,\alpha)^2+(cos\,\alpha)^2} \quad (6.2.71)$$

Design stress: $$\sigma_{c,\alpha,d} = \frac{F_{c,\alpha,d}}{A} = \frac{0{,}01174MN}{7{,}53 \cdot 10^{-2}\,m^2} = 1{,}56\,\frac{N}{mm^2} \quad (6.2.72)$$

With: $$F_{c,\alpha,d} = \sin\alpha \cdot F_{c,ED,left} \quad (6.2.73)$$

$$F_{c,\alpha,d} = \sin 50^{\circ} \cdot 182{,}6\ kN = 117{,}4\ kN$$

$$A = b \cdot l = 0{,}215 \cdot 0{,}350 = 7{,}53 \cdot 10^{-2}\ m^2 \quad (6.2.74)$$

$$l = \frac{h_{truss}}{sin\,\alpha} = \frac{225mm}{\sin 40^{\circ}} = 350\ \text{mm} \quad (6.2.75)$$

Design strength: $$f_{c,90,d} = k_{mod} \cdot \frac{f_{c,90,k}}{\gamma_M} = 0{,}9 \cdot \frac{3{,}0}{1{,}3} = 2{,}08\,\frac{N}{mm^2} \quad (6.2.76)$$

$$f_{c,0,d} = k_{mod} \cdot \frac{f_{c,0,k}}{\gamma_M} = 0{,}9 \cdot \frac{26{,}5}{1{,}3} = 18{,}35\,\frac{N}{mm^2} \quad (6.2.77)$$

Where: $k_{c,90}$ a factor taking into account the effect of stresses perpendicular to the grain

$k_{c,90} = 1{,}75$ $l \leq 400\ mm$ EC5-1-1, 6.1.5(4)

According to (6.2.58): $\mathbf{1{,}56\,\frac{N}{mm^2} \leq \frac{18{,}35}{\frac{18{,}35}{1{,}75 \cdot 2{,}08}(sin\,50)^2+(cos\,50)^2} = 5{,}44\,\frac{N}{mm^2}}$ **OK**

6.3. Connections between frame members / hanger / rods

A steel-to-timber connection with 2 plates as the outer members of double shear connections is chosen. As fasteners **2 x 2 bolts** with a diameter of **12 mm** and strength of **4.8** are used.

In the interest of simplification, it has been tried to design the connections between beam and struts as well as between struts, hangers and rods as similar as possible.

According to EC5-1-1, 8.2.1(1), for the determination of the characteristic load-carrying capacity of connections with metal dowel-type fasteners the contributions of the yield strength, the embedment strength, and the withdrawal strength of the fastener shall be considered.

The possible failure modes of this steel-to-timber connection are pictured in Figure 6.15.

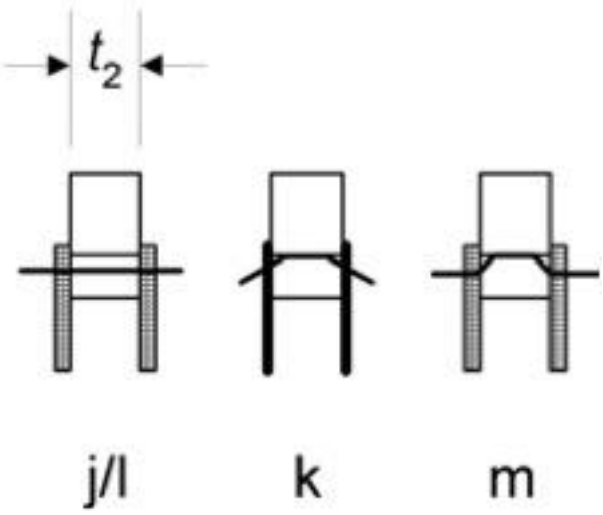

Figure 6.15 Failure modes for steel-to-timber connections (EC5-1-1, Figure 8.3)

<u>According to EC5-1-1, 8.2.3(1):</u>

Thin plates $t_s \leq 0{,}5d = 6\ mm$ (6.3.1)

Thick plates $t_s \geq d = 12\ mm$ (6.3.2)

Where: t_s the steel plate thickness [mm]

d the fastener diameter [mm]

The characteristic load-carrying capacity of connections with steel plate thickness between a thin and a thick plate should be calculated by linear interpolation between the limiting thin and thick plate values

6.3.1 Connection: Beam-Strut

The timber struts are connected to the timber beam at angles of 76˚ and 24˚.

Every strut is subjected once along the half curved structure to tension instead of compression. This tension will be taken by the connections.

Table 6.12 shows the maximum value and the position of the tension force in both struts.

	Angle	Symbol	Frame	Maximum value
left strut	α=76˚	**$F_{t,Ed,left}$**	**'1'**	**24,9 kN**
right strut	α=24˚	**$F_{t,Ed,right}$**	**'11'**	**57,9 kN**

Table 6.12 Tensile forces in timber struts

With regard to (6.3.1) and (6.3.2):

In this case: $t_s = 8\ mm \begin{cases} \geq 6\ mm \\ \leq 12\ mm \end{cases}$

The characteristic load-carrying capacity of connections should be calculated by linear interpolation between the limiting thin and thick plate values.

According to 8.2.3(2):

The tension forces of maximum 60 kN are not a problem for steel plates with a width of 190mm and a thickness of 8mm.

According to EC3-1-8/NA:2010-12, NCl 4.5.2:

$$a \geq \sqrt{\max t} - 0{,}5 = \sqrt{8} - 0{,}5 = 2{,}33\ mm \qquad (6.3.3)$$

According to EC3-1-8:2010-12, 4.1(1):

The welded joints are designed constructively: $\boldsymbol{a = 4\ mm}$ **OK**

6.3.1.1 Connection: Beam-Left timber strut

Steel-to-timber connection in beam

The angle $\alpha = 76^{\circ}$ is the angle of the load to the grain.

Spacing and end / edge distances

Minimum spacings and edge / end distances are shown in Figure 6.16.

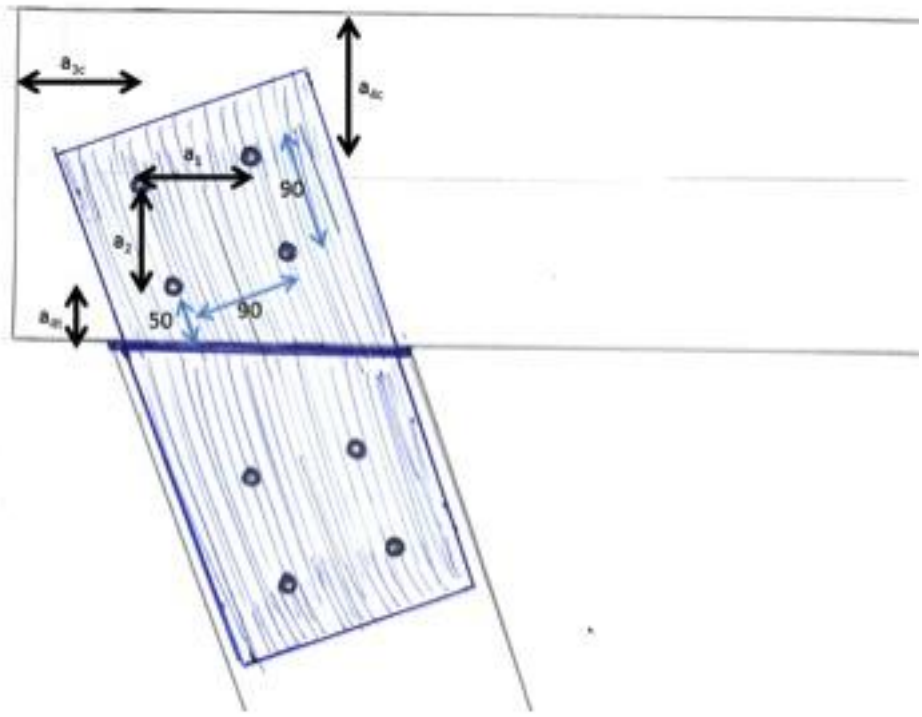

Figure 6.16 Connection between beam and left strut

According to EC5-1-1, Table 8.5:

Spacing and edge/end distances	Angle	Minimum spacing or edge/end distance
a_1 (parallel to the grain)	$0^\circ \leq \alpha \leq 360^\circ$	$(3 + 2\lvert\cos\alpha\rvert)d$ $=(3 + 2\lvert\cos 76\rvert)12 = 41{,}8$ mm
a_2 (perpendicular to the grain)	$0^\circ \leq \alpha \leq 360^\circ$	$3d = 3 \cdot 12 = 36\ mm$
a_{3c} (unloaded end)		$3d = 3 \cdot 12 = 36\ mm$
a_{4t} (loaded edge)	$0^\circ \leq \alpha \leq 180^\circ$	$\max[(2 + 2\sin\alpha)d; 3d] =$ $\max[(2 + 2\sin(180 - 76))12; 3 \cdot 12]$ $= 47{,}3$ mm
a_{4c} (unloaded edge)	$180^\circ \leq \alpha \leq 360^\circ$	$3d = 3 \cdot 12 = 36\ mm$

Table 6.13 Minimum spacings and edge / end distances for dowels

Based on the requirements of Table 6.13, the following spacings and distances are chosen (Table 6.14).

Spacing and edge/end distances	Minimum spacing or edge/end distance
a_1 (parallel to the grain)	$90\ mm \cdot \sin 76 = 87{,}3\ mm$
a_2 (perpendicular to the grain)	$90\ mm \cdot \sin 76 = 87{,}3\ mm$
a_{3c} (unloaded end)	100 mm
a_{4t} (loaded edge)	$50\ mm \cdot \sin 76 = 48{,}5\ mm$
4_{4c} (unloaded edge)	$270 - 2 \cdot 87{,}3 - 90\ mm \cdot \cos 76 = 73{,}6\ mm$

Table 6.14 Spacings and edge / end distances (Fig. 6.16)

Lateral load-carrying capacity of metal dowel-type fasteners

<u>According to EC5-1-1, (8.12); for thin steel plates:</u>

$$F_{v,Rk} = min\begin{cases} 0{,}5 \cdot f_{h,2,k} \cdot t_2 \cdot d \\ 1{,}15 \cdot \sqrt{2 \cdot M_{y,Rk} \cdot f_{h,2,k} \cdot d} + \frac{F_{ax,Rk}}{4} \end{cases} \quad \begin{matrix}(j)\\(k)\end{matrix} \qquad (6.3.4)$$

$$F_{v,Rk} = min\begin{cases} 0{,}5 \cdot 21{,}66 \cdot 215 \cdot 12 \\ 1{,}15 \cdot \sqrt{2 \cdot 76745 \cdot 21{,}66 \cdot 12} + \frac{F_{ax,Rk}}{4} \end{cases}$$

$$F_{v,Rk} = min\begin{cases} 27941N \\ 7264 + \frac{F_{ax,Rk}}{4} = 7264 + 1816 = 9080\ N \end{cases}$$

<u>With regard to (6.3.10)</u>:

$$\frac{F_{ax,Rk}}{4} = min\begin{cases} 0{,}25 \cdot R_{V,Rk,Johansen} \\ 9161/4 = 2290{,}3\ N \end{cases}$$

$$\frac{F_{ax,Rk}}{4} = min\begin{cases} 0{,}25 \cdot 7264 = 1816\ N \\ 9161/4 = 2290{,}3\ N \end{cases} = 1816\ N$$

<u>According to EC5-1-1, (8.12); for thick steel plates:</u>

$$F_{v,Rk} = min\begin{cases} 0{,}5 \cdot f_{h,2,k} \cdot t_2 \cdot d \\ 2{,}3 \cdot \sqrt{M_{y,Rk} \cdot f_{h,2,k} \cdot d} + \frac{F_{ax,Rk}}{4} \end{cases} \quad \begin{matrix}(l)\\(m)\end{matrix} \qquad (6.3.5)$$

$$F_{v,Rk} = min\begin{cases} 0{,}5 \cdot 21{,}66 \cdot 215 \cdot 12 \\ 2{,}3 \cdot \sqrt{76745 \cdot 21{,}66 \cdot 12} + \frac{F_{ax,Rk}}{4} \end{cases}$$

$$F_{v,Rk} = min\begin{cases} 27941\ N \\ 10273 + \frac{F_{ax,Rk}}{4} = 10273 + 2290 = 12563\ N \end{cases}$$

<u>With regard to (6.3.11)</u>:

$$\frac{F_{ax,Rk}}{4} = min\begin{cases} 0{,}25 \cdot R_{V,Rk,Johansen} \\ 9161/4 = 2290\ N \end{cases}$$

$$\frac{F_{ax,Rk}}{4} = min\begin{cases} 0{,}25 \cdot 10273 = 2568{,}3\ N \\ 9161/4 = 2290\ N \end{cases} = 2290\ N$$

<u>According to EC5-1-1, (8.12); in between:</u>

$$F_{v,Rk} = min\begin{cases} 27941\ N \\ \frac{(12563-9080)}{(12-6)} \cdot (8-6) + 9080 = 10241\ N \end{cases} \quad (6.3.6)$$

$$\boldsymbol{F_{v,Rk} = 10241\ N} \qquad \textbf{failure in bolt}$$

With:

$$M_{y,Rk} = 0{,}3 \cdot f_{u,k} \cdot d^{2,6} \quad (6.3.7)$$

$$M_{y,Rk} = 0{,}3 \cdot 400 \cdot 12^{2,6} = 76745\ Nmm$$

$$f_{h,2,k} = \frac{f_{h,0,k}}{k_{90} \cdot (\sin\alpha)^2 + (\cos\alpha)^2} \quad (6.3.8)$$

$$f_{h,2,k} = \frac{32{,}47}{1{,}53 \cdot (\sin 76)^2 + (\cos 76)^2} = 21{,}66\,\frac{N}{mm^2}$$

$$f_{h,0,k} = 0{,}082 \cdot (1 - 0{,}01 \cdot d) \cdot \rho_k \quad (6.3.9)$$

$$f_{h,0,k} = 0{,}082 \cdot (1 - 0{,}01 \cdot 12) \cdot 450 = 32{,}47\,\frac{N}{mm^2}$$

$$k_{90} = 1{,}35 + 0{,}015 \cdot d \quad (6.3.10)$$

$$k_{90} = 1{,}35 + 0{,}015 \cdot 12 = 1{,}53$$

Where:

$F_{v,Rk}$ the characteristic load-carrying capacity per shear plane per fastener

$M_{y,Rk}$ the characteristic fastener yield moment [Nmm] EC5-1-1, 8.5.1.1(1)

$f_{h,2,k}, f_{h,0,k}$ the characteristic embedment strength in the timber member / parallel to grain [N/mm^2] EC5-1-1, 8.5.1.1(2)

k_{90} for softwoods EC5-1-1, (8.33)

$F_{ax,Rk}$ the characteristic withdrawal capacity of the fastener

$f_{u,k}$ the characteristic tensile strength ($f_{u,k} = 400\,\frac{N}{mm^2}$, bolt 4.8)

t_2 the thickness of the timber middle member (Fig. 6.15) [mm]

ρ_k the characteristic timber density ($\rho_k = 450\,\frac{kg}{m^3}$, cf. Table 5.1)

According to EC5-1-1, 8.2.3(4): For the limitation of the rope effect $F_{ax,Rk}$ 8.2.2(2) applies.

In the equations (6.3.4) and (6.3.5) the first term on the right hand side is the load-carrying capacity according to the Johansen yield theory, whilst the second term $\frac{F_{ax,Rk}}{4}$ is the contribution from the rope effect.

The contribution to the load-carrying capacity due to the rope effect should be limited to following percentages of the Johansen part: 25% (bolts)

As a consequence:
$$\boxed{\frac{F_{ax,Rk}}{4} = min\begin{cases} 0{,}25 \cdot R_{V,Rk,Johansen} \\ 3{,}0 \cdot f_{c,90,k} \cdot A_{washer}/4 \end{cases}} \quad (6.3.11)$$

$$\frac{F_{ax,Rk}}{4} = min\begin{cases} 0{,}25 \cdot R_{V,Rk,Johansen} \\ 9161/4 = 2293\ N \end{cases}$$

With:
$$F_{ax,Rk} = 3{,}0 \cdot f_{c,90,k} \cdot A_{washer} \quad (6.3.12)$$

$$F_{ax,Rk} = 3{,}0 \cdot 3{,}00 \cdot 1018 = 9161\ N$$

$$A_{washer} = \frac{(3 \cdot d)^2}{4} \cdot \pi = \frac{(3 \cdot 12)^2}{4} \cdot \pi = 1018\ mm^2 \quad (6.3.13)$$

Where: $F_{ax,Rk}$ the rope effect EC5-1-1, 8.5.2(2)

A_{washer} the contact area of washer EC5-1-1, 10.4.3(2)

Multiple fastener connections

For one row of fasteners parallel to the grain direction, the effective characteristic load-carrying capacity parallel to the row should be taken as:

According to EC5-1-1, 8.1.2(4): $\boxed{F_{v,ef,Rk} = n_{ef} \cdot F_{v,Rk}}$ (6.3.14)

With: parallel to the grain
$$n_{ef} = min\begin{cases} n \\ n^{0{,}9} \cdot \sqrt[4]{\frac{a_1}{13 \cdot d}} \end{cases} \quad (6.3.15)$$

$$n_{ef} = min\begin{cases} 2 \\ 2^{0{,}9} \cdot \sqrt[4]{\frac{87{,}3}{13 \cdot 12}} = 1{,}36 \end{cases} = 1{,}61$$

Perpendicular to the grain $n_{ef} = n$ (6.3.16)

For angles $o^\circ < \alpha < 90^\circ$ between load and grain direction, n_{ef} may be determined by linear interpolation between equations (6.3.15) and (6.3.16).

$$n_{ef} = \frac{(2-1{,}61)}{(90-0)} \cdot (76-0) + 1{,}61 = \mathbf{1{,}94} \qquad (6.3.17)$$

Where: n_{ef} the effective number in line parallel to the grain EC5-1-1, 8.5.1.1(4)

n the number of bolts in the row

a_1 the spacing between bolts in the grain direction (cf. Fig. 6.16)

Total effective design load-carrying capacity

The load-carrying capacity of this steel-to-timber connection with **2** plates as the outer members of double shear connections and **2 x 2 bolts** is:

With regard to (6.0.1): $\boxed{F_{v,ef,Rd} = k_{mod} \cdot \frac{F_{v,ef,Rk}}{\gamma_M}}$

$$F_{v,ef,Rd} = 0{,}90 \cdot \frac{77{,}8}{1{,}1} = \mathbf{66{,}0\ kN}$$

With: $$F_{v,ef,Rk} = 2 \cdot 2 \cdot n_{ef} \cdot F_{v,Rk} \qquad (6.3.18)$$

$$F_{v,ef,Rk} = 2 \cdot 2 \cdot 1{,}94 \cdot 10241\ N = 79{,}5\ kN$$

Where: γ_M the partial factor for a material property ($\gamma_M = 1{,}1$, failure in bolt)

$F_{v,Rk}$ see equation (6.3.6)

Ultimate Limit State

$$\boxed{\boldsymbol{F_{t,Ed,left} \leq F_{v,ef,Rd}}} \qquad (6.3.19)$$

$$\mathbf{24{,}9\ kN \leq 65{,}0\ kN} \qquad \textbf{OK}$$

With: $$F_{t,Ed,left} = 24{,}9\ kN$$

Where: $F_{t,Ed,left}$ see Table 6.12

Steel-to-timber connection in strut

The angle $\alpha = 0^{\circ}$ is the angle of the load to the grain. The fasteners are located parallel to the grain.

Spacing and end / edge distances

Minimum spacings and edge / end distances are shown in Figure 6.17.

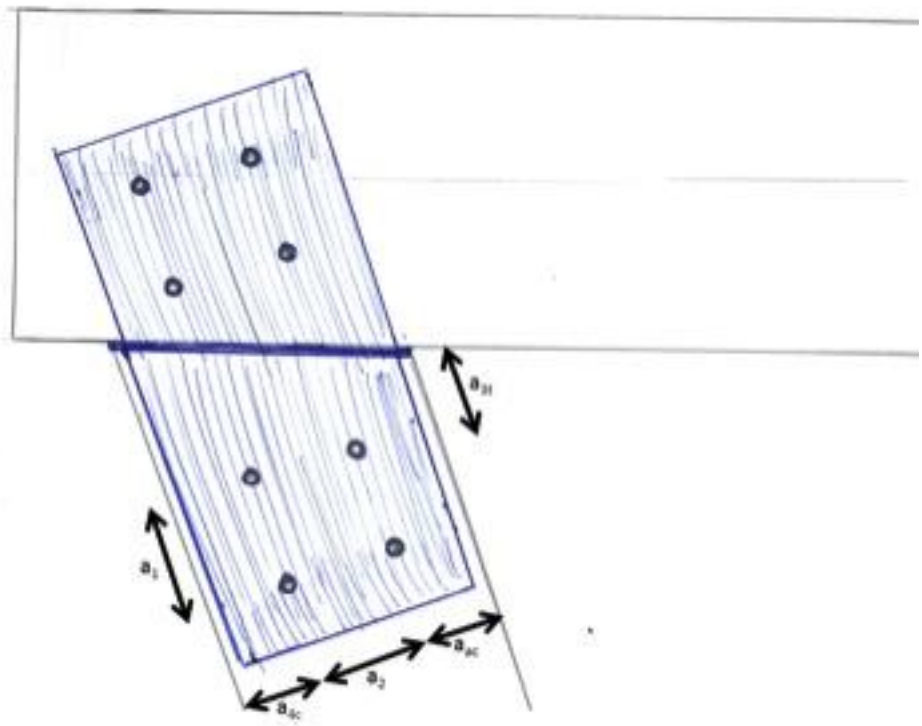

Figure 6.17 Connection between beam and left strut

According to EC5-1-1, Table 8.5:

Spacing and edge/end distances	Angle	Minimum spacing or edge/end distance
a_1 (parallel to the grain)	$0^{\circ} \leq \alpha \leq 360^{\circ}$	$(3 + 2\lvert\cos\alpha\rvert)d$ $=(3 + 2\lvert\cos 0\rvert)12 = 60\ mm$
a_2 (perpendicular to the grain)	$-90^{\circ} \leq \alpha \leq 90^{\circ}$	$\max(7d; 80mm) = 84\ mm$
a_{3t} (loaded end)	$180^{\circ} \leq \alpha \leq 360^{\circ}$	$3d = 3 \cdot 12 = 36\ mm$
a_{4c} (unloaded edge)	$180^{\circ} \leq \alpha \leq 360^{\circ}$	$3d = 3 \cdot 12 = 36\ mm$

Table 6.15 Minimum spacings and edge / end distances for dowels

Based on the requirements of Table 6.15, the following spacings and distances are chosen (Table 6.16).

Spacing and edge/end distances	Minimum spacing or edge/end distance
a_1 (parallel to the grain)	$90\ mm$
a_2 (perpendicular to the grain)	$90\ mm$
a_{3t} (loaded end)	$90\ mm$
4_{4c} (unloaded edge)	$0{,}5 \cdot (225 - 90) = 67{,}5\ mm$

Table 6.16 Spacings and edge / end distances (Fig. 6.17)

Lateral load-carrying capacity of metal dowel-type fasteners

According to EC5-1-1, (8.12); for thin steel plates:

$$F_{v,Rk} = min\begin{cases} 0{,}5 \cdot f_{h,2,k} \cdot t_2 \cdot d \\ 1{,}15 \cdot \sqrt{2 \cdot M_{y,Rk} \cdot f_{h,2,k} \cdot d} + \frac{F_{ax,Rk}}{4} \end{cases} \quad \begin{matrix}(j)\\(k)\end{matrix} \qquad (6.3.20)$$

$$F_{v,Rk} = min\begin{cases} 0{,}5 \cdot 32{,}47 \cdot 215 \cdot 12 \\ 1{,}15 \cdot \sqrt{2 \cdot 76745 \cdot 32{,}47 \cdot 12} + \frac{F_{ax,Rk}}{4} \end{cases}$$

$$F_{v,Rk} = min\begin{cases} 41886\ N \\ 8893 + \frac{F_{ax,Rk}}{4} = 8893 + 2223 = 11116\ N \end{cases}$$

With regard to (6.3.26):

$$\frac{F_{ax,Rk}}{4} = min\begin{cases} 0{,}25 \cdot R_{V,Rk,Johansen} \\ 9161/4 = 2290\ N \end{cases}$$

$$\frac{F_{ax,Rk}}{4} = min\begin{cases} 0{,}25 \cdot 8893 = 2223\ N \\ 9161/4 = 2290\ N \end{cases} = 2223\ N$$

According to EC5-1-1, (8.12); for thick steel plates:

$$F_{v,Rk} = min\begin{cases} 0{,}5 \cdot f_{h,2,k} \cdot t_2 \cdot d \\ 2{,}3 \cdot \sqrt{M_{y,Rk} \cdot f_{h,2,k} \cdot d} + \frac{F_{ax,Rk}}{4} \end{cases} \quad \begin{matrix}(l)\\(m)\end{matrix} \qquad (6.3.21)$$

$$F_{v,Rk} = min\begin{cases} 0{,}5 \cdot 32{,}47 \cdot 215 \cdot 12 \\ 2{,}3 \cdot \sqrt{76745 \cdot 32{,}47 \cdot 12} + \frac{F_{ax,Rk}}{4} \end{cases}$$

$$F_{v,Rk} = min\begin{cases} 41886\ N \\ 12577 + \frac{F_{ax,Rk}}{4} = 12577 + 2290{,}3 = 14867\ N \end{cases}$$

With regard to (6.3.27):

$$\frac{F_{ax,Rk}}{4} = min\begin{cases} 0{,}25 \cdot R_{V,Rk,Johansen} \\ 9161/4 = 2290\ N \end{cases}$$

$$\frac{F_{ax,Rk}}{4} = min\begin{cases} 0{,}25 \cdot 12577 = 3144\ N \\ 9161/4 = 2290\ N \end{cases} = 2290\ N$$

According to EC5-1-1, (8.12); in between:

$$F_{v,Rk} = min\begin{cases} 41886\ N \\ \frac{(14867-11116)}{(12-6)} \cdot (8-6) + 11116 = 12366\ N \end{cases} \quad (6.3.22)$$

$$\boldsymbol{F_{v,Rk} = 12366\ N} \qquad \textbf{failure in bolt}$$

With:

$$M_{y,Rk} = 0{,}3 \cdot f_{u,k} \cdot d^{2,6} \quad (6.3.23)$$

$$M_{y,Rk} = 0{,}3 \cdot 400 \cdot 12^{2,6} = 76745\ Nmm$$

$$\boldsymbol{f_{h,2,k} = f_{h,0,k}} \quad (6.3.24)$$

$$f_{h,0,k} = 0{,}082 \cdot (1 - 0{,}01 \cdot d) \cdot \rho_k \quad (6.3.25)$$

$$f_{h,0,k} = 0{,}082 \cdot (1 - 0{,}01 \cdot 12) \cdot 450 = 32{,}47\ \frac{N}{mm^2}$$

$$k_{90} = 1{,}35 + 0{,}015 \cdot d \quad (6.3.26)$$

$$k_{90} = 1{,}35 + 0{,}015 \cdot 12 = 1{,}53$$

Where:

$F_{v,Rk}$	the characteristic load-carrying capacity per shear plane per fastener	
$M_{y,Rk}$	the characteristic fastener yield moment [Nmm]	EC5-1-1, 8.5.1.1(1)
$f_{h,2,k}, f_{h,0,k}$	the characteristic embedment strength in the timber member / parallel to grain [N/mm^2]	EC5-1-1, 8.5.1.1(2)
k_{90}	for softwoods	EC5-1-1, (8.33)
$F_{ax,Rk}$	the characteristic withdrawal capacity of the fastener	
$f_{u,k}$	the characteristic tensile strength ($f_{u,k} = 400\ \frac{N}{mm^2}$, bolt 4.8)	
t_2	the thickness of the timber middle member (Fig. 6.15) [mm]	
ρ_k	the characteristic timber density ($\rho_k = 450\ \frac{kg}{m^3}$, cf. Table 5.1)	

According to EC5-1-1, 8.2.3(4): For the limitation of the rope effect $F_{ax,Rk}$ 8.2.2(2) applies.

In the equations (6.3.20) and (6.3.21) the first term on the right hand side is the load-carrying capacity according to the Johansen yield theory, whilst the second term $\frac{F_{ax,Rk}}{4}$ is the contribution from the rope effect.

The contribution to the load-carrying capacity due to the rope effect should be limited to following percentages of the Johansen part: 25% (bolts)

As a consequence:
$$\boxed{\frac{F_{ax,Rk}}{4} = min\begin{cases} 0{,}25 \cdot R_{V,Rk,Johansen} \\ 3{,}0 \cdot f_{c,90,k} \cdot A_{washer}/4 \end{cases}} \quad (6.3.27)$$

$$\frac{F_{ax,Rk}}{4} = min\begin{cases} 0{,}25 \cdot R_{V,Rk,Johansen} \\ 9161/4 = 2290\ N \end{cases}$$

With:
$$F_{ax,Rk} = 3{,}0 \cdot f_{c,90,k} \cdot A_{washer} \quad (6.3.28)$$

$$F_{ax,Rk} = 3{,}0 \cdot 3{,}00 \cdot 1018 = 9161\ N$$

$$A_{washer} = \frac{(3 \cdot d)^2}{4} \cdot \pi = \frac{(3 \cdot 12)^2}{4} \cdot \pi = 1018\ mm^2 \quad (6.3.29)$$

Where: $F_{ax,Rk}$ the rope effect EC5-1-1, 8.5.2(2)

A_{washer} the contact area of washer EC5-1-1, 10.4.3(2)

Multiple fastener connections

For one row of fasteners parallel to the grain direction, the effective characteristic load-carrying capacity parallel to the row should be taken as:

According to EC5-1-1, 8.1.2(4): $\boxed{F_{v,ef,Rk} = n_{ef} \cdot F_{v,Rk}}$ (6.3.30)

With: parallel to the grain
$$n_{ef} = min\begin{cases} n \\ n^{0,9} \cdot \sqrt[4]{\frac{a_1}{13 \cdot d}} \end{cases} \quad (6.3.31)$$

$$n_{ef} = min\begin{cases} 2 \\ 2^{0,9} \cdot \sqrt[4]{\frac{90}{13 \cdot 12}} = 1{,}36 \end{cases} = \mathbf{1{,}63}$$

Where: n_{ef} the effective number in line parallel to the grain EC5-1-1, 8.5.1.1(4)

n the number of bolts in the row

a_1 the spacing between bolts in the grain direction (cf. Fig. 6.17)

Total effective design load-carrying capacity

The load-carrying capacity of this steel-to-timber connection with **2** plates as the outer members of double shear connections and **2 x 2 bolts** is:

With regard to (6.0.1): $\boxed{F_{v,ef,Rd} = k_{mod} \cdot \frac{F_{v,ef,Rk}}{\gamma_M}}$

$$F_{v,ef,Rd} = 0{,}90 \cdot \frac{80{,}6}{1{,}1} = \mathbf{66{,}0\ kN}$$

With: $$F_{v,ef,Rk} = 2 \cdot 2 \cdot n_{ef} \cdot F_{v,Rk} \qquad (6.3.32)$$

$$F_{v,ef,Rk} = 2 \cdot 2 \cdot 1{,}63 \cdot 12366\ N = 80{,}6\ kN$$

Where: γ_M the partial factor for a material property ($\gamma_M = 1{,}1$, failure in bolt)

$F_{v,Rk}$ see equation (6.3.22)

Ultimate Limit State

$$\boxed{\boldsymbol{F_{t,Ed,left} \leq F_{v,ef,Rd}}} \qquad (6.3.33)$$

$$\mathbf{24{,}9\ kN \leq 66{,}0\ kN} \qquad \textbf{OK}$$

With: $$F_{t,Ed,left} = 24{,}9\ kN$$

Where: $F_{t,Ed,left}$ see Table 6.12

6.3.1.2 Connection: Beam-Right timber strut

Steel-to-timber connection in beam

The angle $\alpha = 24^{\circ}$ is the angle of the load to the grain.

Spacing and end / edge distances

Minimum spacings and edge / end distances are shown in Figure 6.18.

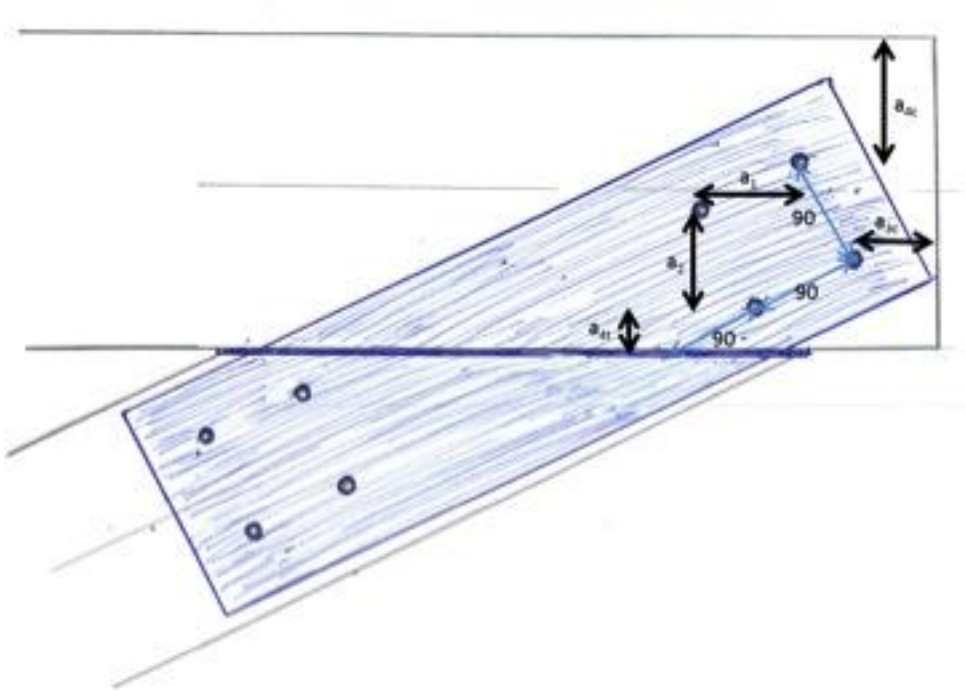

Figure 6.18 Connection between beam and left strut

<u>According to EC5-1-1, Table 8.5:</u>

Spacing and edge/end distances	Angle	Minimum spacing or edge/end distance
a_1 (parallel to the grain)	$0^\circ \leq \alpha \leq 360^\circ$	$(3 + 2\lvert\cos\alpha\rvert)d$ $=(3 + 2\lvert\cos 24\rvert)12 = 57{,}9$ mm
a_2 (perpendicular to the grain)	$0^\circ \leq \alpha \leq 360^\circ$	$3d = 3 \cdot 12 = 36\ mm$
a_{3c} (unloaded end)		$3d = 3 \cdot 12 = 36\ mm$
a_{4t} (loaded edge)	$0^\circ \leq \alpha \leq 180^\circ$	$\max[(2 + 2\sin\alpha)d; 3d] =$ $\max[(2 + 2\sin(180 - 24))12; 3 \cdot 12]$ $= 36$ mm
a_{4c} (unloaded edge)	$180^\circ \leq \alpha \leq 360^\circ$	$3d = 3 \cdot 12 = 36\ mm$

Table 6.17 Minimum spacings and edge / end distances for dowels

Based on the requirements of Table 6.17, the following spacings and distances are chosen (Table 6.18).

Spacing and edge/end distances	Minimum spacing or edge/end distance
a_1 (parallel to the grain)	$90\ mm \cdot \cos 24 = 82{,}2$
a_2 (perpendicular to the grain)	$90\ mm \cdot \cos 24 = 82{,}2$
a_{3c} (unloaded end)	75 mm
a_{4t} (loaded edge)	$90\ mm \cdot \sin 24 = 36{,}6\ mm$
4_{4c} (unloaded edge)	$270 - 82{,}2 - 2 \cdot 90\ mm \cdot \sin 24 = 114{,}6\ mm$

Table 6.18 Spacings and edge / end distances (Fig. 6.18)

Lateral load-carrying capacity of metal dowel-type fasteners

<u>According to EC5-1-1, (8.12); for thin steel plates:</u>

$$F_{v,Rk} = min\begin{cases} 0{,}5 \cdot f_{h,2,k} \cdot t_2 \cdot d \\ 1{,}15 \cdot \sqrt{2 \cdot M_{y,Rk} \cdot f_{h,2,k} \cdot d} + \frac{F_{ax,Rk}}{4} \end{cases} \quad \begin{matrix}(j)\\(k)\end{matrix} \qquad (6.3.34)$$

$$F_{v,Rk} = min\begin{cases} 0{,}5 \cdot 29{,}85 \cdot 215 \cdot 12 \\ 1{,}15 \cdot \sqrt{2 \cdot 76745 \cdot 29{,}85 \cdot 12} + \frac{F_{ax,Rk}}{4} \end{cases}$$

$$F_{v,Rk} = min\begin{cases} 38507\ N \\ 8527 + \frac{F_{ax,Rk}}{4} = 8527 + 2132 = 10659\ N \end{cases}$$

<u>With regard to (6.3.41)</u>: $\frac{F_{ax,Rk}}{4} = min\begin{cases} 0{,}25 \cdot R_{V,Rk,Johansen} \\ 9161/4 = 2290\ N \end{cases}$

$$\frac{F_{ax,Rk}}{4} = min\begin{cases} 0{,}25 \cdot 8527 = 2132\ N \\ 9161/4 = 2290\ N \end{cases} = 2132\ N$$

<u>According to EC5-1-1, (8.12); for thick steel plates:</u>

$$F_{v,Rk} = min\begin{cases} 0{,}5 \cdot f_{h,2,k} \cdot t_2 \cdot d \\ 2{,}3 \cdot \sqrt{M_{y,Rk} \cdot f_{h,2,k} \cdot d} + \frac{F_{ax,Rk}}{4} \end{cases} \quad \begin{matrix}(l)\\(m)\end{matrix} \qquad (6.3.35)$$

$$F_{v,Rk} = min\begin{cases} 0{,}5 \cdot 21{,}66 \cdot 215 \cdot 12 \\ 2{,}3 \cdot \sqrt{76745 \cdot 29{,}85 \cdot 12} + \frac{F_{ax,Rk}}{4} \end{cases}$$

$$F_{v,Rk} = min\begin{cases} 38507\ N \\ 12059 + \frac{F_{ax,Rk}}{4} = 12059 + 2290 = 14349\ N \end{cases}$$

<u>With regard to (6.3.9)</u>: $\frac{F_{ax,Rk}}{4} = min\begin{cases} 0{,}25 \cdot R_{V,Rk,Johansen} \\ 9161/4 = 2290\ N \end{cases}$

$$\frac{F_{ax,Rk}}{4} = min\begin{cases} 0{,}25 \cdot 12059 = 3014{,}8\ N \\ 9161/4 = 2290\ N \end{cases} = 2290\ N$$

According to EC5-1-1, (8.12); in between:

$$F_{v,Rk} = min\begin{cases} 38507\ N \\ \frac{(14349-10659)}{(12-6)} \cdot (8-6) + 10659 = 11889\ N \end{cases} \quad (6.3.36)$$

$$\boldsymbol{F_{v,Rk} = 11889\ N} \qquad \textbf{failure in bolt}$$

With:

$$M_{y,Rk} = 0{,}3 \cdot f_{u,k} \cdot d^{2,6} \quad (6.3.37)$$

$$M_{y,Rk} = 0{,}3 \cdot 400 \cdot 12^{2,6} = 76745\ Nmm$$

$$f_{h,2,k} = \frac{f_{h,0,k}}{k_{90} \cdot (\sin\alpha)^2 + (\cos\alpha)^2} \quad (6.3.38)$$

$$f_{h,2,k} = \frac{32{,}47}{1{,}53 \cdot (\sin 24)^2 + (\cos 24)^2} = 29{,}85\,\frac{N}{mm^2}$$

$$f_{h,0,k} = 0{,}082 \cdot (1 - 0{,}01 \cdot d) \cdot \rho_k \quad (6.3.39)$$

$$f_{h,0,k} = 0{,}082 \cdot (1 - 0{,}01 \cdot 12) \cdot 450 = 32{,}47\,\frac{N}{mm^2}$$

$$k_{90} = 1{,}35 + 0{,}015 \cdot d \quad (6.3.40)$$

$$k_{90} = 1{,}35 + 0{,}015 \cdot 12 = 1{,}53$$

Where:

$F_{v,Rk}$	the characteristic load-carrying capacity per shear plane per fastener	
$M_{y,Rk}$	the characteristic fastener yield moment [Nmm]	EC5-1-1, 8.5.1.1(1)
$f_{h,2,k}, f_{h,0,k}$	the characteristic embedment strength in the timber member / parallel to grain [N/mm^2]	EC5-1-1, 8.5.1.1(2)
k_{90}	for softwoods	EC5-1-1, (8.33)
$F_{ax,Rk}$	the characteristic withdrawal capacity of the fastener	
$f_{u,k}$	the characteristic tensile strength ($f_{u,k} = 400\,\frac{N}{mm^2}$, bolt 4.8)	
t_2	the thickness of the timber middle member (Fig. 6.15) [mm]	
ρ_k	the characteristic timber density ($\rho_k = 450\,\frac{kg}{m^3}$, cf. Table 5.1)	

According to EC5-1-1, 8.2.3(4): For the limitation of the rope effect $F_{ax,Rk}$ 8.2.2(2) applies.

In the equations (6.3.34) and (6.3.35) the first term on the right hand side is the load-carrying capacity according to the Johansen yield theory, whilst the second term $\frac{F_{ax,Rk}}{4}$ is the contribution from the rope effect.

The contribution to the load-carrying capacity due to the rope effect should be limited to following percentages of the Johansen part: 25% (bolts)

As a consequence:
$$\boxed{\frac{F_{ax,Rk}}{4} = min\begin{cases} 0{,}25 \cdot R_{V,Rk,Johansen} \\ 3{,}0 \cdot f_{c,90,k} \cdot A_{washer}/4 \end{cases}} \quad (6.3.41)$$

$$\frac{F_{ax,Rk}}{4} = min\begin{cases} 0{,}25 \cdot R_{V,Rk,Johansen} \\ 9161/4 = 2290\ N \end{cases}$$

With:
$$F_{ax,Rk} = 3{,}0 \cdot f_{c,90,k} \cdot A_{washer} \quad (6.3.42)$$

$$F_{ax,Rk} = 3{,}0 \cdot 3{,}00 \cdot 1018 = 9161\ N$$

$$A_{washer} = \frac{(3 \cdot d)^2}{4} \cdot \pi = \frac{(3 \cdot 12)^2}{4} \cdot \pi = 1018\ mm^2 \quad (6.3.43)$$

Where: $F_{ax,Rk}$ the rope effect EC5-1-1, 8.5.2(2)

A_{washer} the contact area of washer EC5-1-1, 10.4.3(2)

Multiple fastener connections

For one row of fasteners parallel to the grain direction, the effective characteristic load-carrying capacity parallel to the row should be taken as:

According to EC5-1-1, 8.1.2(4): $\boxed{F_{v,ef,Rk} = n_{ef} \cdot F_{v,Rk}}$ (6.3.44)

With: parallel to the grain
$$n_{ef} = min\begin{cases} n \\ n^{0{,}9} \cdot \sqrt[4]{\frac{a_1}{13 \cdot d}} \end{cases} \quad (6.3.45)$$

$$n_{ef} = min\begin{cases} 2 \\ 2^{0{,}9} \cdot \sqrt[4]{\frac{82{,}2}{13 \cdot 12}} = 1{,}36 \end{cases} = 1{,}59$$

Perpendicular to the grain $n_{ef} = n$ (6.3.46)

For angles $o^\circ < \alpha < 90^\circ$ between load and grain direction, n_{ef} may be determined by linear interpolation between equations (6.3.45) and (6.3.46).

$$n_{ef} = \frac{(2-1{,}59)}{(90-0)} \cdot (24-0) + 1{,}59 = \mathbf{1,70} \qquad (6.3.47)$$

Where: n_{ef} the effective number in line parallel to the grain EC5-1-1, 8.5.1.1(4)

n the number of bolts in the row

a_1 the spacing between bolts in the grain direction (cf. Fig. 6.18)

Total effective design load-carrying capacity

The load-carrying capacity of this steel-to-timber connection with **2** plates as the outer members of double shear connections and **2 x 2 bolts** is:

With regard to (6.0.1): $\boxed{F_{v,ef,Rd} = k_{mod} \cdot \frac{F_{v,ef,Rk}}{\gamma_M}}$

$$F_{v,ef,Rd} = 0{,}90 \cdot \frac{90{,}8}{1{,}1} = \mathbf{66,15\ kN}$$

With: $$F_{v,ef,Rk} = 2 \cdot 2 \cdot n_{ef} \cdot F_{v,Rk} \qquad (6.3.48)$$

$$F_{v,ef,Rk} = 2 \cdot 2 \cdot 1{,}70 \cdot 11889\ N = 80{,}8\ kN$$

Where: γ_M the partial factor for a material property ($\gamma_M = 1{,}1$, failure in bolt)

$F_{v,Rk}$ see equation (6.3.36)

Ultimate Limit State

$$\boxed{\boldsymbol{F_{t,Ed,left} \leq F_{v,ef,Rd}}} \qquad (6.3.49)$$

$$\mathbf{57,9\ kN \leq 66,15\ kN} \qquad \textbf{OK}$$

With: $F_{t,Ed,right} = 57{,}9\ kN$

Where: $F_{t,Ed,right}$ see Table 6.12

Steel-to-timber connection in strut

The angle $\alpha = 0^\circ$ is the angle of the load to the grain.

Spacing and end / edge distances

Minimum spacings and edge / end distances are shown in Figure 6.19.

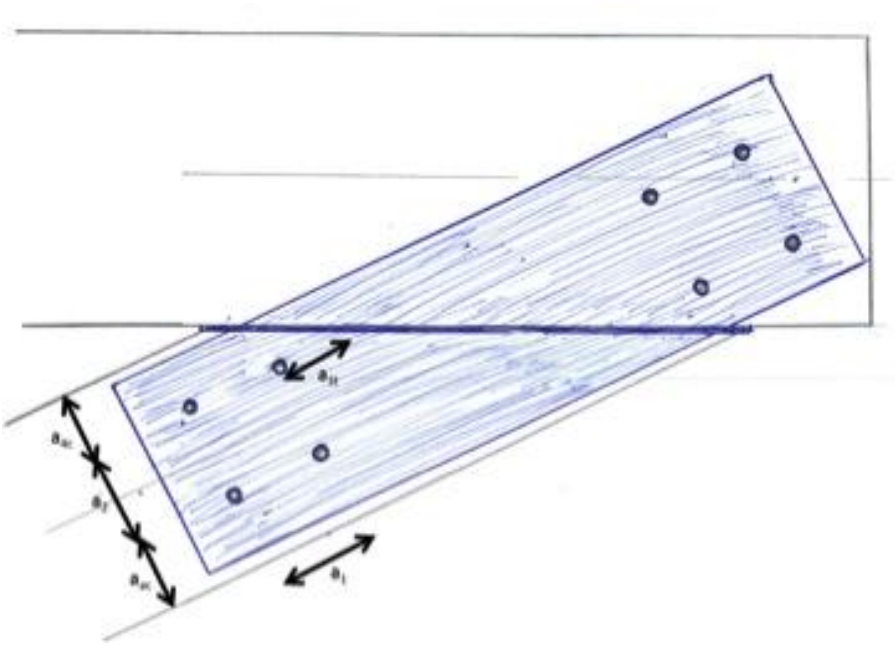

Figure 6.19 Connection between beam and left strut

<u>According to EC5-1-1, Table 8.5:</u>

Spacing and edge/end distances	Angle	Minimum spacing or edge/end distance
a_1 (parallel to the grain)	$0^\circ \leq \alpha \leq 360^\circ$	$(3 + 2\lvert\cos\alpha\rvert)d$ $=(3 + 2\lvert\cos 0\rvert)12 = 60\ mm$
a_2 (perpendicular to the grain)	$-90^\circ \leq \alpha \leq 90^\circ$	$\max(7d; 80mm) = 84\ mm$
a_{3t} (loaded end)	$180^\circ \leq \alpha \leq 360^\circ$	$3d = 3 \cdot 12 = 36\ mm$
a_{4c} (unloaded edge)	$180^\circ \leq \alpha \leq 360^\circ$	$3d = 3 \cdot 12 = 36\ mm$

Table 6.19 Minimum spacings and edge / end distances for dowels

Based on the requirements of Table 6.19, the following spacings and distances are chosen (Table 6.20).

Spacing and edge/end distances	Minimum spacing or edge/end distance
a_1 (parallel to the grain)	$90\ mm$
a_2 (perpendicular to the grain)	$90\ mm$
a_{3t} (loaded end)	$90\ mm$
4_{4c} (unloaded edge)	$0{,}5 \cdot (225 - 90) = 67{,}5\ mm$

Table 6.20 Spacings and edge / end distances (Fig. 6.19)

Ultimate Limit State

The results of subchapter 6.3.1.1 about the connection resistance between beam and left strut can be taken over. The whole connection is identical.

$$\boxed{\boldsymbol{F_{t,Ed,right} \leq F_{v,ef,Rd}}} \qquad (6.3.50)$$

$$\boldsymbol{57,9\ kN \leq 66,0\ kN} \qquad \textbf{OK}$$

With: $F_{t,Ed,right} = 57{,}9\ kN$

Where: $F_{t,Ed,right}$ see Table 6.12

$F_{v,ef,Rd}$ see equation (6.3.33)

6.3.2 Connection: Hanger

At the connection point beneath the deck the struts are connected to the hangers and, at the same time, to the tension rods.

Figure 6.20 demonstrates the developed design of the elaborate connection point. The assembly is chosen in order to assure that the system lines for all members coincide with the center lines and intersect in the center of the connection point.

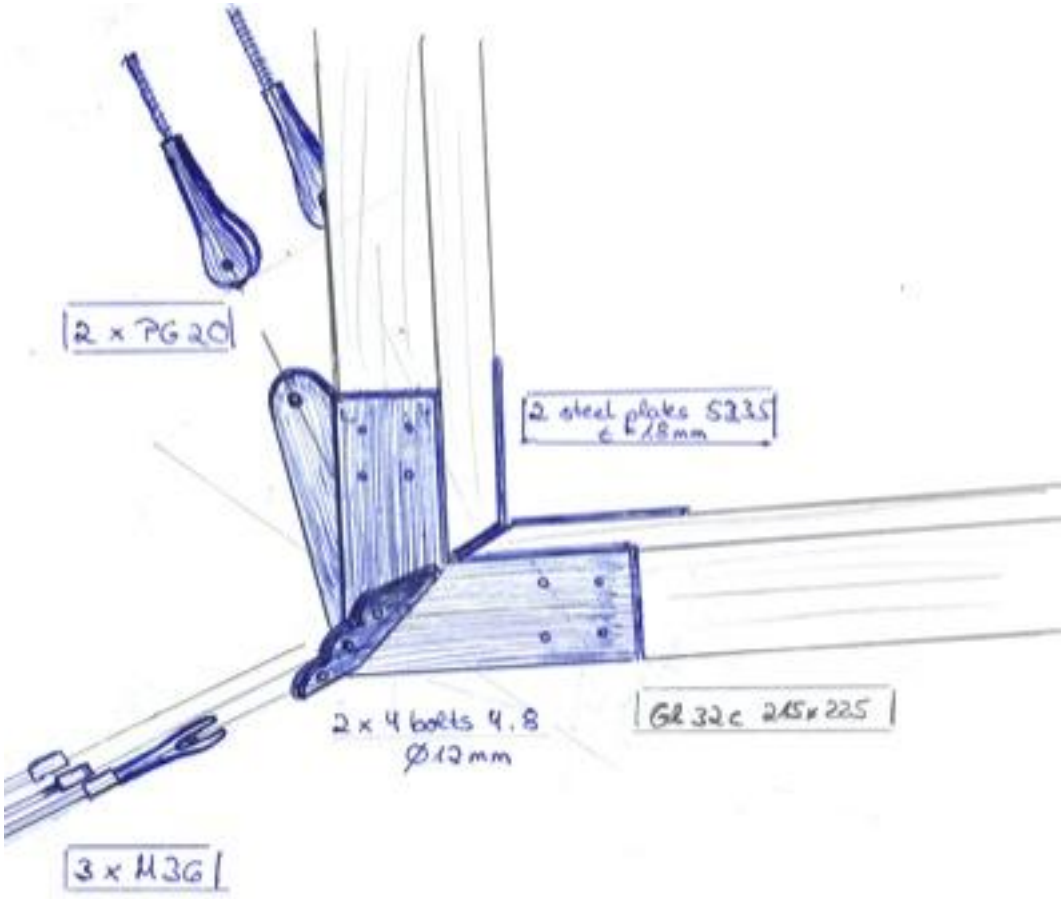

Figure 6.20 Draft of the connection point underneath the deck

Furthermore, it can be seen how the idea of anchoring two hangers per timber frame has been developed. The reason therefore has been the wish to facilitate the breathing of the glulam members. Covering the left timber strut also at the backside with a steel plate would create a whole ‘shoe’ around the connection point. As a consequence, the ventilation of the connection point would be more difficult to assure and the risk of moisture accumulating at the struts backside would increase. That means, the cables’ fork connectors have to be connected directly with the steel plates of the steel-to-timber connection on both sides of the timber struts (2 hangers).

The whole assembly of steel-to-timber connection and anchored hangers is unified to an entire steel plate on each side of the strut. The demanding thickness for the steel plate is the size of 18 mm given by the data sheets of the German company Pfeifer (Fig. 6.22). The data sheets describe exactly how to design the connection of the hanger. For the hanger pairs the chosen cross-section of 20 mm each (cf. subchapter 5.3.1) is sufficient to take the highest tension force of 208 kN at the innermost timber frame (Fig. 6.21).

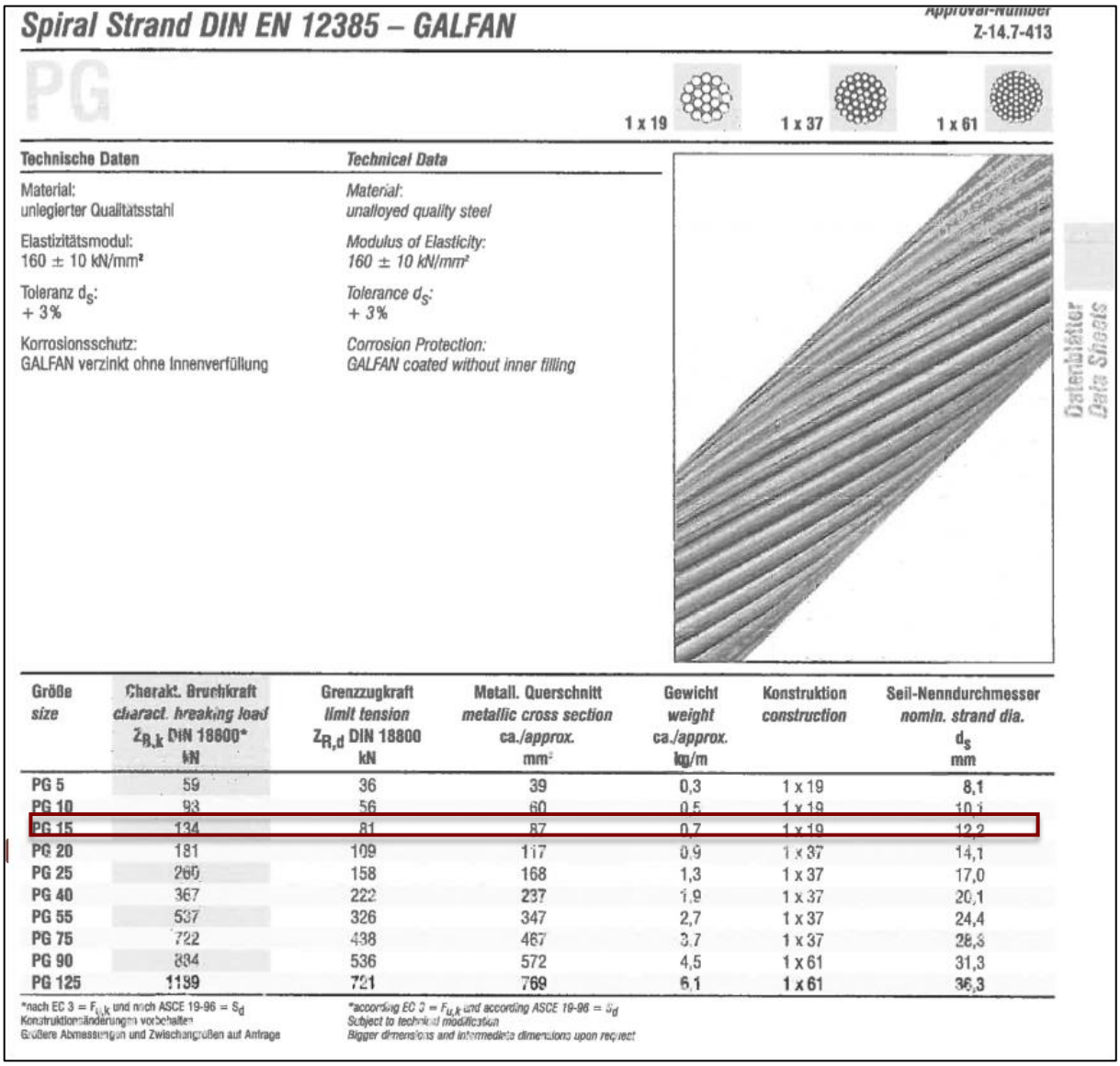

Spiral Strand DIN EN 12385 – GALFAN

Approval-Number Z-14.7-413

PG

1 x 19 1 x 37 1 x 61

Technische Daten

Material:
unlegierter Qualitätsstahl

Elastizitätsmodul:
160 ± 10 kN/mm²

Toleranz d_S:
+ 3%

Korrosionsschutz:
GALFAN verzinkt ohne Innenverfüllung

Technical Data

Material:
unalloyed quality steel

Modulus of Elasticity:
160 ± 10 kN/mm²

Tolerance d_S:
+ 3%

Corrosion Protection:
GALFAN coated without inner filling

Datenblätter Data Sheets

Größe *size*	Charakt. Bruchkraft *charact. breaking load* $Z_{B,k}$ DIN 18800* kN	Grenzzugkraft *limit tension* $Z_{R,d}$ DIN 18800 kN	Metall. Querschnitt *metallic cross section* ca./*approx.* mm²	Gewicht *weight* ca./*approx.* kg/m	Konstruktion *construction*	Seil-Nenndurchmesser *nomin. strand dia.* d_S mm
PG 5	59	36	39	0,3	1 x 19	8,1
PG 10	93	56	60	0,5	1 x 19	10,1
PG 15	134	81	87	0,7	1 x 19	12,2
PG 20	181	109	117	0,9	1 x 37	14,1
PG 25	265	158	168	1,3	1 x 37	17,0
PG 40	367	222	237	1,9	1 x 37	20,1
PG 55	537	326	347	2,7	1 x 37	24,4
PG 75	722	438	467	3,7	1 x 37	28,3
PG 90	884	536	572	4,5	1 x 61	31,3
PG 125	1199	721	769	6,1	1 x 61	36,3

*nach EC 3 = $F_{u,k}$ und nach ASCE 19-96 = S_d
Konstruktionsänderungen vorbehalten
Größere Abmessungen und Zwischengrößen auf Anfrage

*according EC 3 = $F_{u,k}$ and according ASCE 19-96 = S_d
Subject to technical modification
Bigger dimensions and intermediate dimensions upon reqiest

Figure 6.21 Data sheet of cable PG (PFEIFER 2011)

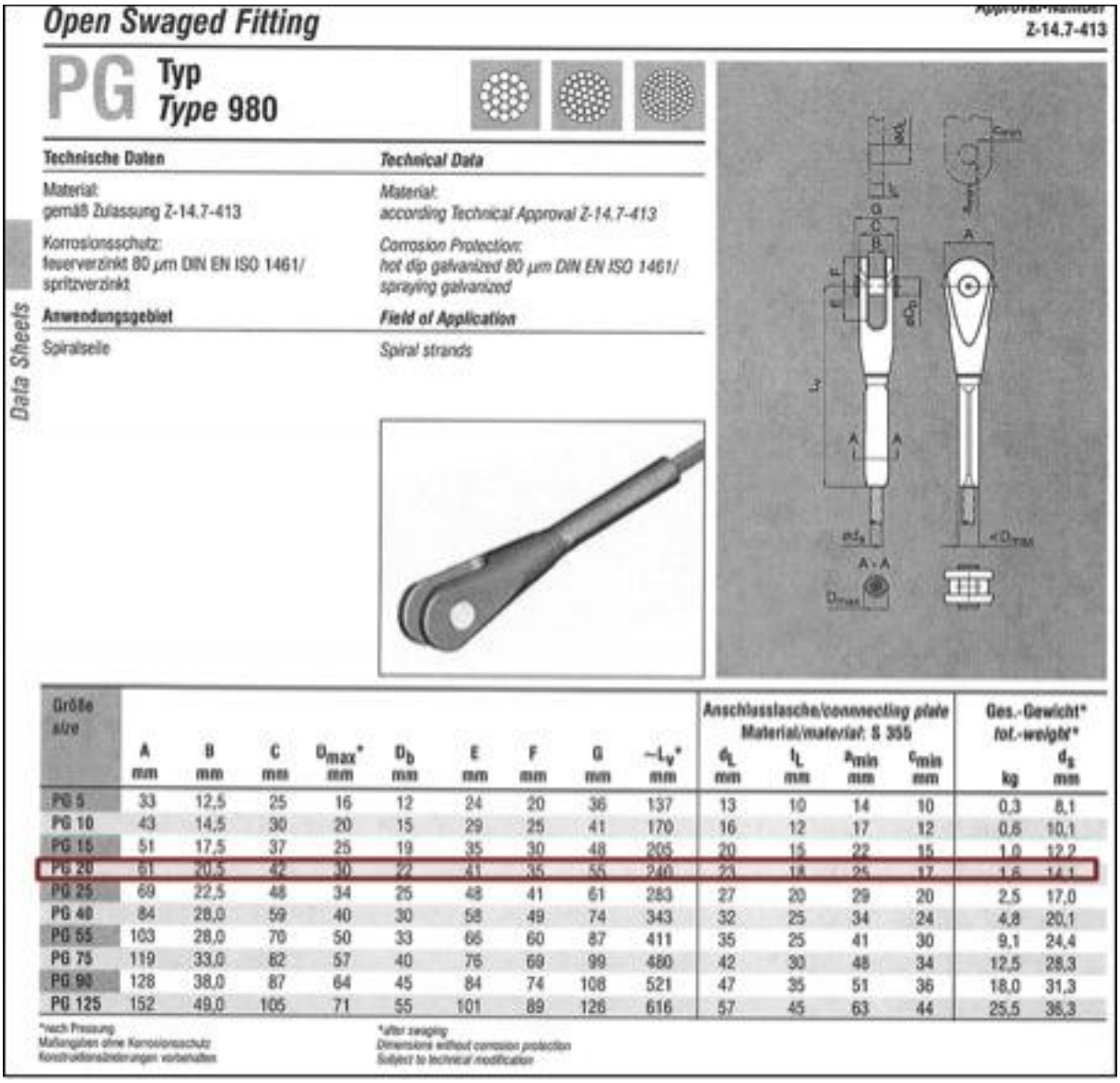

Open Swaged Fitting

Z-14.7-413

PG Typ / Type 980

Data Sheets

Technische Daten	Technical Data
Material: gemäß Zulassung Z-14.7-413	Material: according Technical Approval Z-14.7-413
Korrosionsschutz: feuerverzinkt 80 µm DIN EN ISO 1461/ spritzverzinkt	Corrosion Protection: hot dip galvanized 80 µm DIN EN ISO 1461/ spraying galvanized
Anwendungsgebiet	**Field of Application**
Spiralseile	Spiral strands

Größe size	A mm	B mm	C mm	D_{max}* mm	D_b mm	E mm	F mm	G mm	$\sim L_v$* mm	Anschlusslasche/connecting plate Material/material: S 355 d_L mm	l_L mm	a_{min} mm	c_{min} mm	Ges.-Gewicht* tot.-weight* kg	d_s mm
PG 5	33	12,5	25	16	12	24	20	36	137	13	10	14	10	0,3	8,1
PG 10	43	14,5	30	20	15	29	25	41	170	16	12	17	12	0,6	10,1
PG 15	51	17,5	37	25	19	35	30	48	205	20	15	22	15	1,0	12,2
PG 20	61	20,5	42	30	22	41	35	55	240	23	18	25	17	1,6	14,1
PG 25	69	22,5	48	34	25	48	41	61	283	27	20	29	20	2,5	17,0
PG 40	84	28,0	59	40	30	58	49	74	343	32	25	34	24	4,8	20,1
PG 55	103	28,0	70	50	33	66	60	87	411	35	25	41	30	9,1	24,4
PG 75	119	33,0	82	57	40	76	69	99	480	42	30	48	34	12,5	28,3
PG 90	128	38,0	87	64	45	84	74	108	521	47	35	51	36	18,0	31,3
PG 125	152	49,0	105	71	55	101	89	126	616	57	45	63	44	25,5	38,3

*nach Pressung
Maßangaben ohne Korrosionsschutz
Konstruktionsänderungen vorbehalten

*after swaging
Dimensions without corrosion protection
Subject to technical modification

Figure 6.22 Data sheet of cable connector PG Type 980 (PFEIFER 2011)

In Figure 6.23 more discarded variants are shown. The slotted-in plate variant did not convince since the risk for moisture seems to increase. Another variant shows all connections centralized in the center of the connection point. In this case, the very tight positioning of all connection members did not appeal. The last variant shows the former version of the final variant. Here, the advantageous fact that all connection members are located in the same system lines is not guaranteed.

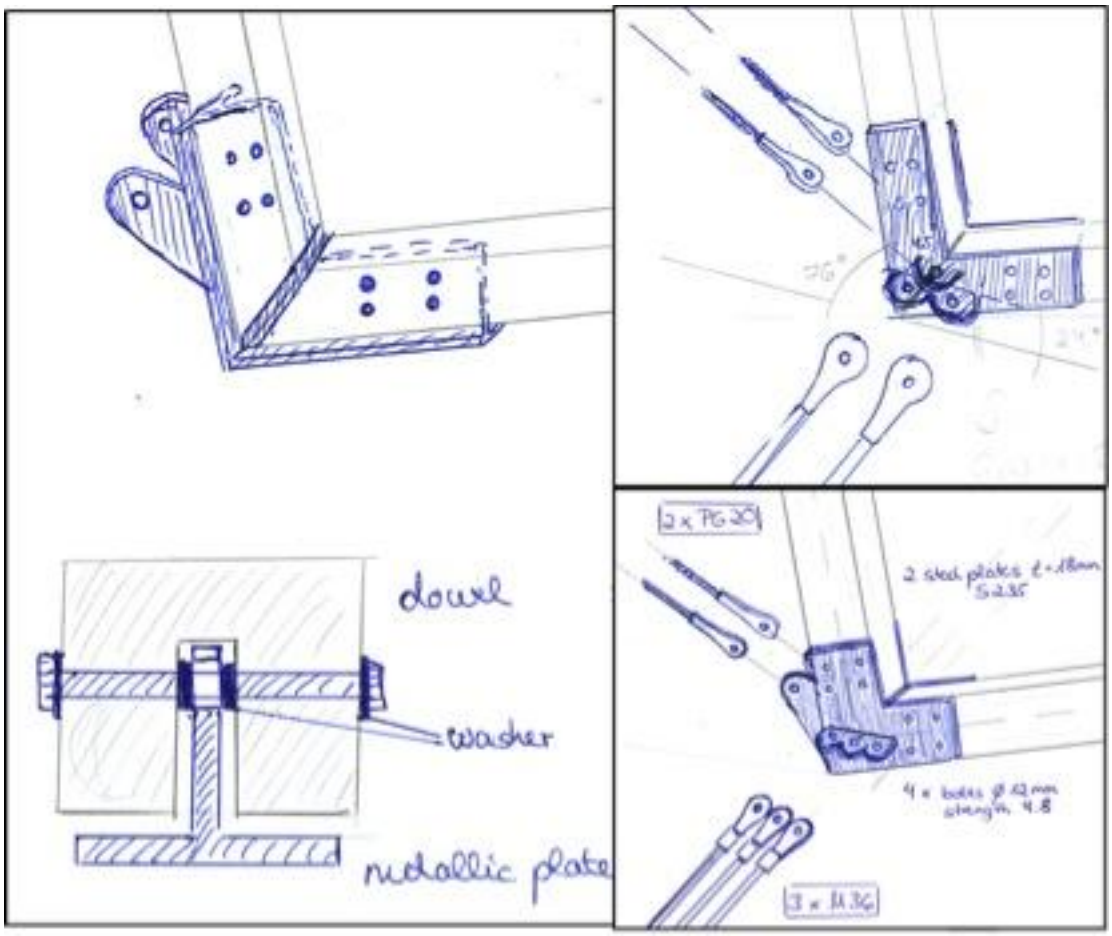

Figure 6.23 Discarded variants of the connection point between struts / hangers / rods

6.3.3 Connection: Strut-Strut

Every strut is subjected once along the half curved structure to tension instead of compression. This tension will be taken by the connections.

Table 6.21 shows the maximum value and the position of the tension force in both struts.

	Angle	Symbol	Frame	Maximum value
left strut	α=76˚	$\mathbf{F_{t,Ed,left}}$	**‘1’**	**24,90 kN**
right strut	α=24˚	$\mathbf{F_{t,Ed,right}}$	**‘11’**	**57,90 kN**

Table 6.21 Tensile forces in timber struts

The angle $\alpha = 0^{\circ}$ is the angle of the load to the grain. The fasteners are located parallel to the grain.

With regard to (6.3.2):

In this case: Thick plates $t_s = 18\ mm \geq d = 12\ mm$

Spacing and end / edge distances

Minimum spacings and edge / end distances are shown in Figure 6.24.

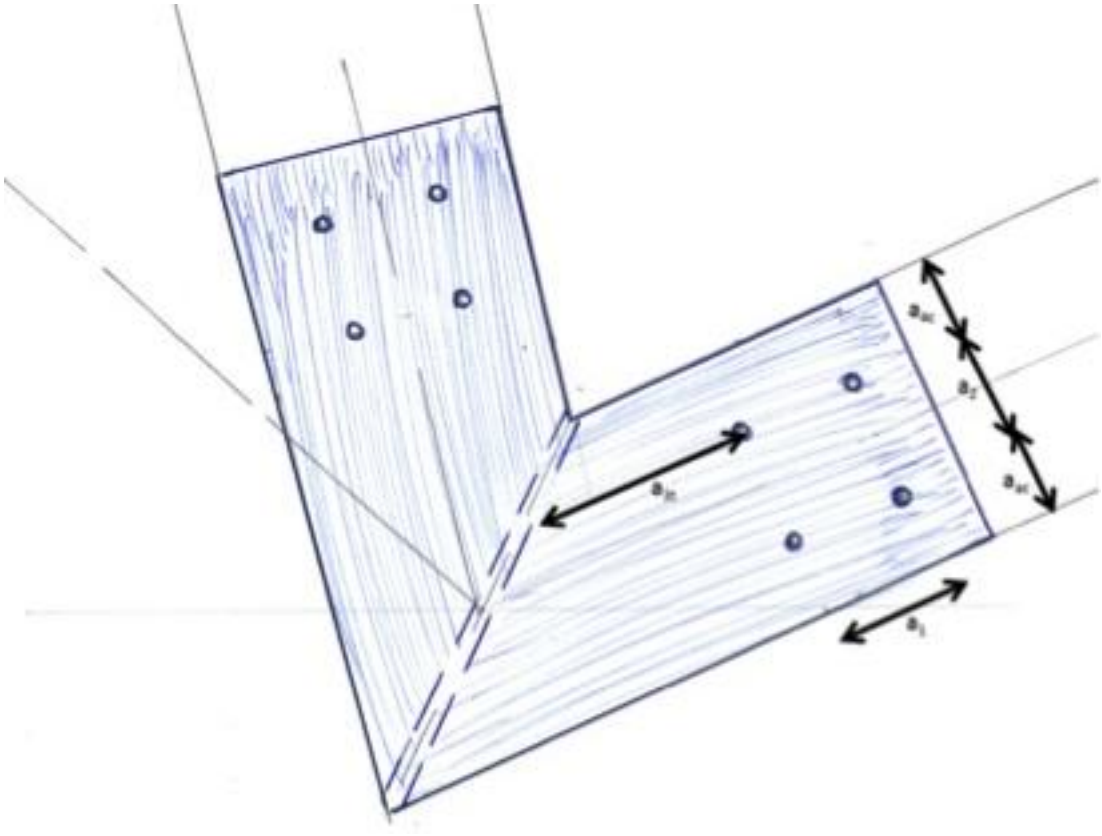

Figure 6.24 Connection between struts

According to EC5-1-1, Table 8.5:

Spacing and edge/end distances	Angle	Minimum spacing or edge/end distance
a_1 (parallel to the grain)	$0^\circ \leq \alpha \leq 360^\circ$	$(3 + 2\lvert\cos\alpha\rvert)d$ $=(3 + 2\lvert\cos 0\rvert)12 = 60\ mm$
a_2 (perpendicular to the grain)	$-90^\circ \leq \alpha \leq 90^\circ$	$\max(7d; 80mm) = 84\ mm$
a_{3t} (loaded end)	$180^\circ \leq \alpha \leq 360^\circ$	$3d = 3 \cdot 12 = 36\ mm$
a_{4c} (unloaded edge)	$180^\circ \leq \alpha \leq 360^\circ$	$3d = 3 \cdot 12 = 36\ mm$

Table 6.22 Minimum spacings and edge / end distances for dowels

Based on the requirements of Table 6.22, the following spacings and distances are chosen (Table 6.23).

Spacing and edge/end distances	Minimum spacing or edge/end distance
a_1 (parallel to the grain)	$90\ mm$
a_2 (perpendicular to the grain)	$90\ mm$
a_{3t} (loaded end)	$180\ mm$
4_{4c} (unloaded edge)	$0{,}5 \cdot (225 - 90) = 67{,}5\ mm$

Table 6.23 Spacings and edge / end distances (Fig. 6.24)

Lateral load-carrying capacity of metal dowel-type fasteners

According to EC5-1-1, (8.12); for thick steel plates:

$$F_{v,Rk} = min\begin{cases} 0{,}5 \cdot f_{h,2,k} \cdot t_2 \cdot d \\ 2{,}3 \cdot \sqrt{M_{y,Rk} \cdot f_{h,2,k} \cdot d} + \frac{F_{ax,Rk}}{4} \end{cases} \quad \begin{matrix}(l)\\(m)\end{matrix} \qquad (6.3.51)$$

$$F_{v,Rk} = min\begin{cases} 0{,}5 \cdot 32{,}47 \cdot 215 \cdot 12 \\ 2{,}3 \cdot \sqrt{76745 \cdot 32{,}47 \cdot 12} + \frac{F_{ax,Rk}}{4} \end{cases}$$

$$F_{v,Rk} = min\begin{cases} 41886\ N \\ 12577 + \frac{F_{ax,Rk}}{4} = 12577 + 2290 = 14867\ N \end{cases}$$

With regard to (6.3.56): $\frac{F_{ax,Rk}}{4} = min\begin{cases} 0{,}25 \cdot R_{V,Rk,Johansen} \\ 9161/4 = 2290\ N \end{cases}$

$$\frac{F_{ax,Rk}}{4} = min\begin{cases} 0{,}25 \cdot 12577 = 3144\ N \\ 9161/4 = 2290\ N \end{cases} = 2290\ N$$

$$\boldsymbol{F_{v,Rk} = 14867\ N} \qquad \textbf{failure in bolt}$$

With:
$$M_{y,Rk} = 0{,}3 \cdot f_{u,k} \cdot d^{2,6} \qquad (6.3.52)$$

$$M_{y,Rk} = 0{,}3 \cdot 400 \cdot 12^{2,6} = 76745\ Nmm$$

$$\boldsymbol{f_{h,2,k} = f_{h,0,k}} \qquad (6.3.53)$$

$$f_{h,0,k} = 0{,}082 \cdot (1 - 0{,}01 \cdot d) \cdot \rho_k \qquad (6.3.54)$$

$$f_{h,0,k} = 0{,}082 \cdot (1 - 0{,}01 \cdot 12) \cdot 450 = 32{,}47\ \frac{N}{mm^2}$$

$$k_{90} = 1{,}35 + 0{,}015 \cdot d \qquad (6.3.55)$$

$$k_{90} = 1{,}35 + 0{,}015 \cdot 12 = 1{,}53$$

Where:
- $F_{v,Rk}$ the characteristic load-carrying capacity per shear plane per fastener
- $M_{y,Rk}$ the characteristic fastener yield moment [Nmm] EC5-1-1, 8.5.1.1(1)
- $f_{h,2,k}, f_{h,0,k}$ the characteristic embedment strength in the timber member / parallel to grain [N/mm^2] EC5-1-1, 8.5.1.1(2)
- k_{90} for softwoods EC5-1-1, (8.33)
- $F_{ax,Rk}$ the characteristic withdrawal capacity of the fastener
- $f_{u,k}$ the characteristic tensile strength ($f_{u,k} = 400\,\frac{N}{mm^2}$, bolt 4.8)
- t_2 the thickness of the timber middle member (Fig. 6.15) [mm]
- ρ_k the characteristic timber density ($\rho_k = 450\,\frac{kg}{m^3}$, cf. Table 5.1)

According to EC5-1-1, 8.2.3(4): For the limitation of the rope effect $F_{ax,Rk}$ 8.2.2(2) applies.

In the equation (6.3.51) the first term on the right hand side is the load-carrying capacity according to the Johansen yield theory, whilst the second term $\frac{F_{ax,Rk}}{4}$ is the contribution from the rope effect.

The contribution to the load-carrying capacity due to the rope effect should be limited to following percentages of the Johansen part: 25% (bolts)

As a consequence:
$$\boxed{\frac{F_{ax,Rk}}{4} = min\begin{cases} 0{,}25 \cdot R_{V,Rk,Johansen} \\ 3{,}0 \cdot f_{c,90,k} \cdot A_{washer}/4 \end{cases}} \qquad (6.3.56)$$

$$\frac{F_{ax,Rk}}{4} = min\begin{cases} 0{,}25 \cdot R_{V,Rk,Johansen} \\ 9161/4 = 2290\ N \end{cases}$$

With: $$F_{ax,Rk} = 3{,}0 \cdot f_{c,90,k} \cdot A_{washer} \quad (6.3.57)$$

$$F_{ax,Rk} = 3{,}0 \cdot 3{,}00 \cdot 1018 = 9161\ N$$

$$A_{washer} = \frac{(3 \cdot d)^2}{4} \cdot \pi = \frac{(3 \cdot 12)^2}{4} \cdot \pi = 1018\ mm^2 \quad (6.3.58)$$

Where: $F_{ax,Rk}$ the rope effect EC5-1-1, 8.5.2(2)

A_{washer} the contact area of washer EC5-1-1, 10.4.3(2)

Multiple fastener connections

For one row of fasteners parallel to the grain direction, the effective characteristic load-carrying capacity parallel to the row should be taken as:

According to EC5-1-1, 8.1.2(4): $$\boxed{F_{v,ef,Rk} = n_{ef} \cdot F_{v,Rk}} \quad (6.3.59)$$

With: parallel to the grain $$n_{ef} = min\begin{cases} n \\ n^{0{,}9} \cdot \sqrt[4]{\frac{a_1}{13 \cdot d}} \end{cases} \quad (6.3.60)$$

$$n_{ef} = min\begin{cases} 2 \\ 2^{0{,}9} \cdot \sqrt[4]{\frac{90}{13 \cdot 12}} = 1{,}36 \end{cases} = \mathbf{1{,}63}$$

Where: n_{ef} the effective number in line parallel to the grain EC5-1-1, 8.5.1.1(4)

n the number of bolts in the row

a_1 the spacing between bolts in the grain direction (cf. Fig. 6.24)

Total effective design load-carrying capacity

The load-carrying capacity of this steel-to-timber connection with **2** plates as the outer members of double shear connections and **2 x 2 bolts** is:

With regard to (6.0.1): $$\boxed{F_{v,ef,Rd} = k_{mod} \cdot \frac{F_{v,ef,Rk}}{\gamma_M}}$$

$$F_{v,ef,Rd} = 0{,}90 \cdot \frac{97{,}0}{1{,}1} = \mathbf{79{,}4\ kN}$$

With: $$F_{v,ef,Rk} = 2 \cdot 2 \cdot n_{ef} \cdot F_{v,Rk} \quad (6.3.61)$$

$$F_{v,ef,Rk} = 2 \cdot 2 \cdot 1{,}63 \cdot 14867\ N = 97{,}0\ kN$$

Where: γ_M the partial factor for a material property ($\gamma_M = 1{,}1$, failure in bolt)

$F_{v,Rk}$ see equation (6.3.51)

Ultimate Limit State

$$\boxed{\boldsymbol{F_{t,Ed,max} \leq F_{v,ef,Rd}}} \qquad (6.3.62)$$

$$\mathbf{57,9\ kN \leq 97,4\ kN} \qquad \textbf{OK}$$

With: $F_{t,Ed,max} = 57{,}9\ kN$

Where: $F_{t,Ed,max}$ see Table 6.21

6.3.4 Connection: Tension rods

The fork connectors of the three tension rods are anchored from one timber frame to the next. Therefore, steel plates have to be welded to the 18 mm steel plates of the steel-to-timber connection. Three connection points are needed for the fork connectors (Fig. 6.25). The welded joint has to take the high-tension force. The rods' cross-sections of 36 mm (cf. subchapter 5.3.1) are chosen by the highest tension force in the tension arch of 992 kN (Fig. 6.26).

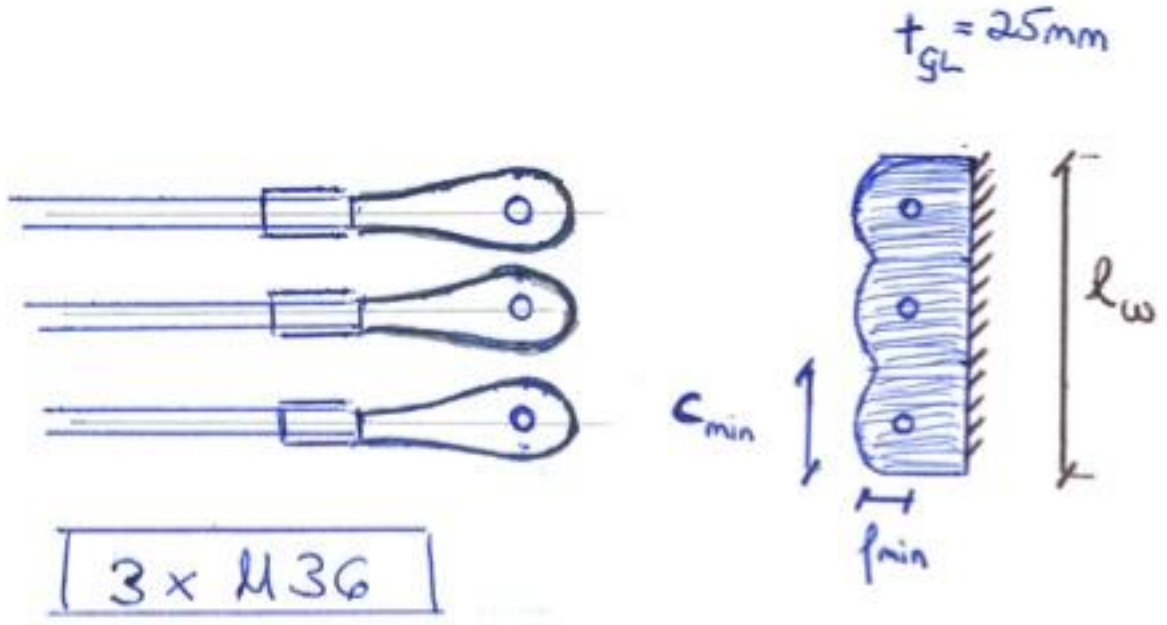

Figure 6.25 Draft of the connection between fork connectors and steel plate on one side of the struts (Tension arch)

According to EC3-1-8:2010-12, 4.5.3.2(6):

$$\sigma_\perp \leq 0{,}9 \cdot \frac{f_{u,k}}{\gamma_{M2}} \tag{6.3.63}$$

With:

$$\sigma_\perp = \frac{F_{t,Ed,max}}{A_w} \tag{6.3.64}$$

$$A_w = 2 \cdot l_w \cdot a \tag{6.3.65}$$

$$l_w = \min(3 \cdot c_{min}) = \min(270\ mm) \tag{6.3.66}$$

Where: $\sigma_\perp$ normal stress perpendicular to the axis of the weld

$F_{t,Ed,max}$ maximum tension force in the tension arch

SAP-result: $F_{t,Ed,max} = 992\ kN$

l_w weld length (cf. Fig. 6.25) EC3-1-8, 4.5.1

a fillet weld thickness EC3-1-8, 4.5.2

c_{min} (cf. Fig. 6.27)

$f_{u,k}$ tensile strength ($f_{u,k} = 360 \frac{N}{mm^2}$, S235 $t \leq 40\ mm$) EC3-1-1, Table 3.1

γ_{M2} partial factor for steel, $\gamma_{M2} = 1{,}25$ EC3-1-1/NA:2010-12, NDP 6.1(1)

According to (6.3.63) and (6.3.64): $a \geq \frac{F_{t,Ed,max}}{0{,}9 \cdot \frac{f_{u,k}}{\gamma_{M2}} \cdot l_w}$ (6.3.67)

$$a \geq \frac{0{,}992\ MN}{0{,}9 \cdot \frac{360}{1{,}25} \cdot 2 \cdot 0{,}27\ m} \geq 7{,}1\ mm$$

According to EC5-1-1, 8.1.2(4): $a \geq \sqrt{\max t} - 0{,}5 = \sqrt{\ } - 0{,}5 =\ mm$ (6.3.68)

With: $\max t = t_{Gl} = 25\ mm$

Where: t_{Gl} thickness of connection steel plate of fork connector cf. Figure 6.27

$$\boldsymbol{a = 8\ mm}$$ **OK**

As transmitter works the steel plate between the two struts which has to be thick enough to transmit this high tension force acting along the tension arch to the next tension rod connectors.

According to EC3-1-1:2010-12, 6.2.3:

$$\boxed{\frac{N_{Ed}}{N_{t,Rd}} \leq 1} \quad (6.3.69)$$

With: $N_{t,Rd} = \frac{A \cdot f_{y,k}}{\gamma_{M0}}$ (6.3.70)

$N_{Ed} = F_{t,Ed,max}$ (6.3.71)

$A = b \cdot t = 350\ mm \cdot t$ (6.3.72)

Where: $N_{t,Rd}$ the design tension resistance

$F_{t,Ed,max}$ maximum tension force in the tension arch

SAP-result: $F_{t,Ed,max} = 992\ kN$

$f_{y,k}$ yield strength ($f_{y,k} = 235 \frac{N}{mm^2}$, S235 $t \leq 40\ mm$) EC3-1-1, Table 3.1

γ_{M0}	partial factor for steel, $\gamma_{M0} = 1{,}0$	EC3-1-1/NA:2010-12, NDP 6.1(1)
b	contact length between timber struts	cf. Figure 6.13

According to (6.3.69) until (6.3.70): $t \geq \frac{F_{t,Ed,max} \cdot \gamma_{M0}}{f_{y,k} \cdot b}$ (6.3.73)

$$t \geq \frac{0{,}992\ MN \cdot 1{,}0}{235 \cdot 0{,}35\ m} = 12{,}1\ mm$$

$$\boldsymbol{t = 14\ mm} \qquad \textbf{OK}$$

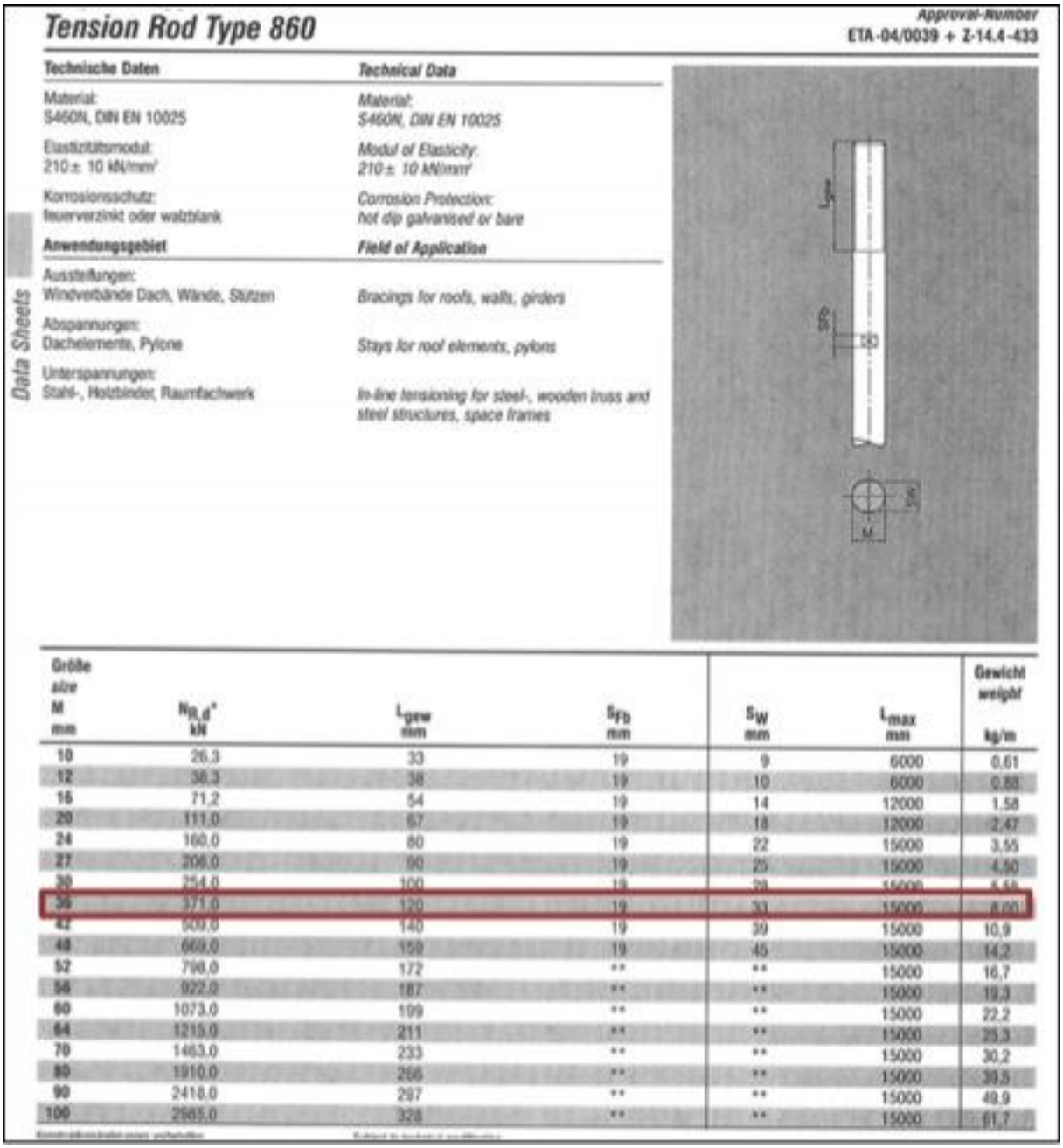

Tension Rod Type 860

Approval-Number
ETA-04/0039 + Z-14.4-433

Data Sheets

Technische Daten	Technical Data
Material: S460N, DIN EN 10025	Material: S460N, DIN EN 10025
Elastizitätsmodul: 210 ± 10 kN/mm²	Modul of Elasticity: 210 ± 10 kN/mm²
Korrosionsschutz: feuerverzinkt oder walzblank	Corrosion Protection: hot dip galvanised or bare
Anwendungsgebiet	***Field of Application***
Aussteifungen: Windverbände Dach, Wände, Stützen	*Bracings for roofs, walls, girders*
Abspannungen: Dachelemente, Pylone	*Stays for roof elements, pylons*
Unterspannungen: Stahl-, Holzbinder, Raumfachwerk	*In-line tensioning for steel-, wooden truss and steel structures, space frames*

Größe size M mm	N_{Rd}* kN	L_{gew} mm	S_{Fb} mm	S_W mm	L_{max} mm	Gewicht weight kg/m
10	26.3	33	19	9	6000	0.61
12	38.3	38	19	10	6000	0.88
16	71.2	54	19	14	12000	1.58
20	111.0	67	19	18	12000	2.47
24	160.0	80	19	22	15000	3.55
27	206.0	90	19	25	15000	4.50
30	254.0	100	19	28	15000	5.55
36	371.0	120	19	33	15000	8.00
42	509.0	140	19	39	15000	10.9
48	669.0	159	19	45	15000	14.2
52	798.0	172	**	**	15000	16.7
56	922.0	187	**	**	15000	19.3
60	1073.0	199	**	**	15000	22.2
64	1215.0	211	**	**	15000	25.3
70	1463.0	233	**	**	15000	30.2
80	1910.0	266	**	**	15000	39.5
90	2418.0	297	**	**	15000	49.9
100	2985.0	328	**	**	15000	61.7

Figure 6.26 Data sheet of Tension Rod Type 860 (PFEIFER 2011)

Fork Connector Type 860

Approval-Number
ETA-04/0039 + Z-14.4-433

Technische Daten / ***Technical Data***

Material: EN-GJS-400-18-LT DIN EN 1563 / *Material: EN-GJS-400-18-LT DIN EN 1563*

Bolzen: 34CrNiMoSV, W. Nr. 1.6582 DIN EN 10083-1 / *Pin: 34CrNiMoSV, W. Nr. 1.6582 DIN EN 10083-1*

Kontermutter: S355J2G3, DIN EN 10025 / *Locking Nut: S355J2G3, DIN EN 10025*

Anschlussblech: S355J2G3 / *Connecting Plate: S355J2G3*

Anwendungsgebiet / ***Field of Application***

Zugstab / *Tension Rod*

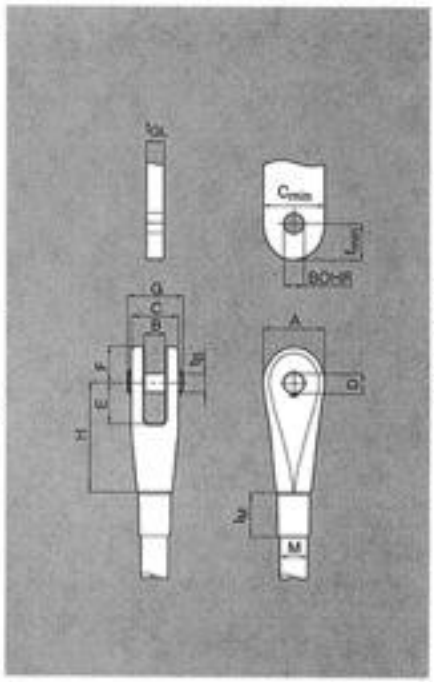

Größe size M mm	Gabelkopf fork connector A mm	B mm	C mm	D mm	E mm	F mm	H mm	Bolzen pin d_B mm	G mm	Kontermutter lock nut l_M mm	Anschlussblech connecting plate l_{GL} mm	f_{min} mm	c_{min} mm	BOHR mm	Ges.Gewicht tot.weight kg
10	25	10	20	10	19	16	52	9	27,0	21	8	16	25	10	0,12
12	29	12	24	11	21	18	58	10	31,0	25	10	17	29	11	0,20
16	42	15	32	15	30	26	77	14	41,0	33	12	23	42	15	0,53
20	52	18	40	17	35	31	93	16	50,2	41	15	27	52	17	0,95
24	58	23	48	23	46	39	115	22	59,8	49	20	36	58	23	1,57
27	68	23	54	25	47	44	125	24	66,6	55	20	39	68	25	2,34
30	77	28	60	29	52	51	138	28	74,8	62	25	47	77	30	3,44
36	90	28	72	33	64	58	167	32	89,3	74	25	53	90	34	5,57
42	104	33	84	37	70	66	190	36	103,0	86	30	59	104	38	8,74
48	120	38	96	41	78	74	213	40	118,0	99	35	66	120	42	12,7
52	136	43	104	46	85	84	231	45	126,0	107	40	73	136	47	16,5
56	148	43	112	51	95	91	254	50	138,0	115	40	81	148	52	21,9
60	162	48	120	56	106	100	275	55	146,0	124	45	90	162	58	27,1
64	170	53	128	56	107	103	286	55	154,0	132	50	90	170	58	31,6
70	185	58	140	61	117	113	315	60	166,0	144	55	98	185	63	39,3
80	210	68	160	71	133	132	359	70	187,0	165	65	114	210	73	58,6
90	240	78	180	80	150	150	402	79	211,0	185	75	128	240	82	85,5
100	265	83	200	90	170	165	448	89	232,0	205	80	144	265	92	120,5

Konstruktionsänderungen vorbehalten / *Subject to technical modification*

Datenblätter

Figure 6.27 Data sheet of Fork Connector Type 860 (PFEIFER 2011)

7. Conclusions and further research

Taking a look back, it can be said that the statics of this rather unusual curved and suspended structure have been more difficult than expected. The distribution of loads, especially in the timber beam of the timber frame, demonstrated how important it is to keep in mind the three-dimensional influence of the curvature. Otherwise, it is surprisingly easy to lose the overview during the load-bearing design.

The analyses of the statics made it clear that the one-side-suspension has a great influence on the whole behavior of the bridge. The location of the suspension is a very important decision. The conclusion is the need of stabilization in order to prevent the bridge deck from twisting. When selecting the concept of the inner edge suspension the upper part of the deck has to take tension while the lower part has to take compression. When selecting the concept of the outer edge suspension the forces are just the other way around. Since it is desirable to load the timber deck mostly by compression, the concept of the suspension along the outer edge was chosen for the further progress.

The parameter study visualized that the horizontal force components of the inclined hangers should not be neglected. As a consequence, it is desirable to keep the angle of the hangers as close to 90° as possible. Another result has been that the lever arm of the connection point below the deck should be chosen as small as possible, i.e. the connection point should not be too eccentric regarding the bridge's cross-section.

Along the curvature the loads are accumulated in the centre of the structure. Consequently, the most loaded hangers and timber frames have been the ones closest to the pylon. The shear force in the innermost timber beam was so unusually high that a cross-section was needed which is 3 times higher than the one used for the rest of the timber frames' beams. As a reason, it is suggested to replace the two innermost timber beams by smaller steel profiles as an alternative.

A suggestion to improve the connections between beam and struts could be to arrange the horizontal rows of the dowels more parallel to the grain direction of the beam.

The load-bearing design process has been calculated under the aspect of the bridge's durability. It is clear that in order to use timber and its connections in an efficient way, durability is an important issue to be considered.

The following suggestions are offered as incentives for further research:

- Since the analyses and calculations are limited to a one-curved structure, it would be interesting to expand the system to the real two-curved structure. Of interest could be the differences and similarities between the systems.
- The stress-laminated timber deck should be analyzed further. The behavior and load-bearing design of the deck are very important aspects.
- As already mentioned in the introduction, dynamic analyses have been left out in this thesis. However, these analyses give essential results of the bridge's behaviour. Hence, the conclusions of Daniel Asp's civil engineering thesis should be consulted.

Bringing the thesis to a close, it should be emphasized that the environmentally friendly material timber seems worthwhile to use for constructions. Using timber more frequently in the field of bridge engineering means locking up more carbon. At the same time, very special bridge constructions can be realized like in the case of the project "A Pilgrim's Walk".

8. References

AASHEIM, E.1999: Development of timber bridges in the Nordic countries, Rotorua New Zealand, Pacific Timber Engineering Conference

BORGEBY CASTLE 09/04/2012: http://enjoysweden.se/en/object/borgeby-castle/– website

CAMINO DE SANTIAGO 08/04/2012: http://www.caminodesantiago.me.uk – website

CAMINOS DE EUROPA 08/04/2012: http://www.backpack45.com/images/mappassport.jpg – website

CROCETTI, R. 2012: personal communication

DEUTSCHES MUSEUM 16/06/2012: http://www.deutsches-museum.de/sammlungen/ausgewaehlte-objekte/meisterwerke-vi/besucherbruecke/ - website

DEUTSCHES MUSEUM et al. 1999: Die Brücke im Raum, München, Deutsches Museum

DTI & TRADA undated: Introduction to Timber Engineering - Timber Bridges - Part 1 - Introduction; Historic Background; Modern Applications; Protective Design; Decks and Joinery, Timber Design Knowledge for Professionals of the Future

EKHOLM, K. 2011: Stress-laminated-timber bridge decks subjected to ultimate loads, Diss., Chalmers University of Technology

GEROLD, M. 2006: Economic Viability of Modern Timber Bridges. Lifespan and Costs of Maintenance, Budapest, IABSE Symposium

GEROLD, M. 2007: Holzbrücken am Weg. Einschließlich Geschichte des Holzbrückenbaus unter Berücksichtigung neuester Entwicklungen und heutiger Anwendungsgebiete, Karlsruhe, Harrer Ingenieure

INFORMATIONSDIENST HOLZ 2000 (a): Brücken - Planung. Konstruktion. Berechnung, Holzbau Handbuch Reihe 1 Teil 9 Folge 1, Düsseldorf, Arbeitsgemeinschaft Holz e.V.

INFORMATIONSDIENST HOLZ 2000 (b): Details für Holzbrücken, Holzbau Handbuch Reihe 1 Teil 9 Folge 2, Düsseldorf, Arbeitsgemeinschaft Holz e.V.

INFORMATIONSDIENST HOLZ 2000 (c): Holz im Außenbereich, Holzbau Handbuch Reihe 1 Teil 18 Folge 2, Düsseldorf, Arbeitsgemeinschaft Holz e.V.

ISAKSSON, T. undated: Methods for predicting durability and service life of wood. State-of-the-art,m, Report, Lund Institute of Technology (LTH)

KLEPPE, O. & AASHEIM, E. 1996: Timber Bridges in the Nordic Countries, Madison WI, Forest Products Laboratory, p. 10 - 17

METTEM, C.J. 2011: Timber Bridges, Routledge Chapman & Hall

NATTERER, J. et al. 1991: Holzbau Atlas Zwei, München, Institut für internationale Architektur-Dokumentation GmbH

NATTERER, J. et al. 1996: Holzbau Atlas, Zweite Auflage, Köln, Rudolf Müller Verlagsgesellschaft

PFEIFER 2011: Tension Members – company publication

PFEIFER 05/08/2012: http://www.pfeifer.de/ - website

RITTER, M.A. 1990: Timber Bridges. Design. Construction. Inspection and Maintenance, U.S. Dept. of Agriculture Forest Service Engineering Staff

SCHICKHOFER, G. 2000: Statik im Holzbrückenbau. Fahrbahnkonstruktionen, Vorlesungsskriptum Holzbrückenbau Teil 3 Step A, TU Graz

SÉTRA 2006 (2007): Technical Guide. Timber Bridges. How to ensure their durability, Ministère de l'Ecologie du Développement et de l'Aménagement durables

STRASKY, J. 2005: Stress Ribbon and Cable-supported Pedestrian Bridges, ICE Publishing, p.173-178 & 226-230

SWEDISH WOOD 16/07/2012:
http://www.swedishwood.com/facts_about_wood/glulam/about_glulam - website

SVENSKT TRÄ TM 2012: Hållfasthetsklasser för limträ enligt Eurokod 5 – company publication

TRONDHEIM 08/04/2012: http://www.trondheim.com/pilgrimage - website

APPENDIX A: Excel-Tables: Demonstration of the correlation between distance x and critical angle φ_{crit}

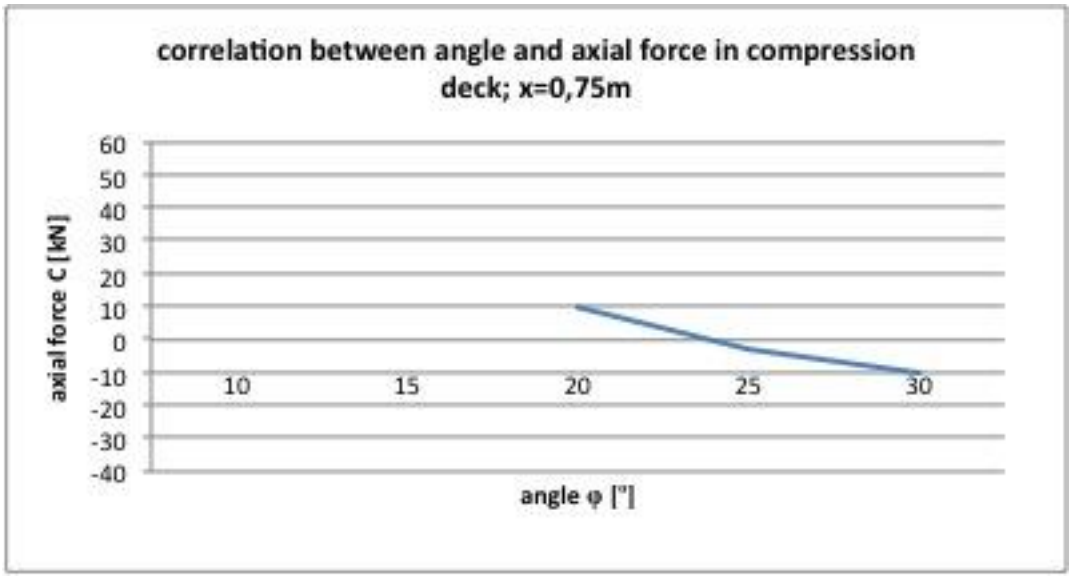

Figure A. 1 Demonstration of the correlation between angle φ and axial force C with the data of the inner node case x=0,75m; $\varphi_{crit} \approx 24^{\circ}$ (cf. Fig. 5.25)

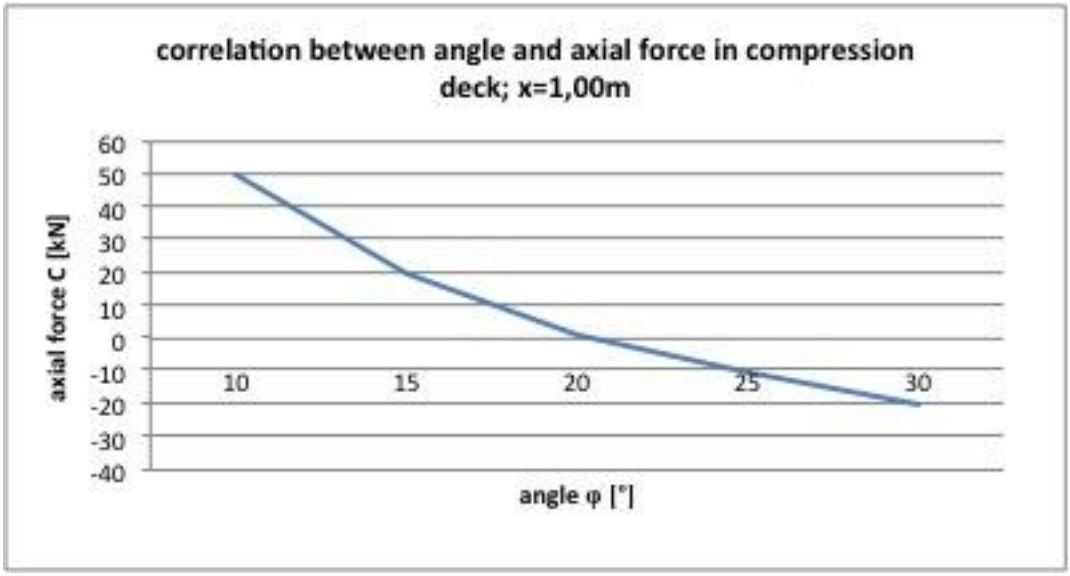

Figure A. 2 Demonstration of the correlation between angle φ and axial force C with the data of the inner node case x=1,00m; $\varphi_{crit} \approx 28^{\circ}$ (cf. Fig. 5.20)

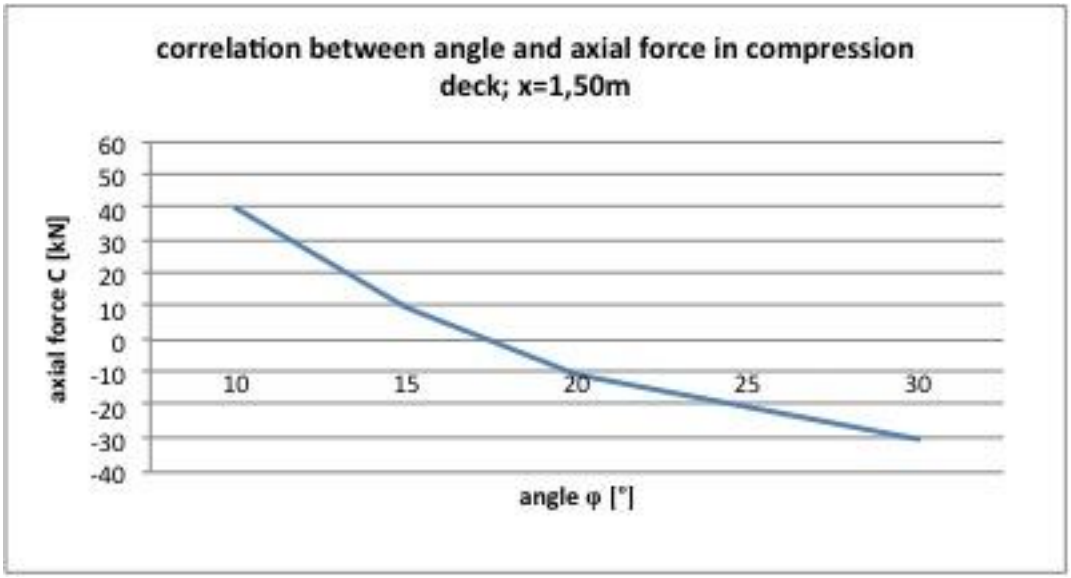

Figure A. 3 Demonstration of the correlation between angle φ and axial force C with the data of the inner node case x=1,50m; $\varphi_{crit} \approx 18^{\circ}$ (cf. Fig. 5.21)